Bicycle aerodynamics

Journal of Wind Engineering & Industrial Aerodynamics 200 (2020) 104134

Contents lists available at ScienceDirect

Journal of Wind Engineering & Industrial Aerodynamics

journal homepage: www.elsevier.com/locate/jweia

Bicycle aerodynamics: History, state-of-the-art and future perspectives

Fabio Malizia [a,b,*], Bert Blocken [a,b]

[a] Department of Civil Engineering, KU Leuven, Kasteelpark Arenberg 40, Bus 2447, 3001, Leuven, Belgium
[b] Department of the Built Environment, Eindhoven University of Technology, P.O. Box 513, 5600 MB, Eindhoven, the Netherlands

ARTICLE INFO

Keywords:
Cycling aerodynamics
Cyclist
Historical overview
Sports review
Wind tunnel test
CFD

ABSTRACT

The importance of aerodynamics in cycling is not a recent discovery. Already in the late 1800s it was recognized as a main source of resistance in cycling. This knowledge was only rediscovered in the late 1970s and 1980s, when aerodynamic concepts were applied to bicycle equipment and cyclist positions, leading to new world hour records and Olympic medals. The renewed interest for cycling aerodynamics is significantly growing with the production of a vast literature, focused on increasing the comprehension of cycling aerodynamics and on improving the aerodynamics of bicycle equipment. Finding the connection between the different subfields of cycling aerodynamics and linking new research with past discoveries is crucial to efficiently drive future studies. Therefore, the present paper provides a comprehensive review of the history and the state-of-the-art in cycling aerodynamics, focusing on one of its main aspects: the bicycle. First, a short history of the bicycle is presented. Next, some cycling power models are outlined and assessment methods for aerodynamic drag are discussed, along with their main advantages and disadvantages. The core of this review paper addresses the components constituting the bicycle: frame and tubes, wheels, handlebar and other equipment. Finally, some future perspectives on bicycle aerodynamics are provided.

1. Introduction

Aerodynamic resistance is a core focus in cycling as it is responsible for about 90% of the total resistance at speeds larger than 40 km/h on flat terrain (Grappe et al., 1997; Kyle and Burke, 1984). The majority of modern bicycles and cyclist postures are therefore optimized in terms of aerodynamic resistance: this optimization can be the result of wind tunnel tests (WT), computational fluid dynamics (CFD) simulations or field tests.

The importance of aerodynamics in cycling was clearly demonstrated by Moser's world hour record (Hinault and Genzling, 1988), achieved using a bicycle and a position developed by means of WT tests and using a special set of so-called 'lenticular' wheels. However, this bicycle was neither the first one to be studied and developed using a WT nor the first one using aerodynamic equipment: aerodynamically shaped frame-tubes and handlebar, recessed cables and aerodynamic water bottles were already in use. To the best of our knowledge, the first WT tests on cyclists date back to the mid-1950s, when Kawamura (1953, reported in Kyle, 1979) and Nonweiler (1956) tested both scaled models and real cyclists and reported an impact of cyclist position on the bicycle and an aerodynamic drag increase when wearing fluttering clothing. This indicates that the awareness about the impact of the frontal area and the influence of clothing on cyclist total resistance was already present. Moreover, aerodynamic equipment, like Lycra skinsuits and streamlined tubes for cycling frames, started to become commercially available already in late 1970s. Despite their availability, this aerodynamic equipment did not create an immediate breakthrough in cycling: for instance Moser's bicycle still had round tubes (Hinault and Genzling, 1988).

Studies and aerodynamic equipment applied to cycling are not only limited to the last decades but they were already present in the late 19th century. The inventions of disc and four-spoke wheels are indeed early examples of aerodynamic equipment. Furthermore, drafting races, where a cyclist was riding behind tandem cyclists, motorcycles or even trains, were common in that period and these were attended by several thousands of spectators (Ritchie, 2011). New bicycle designs were proposed as well, such as recumbent bicycles in 1895 (von Salvisberg, 1897; Wilson, 2004) and streamlined enclosures in 1913 (Schmitz, 1990). Moreover, the first simplified mathematical models of forces acting on cyclists also became available at that time (Bourlet, 1894) and these models showed the large impact of aerodynamics on cyclist performance.

At present, a lot of research on cycling aerodynamics has been

* Corresponding author. Department of Civil Engineering, KU Leuven, Kasteelpark Arenberg 40, bus 2447, 3001, Leuven. Belgium.
E-mail address: fabio.malizia@kuleuven.be (F. Malizia).

https://doi.org/10.1016/j.jweia.2020.104134
Received 22 November 2019; Received in revised form 20 February 2020; Accepted 20 February 2020
Available online 25 March 2020

performed and published and this includes a few review papers covering the state-of-the-art in cycling aerodynamics. To the best of our knowledge, Lukes et al. (2005) was the first to present such a review, summarizing the latest findings from the aerodynamic investigations of different cycling equipment and cyclist positions. Later Gibertini and Grassi (2008) provided an additional review of cycling aerodynamics focused on the work performed at their institution. Most recently, Crouch et al. (2017) provided a review paper including the most recent results obtained by means of WT tests, CFD simulations and field tests. However these very valuable reviews focused mainly on the state-of-the-art and on recent developments in cycling aerodynamics and provided only little or no information on the historical developments that have led to the present-day state-of-the-art. In addition, the field of cycling aerodynamics is developing at an ever increasing pace, with many relevant studies appearing in the past few years that were not yet included in any review paper. Moreover, the interest for aerodynamics has also been growing in para-cycling recently (e.g. Belloli et al., 2014; Mannion et al., 2018a, 2018b, 2019c).

The aim of the present review paper therefore is to provide a comprehensive review of the history and the state-of-the-art in cycling aerodynamics combined with perspectives for future research. In particular, this review paper focuses on bicycle aerodynamics, with particular focus on racing bicycle aerodynamics, which includes the aerodynamics of the frame, wheels, handlebar and other small equipment. It will be shown that the earliest reported work where cycling aerodynamics was considered dates back to the 19th century. The aerodynamic development in early cycling is then linked to the current state-of-the art of modern aerodynamics, which is systematically described together with its impact on bicycle performance. Finally, the missing links in the present knowledge on bicycle aerodynamics are discussed and ongoing research as well as perspectives for future research are described.

The paper is structured in five main sections. Section 2 presents a short historical review of the bicycle, from the "Laufmaschine" to the modern bicycle. Section 3 provides basic information about the forces acting on cyclists, including mathematical models and the available methods to measure these forces. Section 4 focuses on the aerodynamics of the components constituting the bicycle: frame, wheels, handlebar as well as smaller components that may influence the total drag. Finally, Section 5 contains a summary with conclusions and future perspectives.

2. A short history of the bicycle

"Mater artium necessitas"; "Necessity is the mother of invention" - William Horman, 1519

2.1. The Laufmaschine

The years between 1812 and 1816 were characterized by bad agricultural harvests in Northern Europe and North America, with a consequent rise of corn and oat prices. The peak was reached in 1817, after the so-called "year without a summer", caused by the 1815 eruption of Mount Tambora in Indonesia (Hadland and Lessing, 2014). The quest for a horse-less means of transport in a bad harvest period, together with the Napoleonic wars, are probably some of the reasons that pushed the twenty-eight year-old Baron Karl von Drais to develop new driving machines in 1813 (Lessing, 2001). Citing Drais' words: "*In wartime, when horses and their fodder often become scarce, a small fleet of such wagons* [note by the present authors: i.e. Drais' four wheel machine] *at each corps could be important, especially for dispatches over short distances and for carrying the wounded*" (Drais, 1816, reported in Hadland and Lessing, 2014).

Drais designed his first two wheeler machine around 1817 (Fig. 1a), which was initially named "Fahrmaschine" and later "Laufmaschine" (running machine) and is also known as "Velocipede" or "Draisine" in England and "Draisienne" in France (Hadland and Lessing, 2014). The idea to switch from a three or four-wheel driving machine to a two-wheeler machine came to Drais' mind by observing ice skaters (Drais, 1817, reported in Lessing, 2003a). Indeed, the balancing system used on a Draisienne resembled the balancing technique of ice skaters. However, this system made the two-wheel machines difficult to ride for a large part of the population.

The "Laufmaschine" was composed by two wooden wheels held together with iron hoops (Hadland and Lessing, 2014). The propulsion was achieved not by a pedaling system but by direct contact of the feet to the ground. The first public ride of Drais' two-wheeler machine occurred on 12th June 1817. Almost 13 km were traveled in less than 1 h, in the surroundings of Mannheim. This machine became popular also outside Germany and was also used in countries like France, England and the United States (Hadland and Lessing, 2014).

The "Laufmaschine" users were generally riding on sidewalks instead of carriageways, as it was easier to keep their balance on a good shaped sidewalk than on a carriageway. However, the presence of the Laufmaschine on sidewalks created danger for the pedestrians and pushed several municipalities to forbid the use of the Laufmaschine on sidewalks and inside cities, causing a drop of its use and its popularity already around 1820 (Hadland and Lessing, 2014; Lessing, 2003b).

2.2. Towards the contemporary bicycle

The evolution from this first Laufmaschine towards the modern bicycle lasted about 80 years and several inventions occurred during this process. Three inventions are considered to be fundamental: the pedaling propulsion, the tension wire spoking for wheels and the indirect rear wheel drive.

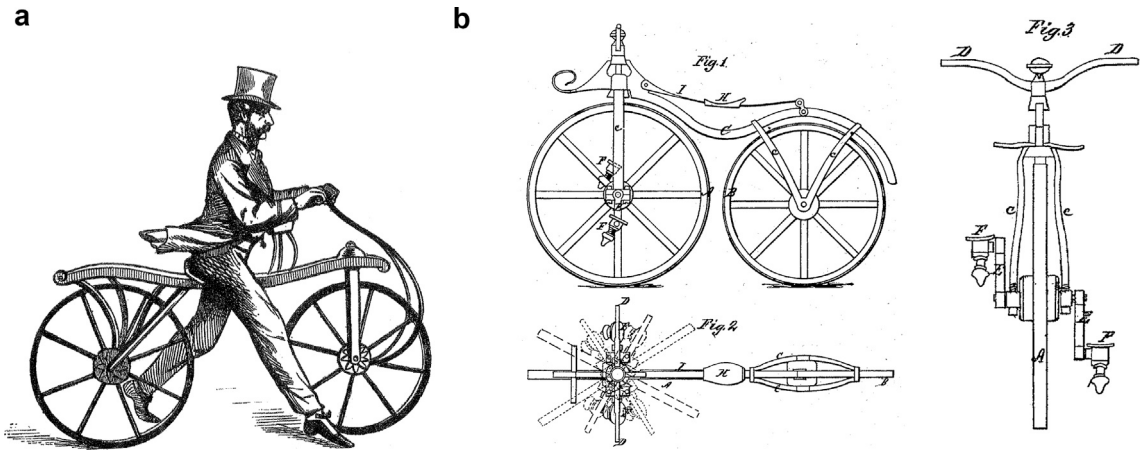

Fig. 1. (a) Draisienne bicycle (source: Sharp, 1896); (b) Lallement's patent of a pedaling system applied to a Draisienne (source: Lallement, 1866).

The first step towards the modern bicycle was established by the introduction of pedaling propulsion. This was achieved by a crank. However, the importance of this step was not the crank itself but the concept of "balancing while cranking" (Hadland and Lessing, 2014; Lessing, 1996). The identity of the true inventor of this driving mechanism is not clear. The dispute about this invention is mainly between Pierre Michaux and Pierre Lallement and several historians have debated it (Hadland and Lessing, 2014; Herlihy, 2004; Wilson, 2004; Woodforde, 1980). One of the few trusted sources about this invention is Lallement's USA patent of a front driven "velocipede", see Fig. 1b (US patent 59,915; November 1866).

The second step was the introduction of the wire wheels. This invention was directly connected to the quest for faster bicycles, since cycling races started to gain popularity in the 1860s (Ritchie, 2011). It is worth noting that at that time "the bicycle was inseparable from the idea of speed" (Kobayashi, 1993, reported in Ritchie, 2011), therefore there was a large demand of innovation in cycling, which could be satisfied only in countries with a large industrial capacity where the bicycle use also spread quicker (Ritchie, 2011). The pedaling system described above was directly connected to the front wheel (Sharp, 1896) thus it had an important limitation: the ratio between the wheel and crank revolution was fixed to one. Therefore the quest for faster bicycles directed the search towards increasing the wheel diameter and thus the path length traveled per unit crank revolution. The manufacturing of larger wheels became only possible after the introduction of the wire wheels: in these wheels the spokes work in traction rather than in compression. The introduction of this tension spoking not only enabled the production of larger wheels but also decreased their weight and removed the buckling problem suffered by compression spokes (Hadland and Lessing, 2014). The wired tension wheel inventor was Eugene Meyer (Hadland and Lessing, 2014), with the 1868 French patent number 86,705 (Fig. 2a). This wheel type was further improved by introducing a tangential "lever bar" designed to tighten all the spokes at once (Herlihy, 2004) (Fig. 2b). This system was mounted on the Ariel bike (Fig. 2b), patented in 1870 by James Starley and William Hillman (British patent number 2,236). Starley was also the first to place the spokes tangential to the hub. This mechanism was described in the 1874 British patent number 3,959 (Hadland and Lessing, 2014). Using this spoke configuration, the forces were acting parallel to the spokes, avoiding the creation of a bending moment which was often responsible for the breaking of radial spokes. Bicycles using these wheels were named "High wheeler", "Ordinary" or "Penny-Farthing" (Heijmans and Mallon, 2011; Ritchie, 2011; Wilson, 2004). The latter name, "Penny-Farthing", referred to the shape of two coins used in Great Britain, the penny and the farthing (quarter-penny) (Hadland and Lessing, 2014). These coins had a large difference in diameter, referring to the difference in diameter between the front and rear wheel of the high wheeler bicycles, respectively up to 1.5 m and about 0.4 m (Boardman, 2015; Hadland and Lessing, 2014). The use of the high wheeler bicycles spread in Europe and the United States for about thirty years, thanks to the higher cycling speed that could be achieved. As a result of this increased cycling speed, the number and type of races increased, leading also to the first world hour record. This record was achieved by Frank Dodds in 1876 using a high wheeler bicycle and riding a total of 26,508 m in 1 h (Heijmans and Mallon, 2011), see Fig. 3. Actually, there were other cyclists that conducted a similar race, prior to Dodds' record. John Thomas Johnson rode his high wheeler bicycle for a total of 22.785 km in 1 h already in 1870 (Kyle and Bassett, 2002). However, accordingly to Kyle and Bassett (2002), only from 1876 the "hour records were kept faithfully", therefore, here the record of Dodds is considered to be the first world hour record. However, these high wheeler bicycles were considered dangerous and common accidents were over-the-handlebar falls, also called "headers", "croppers" or "imperial crown" (Earl of Albemarle and Hillier, 1896). Moreover, the large front wheel caused problems of maneuverability and steering. Therefore many bicycle designers started to focus on creating safer bicycles.

The third step in bicycle progress was the invention of the indirect

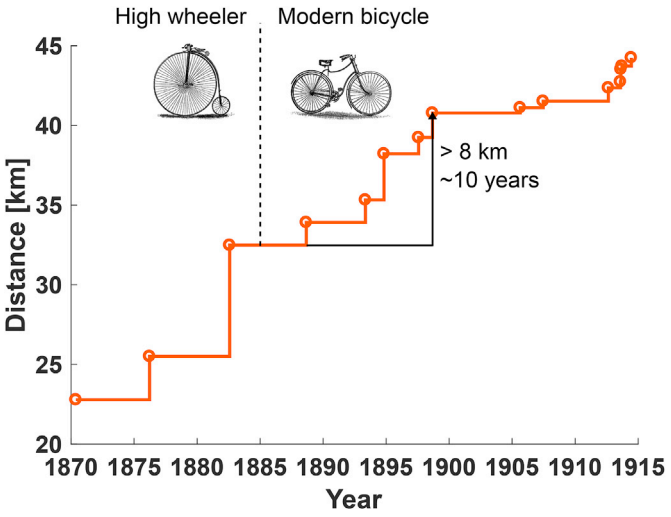

Fig. 3. Fast increase in the world hour record achievements by introduction of safety bicycles in 1885, shown here until 1915. High wheeler and safety modern bicycle picture source: (Sharp, 1896).

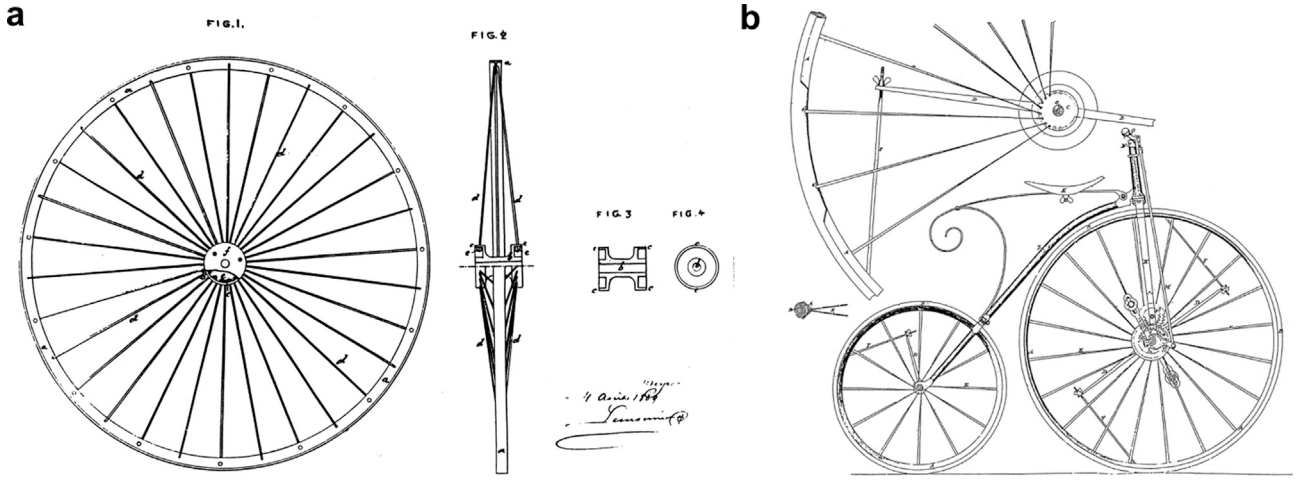

Fig. 2. (a) Drawings included in Meyer's French patent (number 86,705) of a bicycle wheel with tension radial spokes; (b) "Ariel" bicycle with a pair of lever tension wheels (source: Starley and Hillman, 1870; reproduced with permission from "Veteran-Cycle Club online library").

driving system, which enabled a rear wheel propulsion thus avoiding the need of a large and dangerous front wheel. This propulsion type could be achieved in several ways, for instance using lever and crank drives, swinger lever and linear drives, belt, pulleys as well as shaft drives and spur gear drives (Hadland and Lessing, 2014). Nevertheless the most successful indirect driving system, used up to the present day, was the chain drive. Several patents appeared around the mid-1860s, however the bush roller (1880) and block roller (1885) chains of Hans Renold became the commercial standard for track racers and non-racing cycles (Hadland and Lessing, 2014). In the years between 1876 and 1885, many bicycle manufacturers built new and safer bicycles, called "safety" bicycles, with an indirect front or rear wheel driven propulsion, which facilitated the use of smaller wheels. In particular, the bicycles with rear wheel driven propulsion enabled the use of two wheels of similar dimensions and a lower saddle placed in the middle of the wheelbase. The first rear-driving "safety" bicycle was invented by Henry John Lawson in 1879 (Sharp, 1896) carrying the British patent 3,934. This bicycle was named "Bicyclette" for the French market (Hadland and Lessing, 2014). However, the first rear drive bicycle that gained large success was the "Rover safety" of John Kemp Starley and William Sutton in 1885 (Sharp, 1896). The second version of this bike was the prototype of the modern rear drive bicycle (Sharp, 1896). The two models are shown in Fig. 4a and b, together with a 1898 racing model with dropped handlebar and pneumatic tire (Fig. 4c), the latter invented by Dunlop in 1888 (Wilson, 2004). The introduction of safety bicycles represented one of the biggest breakthroughs in cycling history. In the period between 1888 and only 10 years later, the world hour record was broken five times and the traveled distance increased by more than 8 km (Fig. 3).

More details about early bicycle history can be found in the literature (e.g. Earl of Albemarle and Hillier, 1896; Hadland and Lessing, 2014; Herlihy, 2004; Ritchie, 2011; Sharp, 1896; Wilson, 2004). Information on further historical developments of the bicycle and its components is provided in the remainder of this paper.

3. Models and methods

This section discusses the forces acting on a cyclist and describes the cycling power model developed by Martin et al. (1998) (Subsection 3.1). The cycling power model developed by Bourlet (1894) is also introduced, since it represents one of the earliest known cycling power models (Subsection 3.2). The reason cycling mathematical models are created is because they enable a better understanding of how a change in a specific parameter, for instance weight, aerodynamics or training, can influence the overall performance of a cyclist, as done by Jeukendrup and Martin (2001). Lastly, the methods available for the assessment of aerodynamic forces are discussed (Subsection 3.3).

3.1. Cycling power model

The physics of a cyclist riding a bicycle follows the laws from classical mechanics including Newton's second law:

$$\sum \vec{F} = m \cdot \vec{a} \tag{1}$$

which states that an acceleration, a, occurs every time the forces F, propulsive and resistive, are out of balance. Here the mass, m, is considered a proportionality constant. In Fig. 5, the forces and moments acting on the combined cyclist-bicycle system are shown. These forces are the aerodynamic drag, F_D; the aerodynamic moment acting on the rotating wheels, M_{ad}; the rolling resistance of the wheels moving on the ground, F_{rr}; and the bearing friction in the wheels, F_{wb}. In addition, when a slope of angle α is present, the weight W has a component $W_{//}$ along the direction of motion thus slowing down or accelerating the cyclist-bicycle system when riding uphill or downhill, respectively. The slope, or grade,

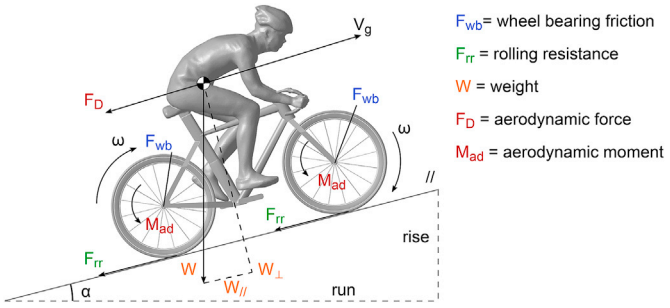

Fig. 5. Force diagram of the cyclist-bicycle system on an inclined road.

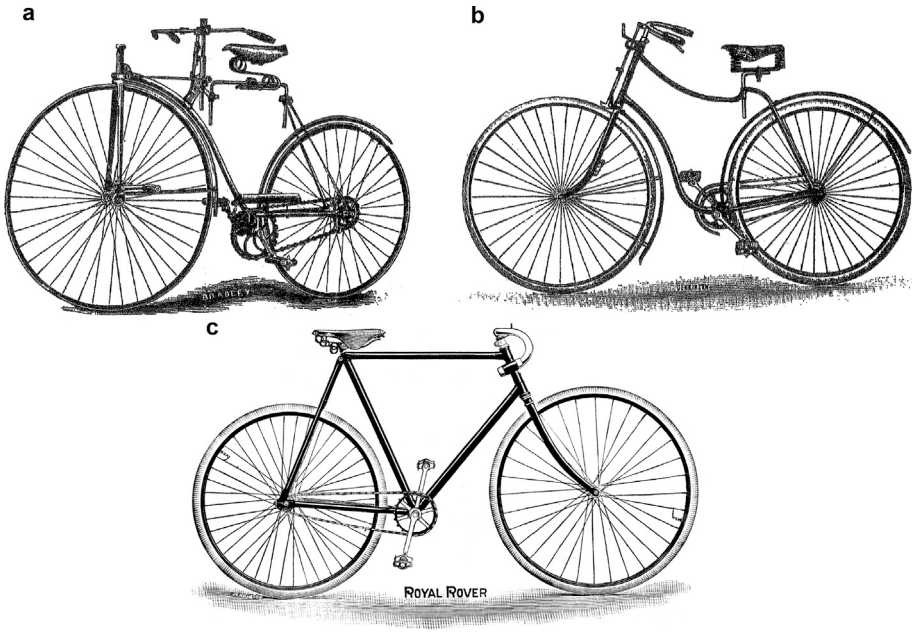

Fig. 4. "Rover" safety bicycle from Starley and Sutton: (a) First model in 1885 (source: Sharp, 1896); (b) Second model (source: Sharp, 1896); and (c) Racing model in 1898 (source: Rover Cycle Company Limited, 1898; reproduced with permission from "Veteran-Cycle Club online library").

is also indicated with the symbol "s" and it is equal to the rise over run ratio:

$$s = \frac{rise}{run} = \tan(\alpha) \tag{2}$$

Often the balance in Eq. (1) is expressed in terms of power since the power generated by a cyclist can be measured easily using power sensors connected to the bicycle. In general, a power model equates the available power, thus the power generated by a cyclist, and the needed power to cycle at a given speed:

$$P_{avail} \cdot \eta = P_{needed} \tag{3}$$

where η is the efficiency of the cyclist power transmission from crank over chain and rear wheel, which is connected to the friction in the drivetrain. The power needed includes five terms (Eq. (4)), namely the power loss due to aerodynamic drag, P_{ad}; due to rolling resistance, P_{rr}; due to friction in wheel bearings, P_{wb}; due to a change in potential energy thus due to terrain slopes, P_{pe}; and due to changes in kinetic energy, P_{ke}. The latter term represents the power to accelerate or the power that becomes available when the system decelerates. These terms are described in detail by Martin et al. (1998). The complete equation for the power needed is reported in Eq. (5) and its simplified version for cases with slope s smaller than 10% is given in Eq. (6).

$$P_{needed} = P_{ad} + P_{rr} + P_{wb} + P_{pe} + P_{ke} \tag{4}$$

$$P_{needed} = 0.5\rho V_a^2 V_g (C_D A + F_w) + V_g \cos\left(\tan^{-1}(s)\right) C_{rr} mg + V_g \left(91 + 8.7 \cdot V_g\right) \cdot 10^{-3} + V_g \sin\left(\tan^{-1}(s)\right) mg + 0.5\left(m\frac{\partial V_g^2}{\partial t} + \frac{I}{r^2}\frac{\partial V_g^2}{\partial t}\right) \tag{5}$$

$$P_{needed} = 0.5\rho V_a^2 V_g (C_D A + F_w) + V_g C_{rr} mg + V_g \left(91 + 8.7 \cdot V_g\right) \cdot 10^{-3} + V_g\, s\, m\, g + 0.5\left(m\frac{\partial V_g^2}{\partial t} + \frac{I}{r^2}\frac{\partial V_g^2}{\partial t}\right) \quad for\ s < 10\% \tag{6}$$

P_{ad} depends on the density ρ, the relative velocity component in the riding direction V_a, which is a function of the riding velocity V_g and the external wind component, the drag coefficient C_D, the frontal area A, and the rotational drag area F_w. P_{rr} depends on V_g, the rolling resistance coefficient C_{rr} and the component of the weight W perpendicular to the ground, where W is expressed by the product between the combined cyclist-bicycle mass m and the gravitational acceleration g. P_{wb} is expressed by an empirical formula where only the riding velocity is present as a variable (Dahn et al., 1991; Martin et al., 1998). P_{pe} is a function of the riding velocity and the weight component parallel to the ground. Lastly, P_{ke} has a translational and rotational component. It is a function of V_g, m, wheel radius r, wheel moment of inertia I and the time derivative of the squared riding velocity V_g.

In the following three subsections, brief descriptions of aerodynamic power losses, aerodynamic forces and moments as well as the available power are provided.

3.1.1. Power loss due to aerodynamics

The aerodynamic power loss consists of a translational and a rotational component. The translational power loss refers to the power associated with the forward movement of the combined cyclist-bicycle system, while the rotational power loss refers to the power needed to keep the wheel spinning, thus associated with the power loss by the aerodynamic moment M_{ad} acting on the two wheels. To the best of our knowledge, the aerodynamic moment M_{ad} has only been measured or computed on isolated wheels (e.g. Jermy et al., 2008; Kyle, 1995b; Malizia and Blocken, 2020). The main limitation when testing/simulating isolated wheels is that the influence of the rider and bicycle on the measured/computed aerodynamic moment of the wheel is neglected. This limitation is mainly affecting the rear wheel, which is located in the wake of several bicycle components and of the cyclist's legs.

The total aerodynamic power loss was already presented in Eq. (5), but it is repeated below to highlight its translational and rotational constituents, respectively $P_{ad,t}$ and $P_{ad,r}$:

$$P_{ad} = P_{ad,t} + P_{ad,r} = 0.5\rho V_a^2 V_g C_D A + 0.5\rho V_a^2 V_g F_w \tag{7}$$

In this equation, the effect of external wind is included inside the relative velocity component in the riding direction, V_a. This velocity is equal to the sum of the riding velocity V_g and the wind velocity component in the cyclist travelling direction $V_{w,a}$ (Martin et al., 1998), as shown in Fig. 6 and Eq. (8):

$$V_a = V_g + V_{w,a} = V_g + V_w \cos(\theta) \tag{8}$$

where ψ is the yaw angle between the riding velocity V_g and the relative speed V_r, and θ is the angle between the riding velocity V_g and the wind velocity V_w. Strictly, the drag coefficient C_D is also a function of the external wind direction, however this dependence is often neglected (e.g. Cummings, 1997; Íñiguez-De-La-Torre and Íñiguez, 2006; Isvan, 1984). Research has however shown that the presence of crosswind has an impact on the measured forces and moments (e.g. Barry et al., 2012; Kyle, 1991a; Mannion et al., 2019b). This influence is highly dependent on the type of bicycle, equipment and cyclist position employed. Moreover, the probability for a cyclist to ride at a given yaw angle not only depends on the wind direction and magnitude, but also on the cyclist traveling speed. For example, Cooper (2003) stated that a road vehicle travelling at 13.41 m/s, similar to professional cyclist's speed, has only 10% probability to exceed yaw angles of 16°, when a wind speed of 3.13 m/s is assumed, i.e. the North-American annual mean wind speed at around 2 m height, and a wind direction equally probable from all directions. Note that in some studies, where the impact of crosswind on cycling was investigated, the resulting velocity V_r (for example Barry et al., 2012; Crane and Morton, 2018; Fintelman et al., 2015; Greenwell et al., 1995) or the ground velocity V_g (for example Godo et al., 2010, 2011) was used to compute the drag and side force coefficients from the measured or computed forces, rather than the relative velocity component in the riding direction V_a.

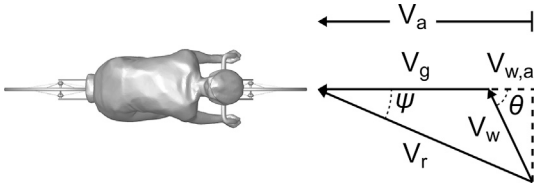

Fig. 6. Cyclist velocity definitions: V_g is the ground or cyclist velocity, V_w is the wind velocity, $V_{w,a}$ is the wind velocity component in the riding direction, V_r is the relative velocity, V_a is the relative velocity component in the riding direction, ψ is the yaw angle, θ is the wind angle.

The drag coefficient and the frontal area are commonly combined in a single parameter called drag area, C_DA. A similar parameter is introduced in the rotational power loss, F_w, and called rotational drag area. This term can be seen as a drag area correction term in the total aerodynamic power loss (Eq. (5)), which takes into account the impact of the wheel rotational moment on the total aerodynamic power loss.

3.1.2. Aerodynamic forces and moments

The most important aerodynamic force in cycling is the drag force, F_D. The main source of aerodynamic drag is the cyclist body, from 60% to 82% of the total drag and depending on the position of the cyclist on the bicycle (Defraeye et al., 2010a; Kyle and Burke, 1984; Nonweiler, 1956), whereas the remaining drag is caused by the bicycle and its components. In Eq. (5), besides the aerodynamic drag force, only the two aerodynamic moments acting on both wheels, M_{ad}, are present. Nevertheless, other forces and moments are generated by the interaction of a cyclist with the air. The definition of these forces and moments is governed by the reference frame (Fig. 7). Two common choices for the reference frame are (i) a reference frame aligned with the relative air velocity, called "wind axes", and indicated in blue in Fig. 7 and (ii) a reference frame aligned with the riding velocity, called "body axes", in red in Fig. 7. In the present paper, the forces and moments are defined in body axes, therefore the drag F_D, commonly indicated with D, is aligned with the riding velocity and the side force F_S, or simply S, is perpendicular to the riding velocity and both forces are parallel to the ground surface, while the lift force F_L is perpendicular to the ground. Considering a reference frame aligned with the riding direction (Fig. 7), three moments can be defined, namely rolling (M_R), pitching (M_P) and yawing (M_Y), oriented respectively longitudinally, laterally and normally to the cyclist-bicycle axis. Their center is located at the wheelbase midpoint, where the wheelbase is defined as the line connecting the front and the rear wheel centers. The reason to use the wheelbase rather than the center of mass is because the latter is usually unknown a-priori, whereas the wheelbase midpoint can be easily identified during WT tests (Genta and Morello, 2009). Forces and moments are generally represented as (Crouch et al., 2017):

$$F_i = \frac{1}{2}\rho C_i A V_r^2 \quad i = D, S, L \tag{9}$$

$$M_j = \frac{1}{2}\rho C_i A V_r^2 l \quad j = R, P, Y \tag{10}$$

where l is the wheelbase length. The velocity used for the forces and moments is the relative velocity V_r, as mentioned in (Crouch et al., 2017) and used in several studies (for example Barry et al., 2012; Crane and Morton, 2018; Fintelman et al., 2015; Greenwell et al., 1995). Note that in aeronautical engineering it is common practice to refer to wind axes

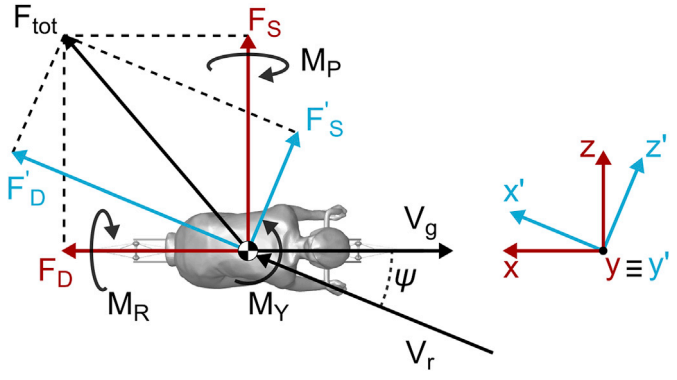

Fig. 7. Forces in relative wind axes (blue) and in body axes (red). Moments in body axes are also presented. (For interpretation of the references to color in this figure legend, the reader is referred to the Web version of this article.)

for aircrafts. In addition, the aerodynamic forces acting on the front wheel generate a steering moment (M_S), which needs to be balanced by the cyclist applying a force (F_{hand}) on each side of the handlebar. Defining b as the length of the handlebar between the two hand positions, the force each hand of the cyclist should apply on the handlebar to compensate M_S is:

$$F_{hand} = \frac{M_S}{b} \tag{11}$$

3.1.3. Power available

The power available is the power produced by the cyclist's muscular activity. The muscular power efficiency, defined as the ratio between the energy transmitted to the crank and the chemical energy in the food, is between 20% and 30%: the remaining energy is dissipated into heat (Wilson, 2004). The chemical energy in the food is stored in the body and employed by means of different metabolic processes, some of them are used for short-term efforts such as the sprint and others for long-term efforts. Moreover, the way the potential chemical energy is converted into work depends on the cyclist's physiological characteristics, therefore a curve establishing the dependence between power and duration is individual. Nevertheless, a curve connecting the maximum recorded duration of a cyclist exerting a given power output can be drawn, as done by Wilson (2004) and shown in Fig. 8. These data were measured or estimated from races by Wilson (2004). A more detailed description of cyclist energetics is out of the scope of this paper, more information can be found in the literature (Capelli et al., 1993, 1998; Casa, 1999; Faria et al. 2005a, 2005b; Ferretti, 2015; Fonda and Šarabon, 2012; Joyner and Coyle, 2008; Martin et al., 2007; Morton and Hodgson, 1996; Wilson, 2004).

3.2. The Bourlet (1894) power model

One of the earliest known mathematical cycling models is presented in the book of Bourlet, published in 1894. This mathematical model includes four sources contributing to the total resistance, namely bicycle passive resistance, including chain losses, drive train and wheel bearing friction; rolling resistance; resistance due to vibrations; and aerodynamic resistance (Bourlet, 1894). In this model, the first term was considered negligible. The second and the third terms, rolling resistance and the resistance due to the vibrations, respectively, are a function of the tire type and the road quality. With the word "vibrations", Bourlet (1894) referred to the vibrations caused by the bumps in the streets that are propagated by the bicycle structure. He found that this term was relevant only when solid tires were used as it became small or negligible for pneumatic tires (Bourlet, 1894). The latter pneumatic tires had been patented by Dunlop only few years earlier, in 1888 (Wilson, 2004). The Bourlet model is given by Eq. (12):

$$P = R \cdot V_g = \left[W\left(a + b \cdot V_g\right) + k \cdot A \cdot V_g^2\right] \cdot V_g \tag{12}$$

Where R is the total resistant force on flat terrain, V_g is the riding velocity, W is the total weight (in kilogram-force), a is a force coefficient related to the rolling resistance, b a force coefficient related to both rolling and vibrational resistance, k an aerodynamic force coefficient and A the frontal area. The forces are expressed in kilogram-force linked to N by the gravity acceleration g, the riding velocity is expressed in m/s and the frontal area in m^2. Bourlet (1894) also introduced a modified version of the model in Eq. (12) that included the effect of a slope s:

$$P = (R + W \cdot s) \cdot V_g = \left[W\left(a + b \cdot V_g\right) + k \cdot A \cdot V_g^2 + W \cdot s\right] \cdot V_g \tag{13}$$

Note that the effect of a slope was described with the same formula used by Martin et al. (1998) and presented in Eq. (6) for cases with slopes $s <$ 10%.

Two types of experiments were described by Bourlet to estimate these

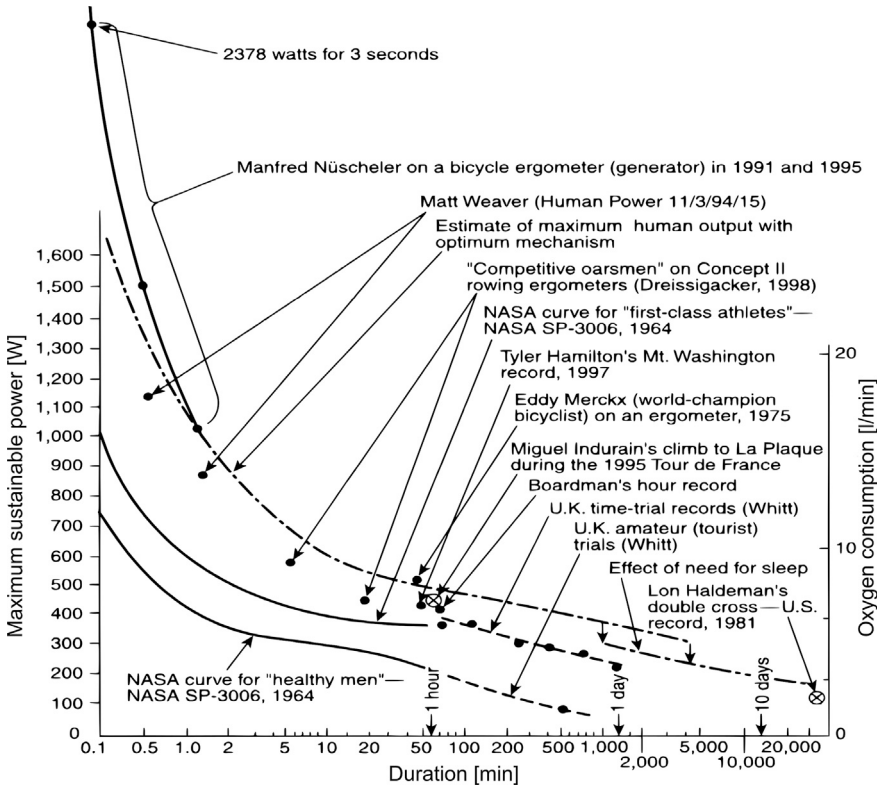

Fig. 8. Envelope of maximum sustainable power as a function of effort duration (source: Wilson, 2004; reproduced with permission from The MIT Press).

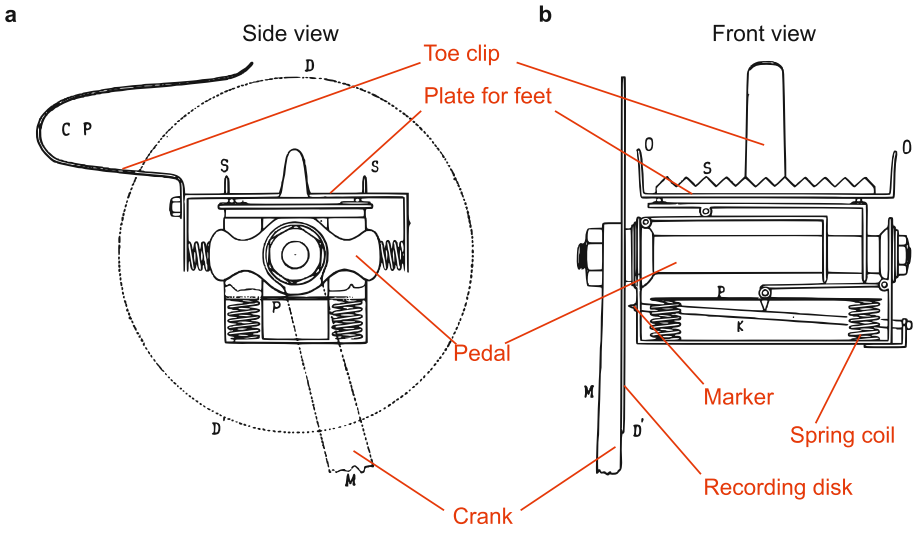

Figure 9. "Pédale Dynamométrique" used for power measurements in late 1890s (adapted from Bouny, 1899; reproduced with permission from "gallica.bnf.fr/BnF").

coefficients. The first experiment involved riding at a constant speed, measuring the terrain slope, the cyclist velocity and the cyclist power, where the latter was measured by the "pédale dynamométrique", patented in 1893 by Maillard and Bardon (Bouny, 1899; Bourlet, 1894). A similar device was already built by Scott in 1889, and called "cyclograph" (Scott, 1889). The "pédale dynamométrique" was improved by M. Marey in 1895 (Bouny, 1899) and its way of use is briefly discussed below to help the readers understand its working principle (Fig. 9). This device consisted of a coil spring connected to the pedal and to a plate where the foot was resting. The cyclist pushing on this pedal deformed the coil springs and moved a lever connected to a marker which reported the displacement caused by the cyclist foot to the coil spring on a recording disk during the entire crank rotation. Bourlet (1894) repeated this experiment at several cycling speeds, from which he gathered the data needed to compute the coefficients a, b and k. The second experiment consisted of measuring the downhill cycling speed of a cyclist on a constant slope: without pedaling, a constant equilibrium velocity, called limit velocity, was reached. At the limit velocity, an equilibrium between the resistive forces, due to rolling, vibrational and aerodynamic resistance, and the propulsive force due to the slope was achieved. Therefore:

$$W\left(a+b\cdot V_g\right)+k\cdot A\cdot V_g^2=-W\cdot s \tag{14}$$

The latter experiment was only described and not performed by Bourlet,

but he mentioned that Guye performed such tests in 1893 (Guye, 1893).

From the first type of experiment, Bourlet found that a was about 0.004 when cycling on track and about 0.009 when cycling on normal road, whereas the average k was 0.06 $kg_f \cdot s^2/m^4$. However, Bourlet mentioned that the coefficient k was dependent on cyclist position, on cyclist size and on both clothing shape and clothing fluttering. The frontal area was estimated to be about 0.5 m^2 for the cyclist-bicycle combination. Bourlet did not provide information about the type of bicycle and the position adopted by the cyclist during the tests. It is likely that the bicycle was similar to a "Rover safety" racing bicycle as shown in Fig. 4c.

The present authors have computed and compared k and a values from more recent studies (Barry et al., 2015; Kyle, 1979; Kyle and Burke, 1984; Nonweiler, 1956; Wilson, 2004) with those reported by Bourlet (1894) as shown in Table 1 for a and Table 2 for k. Considering the different bicycles, cycling equipment and measuring devices used in different historical periods, one could argue that these values present a reasonable agreement.

3.3. Methods to assess forces and power

The mathematical models described in the previous subsection include parameters such as aerodynamic drag coefficient, rolling resistance coefficient and frontal area, which need to be measured or computed. This subsection discusses how to obtain the aerodynamic drag force by means of direct or indirect measurements. The former include experimental and computational techniques such as WT tests and computational fluid dynamics (CFD) simulations, while the latter generally refer to field tests, where quantities like speed, power or terrain slope are measured from which the drag force is inferred through mathematical models. This subsection provides the basic information towards the presentation of the history and state-of-the-art in Section 4, where technological innovations in the bicycle and its main components will be linked to their aerodynamic performance as demonstrated by WT tests, CFD simulations and/or field tests.

3.3.1. Wind tunnel tests

The main hypothesis generally adopted in WT tests of cyclists is that the forces measured on a static or pedaling cyclist with moving air are equal to the ones of a cyclist riding through stagnant air. This equivalence was first stated by Leonardo Da Vinci in the Codex Atlanticus, and referred to by Giacomelli (1930) as the principle of aerodynamic reciprocity (reported in Anderson, 1997). WTs are often classified according to their intended test objects or test conditions (aeronautical WTs, atmospheric boundary layer WTs or automobile WTs), according to their design (open or closed circuit), or their test section (open or closed). An example of a closed circuit WT with a closed test section of 27 m length specifically designed and equipped for cycling tests including team time trials and sprint trains is shown in Fig. 10 and Fig. 11. A more detailed classification of WTs can be found in Barlow et al. (1999).

Probably the first WT tests for cycling were performed by Kawamura in 1953 (reported in Kyle, 1979) and Nonweiler in 1956. The former tested reduced-scale cycling models inside a WT whereas the latter tested real cyclists. Generally, WT tests in cycling are performed on full-size bodies. When a scaled model is used, the same forces as on full-size cyclists can be measured if Reynolds number similarity is satisfied, with the Reynolds number defined as:

Table 1
Comparison of rolling resistance coefficients between the data by Bourlet and modern measurements.

$a = c_{rr}$ [-]	Bourlet (1894)	Kyle and Burke (1984)	Wilson (2004)
Minimum	0.004 (track)	0.0016	0.002
Average	0.009 (road)	0.0034	0.008

Table 2
Comparison of aerodynamic k coefficient between the data by Bourlet and modern measurements.

	Bourlet (1894)	Nonweiler (1956)	Kyle (1979)	Barry et al. (2015)
Methodology	Power measurement	Wind tunnel	Coasting tests	Wind tunnel
Position	Unknown	Dropped	Dropped	Standard dropped
A (m^2)	0.5	0.334	Unknown	0.472
k (kg/m^3)[a,b]	0.588	0.571	0.49[c]	0.422

[a] The Bourlet k coefficient has the unit $[(kg_f \cdot s^2)/(m^4)]$, which is multiplied by gravitational acceleration to convert it to SI units.
[b] Comparing Bourlet and modern models; $k = 0.5\,\rho C_D$.
[c] Air density assumed to be 1.225 kg/m^3.

$$Re = \frac{\rho\, l\, V}{\mu} \tag{16}$$

where ρ is the density, l a reference length, V a reference velocity and μ the dynamic viscosity of air. Considering standard atmosphere and the square root of the cyclist frontal area, e.g. 0.40 m^2, as the reference length (Crouch et al., 2017), the Reynolds number ranges between 4×10^5 and 7×10^5 for speeds between 10 m/s and 16 m/s. The Reynolds number is also used to describe the state of a flow, i.e. laminar, transitional or turbulent. A laminar flow is characterized by a low skin friction and smooth and regular pathlines, whereas a turbulent flow has a higher skin friction and more irregular pathlines (Anderson, 1984). However, turbulent flows are characterized by a higher speed near the walls compared to laminar flows: this helps turbulent flows to delay the flow separation compared to laminar flows (Anderson, 1984), thus generally decreasing the pressure drag on the body. In cycling, the pressure drag is the main resistive component of the drag force for most bicycle components and cyclist body parts, therefore its reduction is generally aimed at. This can be achieved on cyclist body parts by forcing the flow to become turbulent through the addition of surface roughness. For example, in the 2017 Tour de France, one cycling team was equipped with a skinsuit where the fabrics on the upper arms had a dimpled surface: these macroscale roughness elements and other vortex generators have shown the capability to reduce the aerodynamic drag of cylinders and cyclists (e.g. Brownlie et al., 2016; Oggiano et al., 2013; Spurkland et al., 2015). Note that cylinders are generally used to investigate the aerodynamics of new fabrics in WT tests since cylinders can be considered as an approximation of the geometry of several cyclist body parts (e.g. Chowdhury et al., 2010; Hoerner, 1965; Oggiano et al., 2007; Shanebrook and Jaszczak, 1976).

Variables like wheel rotation, cadence and cyclist posture (Flanagan, 1996) introduce uncertainties in the measurements and can affect the experiment reproducibility. Another aspect to consider during WT testing are the WT boundaries: the flow is constrained by these boundaries (WT vertical walls and ceiling) that can affect the forces acting on the measured object (ESDU, 1980). These flow boundaries limit the flow expansion thus causing an inner-flow acceleration, as opposed to an open test section where the jet boundary may over-expand causing a lower velocity acting on the cyclist (Crouch et al., 2017). Several corrections have been developed for closed and open-test section WTs to correct this so-called "blockage effect" (Barlow et al., 1999; Cooper, 1998; ESDU, 1980; Maskell, 1963; Mercker, 1986). A general rule of thumb to limit the blockage effect in a closed test section WT is to have a WT cross-section such that the solid blockage is lower than 5%. The solid blockage is given by the ratio between the projected cyclist-bicycle system frontal area and the test section cross-sectional area. In open test section WTs, the blockage correction is smaller and of opposite sign than for closed test section WTs (Barlow et al., 1999). Other types of corrections are needed in open test section WTs and these are needed because of jet expansion, jet deflection, nozzle blockage, collector blockage and horizontal

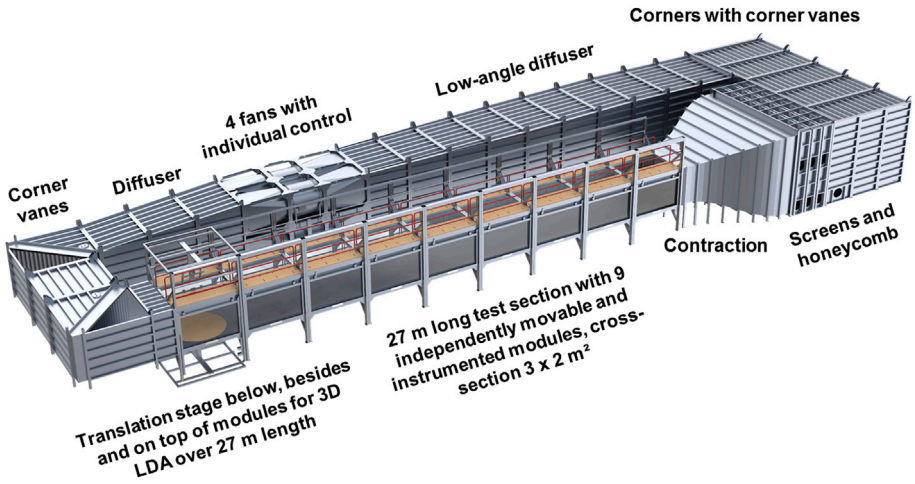

Fig. 10. Closed-circuit wind tunnel with a closed test section at Eindhoven University of Technology in the Netherlands, used also for cycling aerodynamic tests of single riders and time trial teams or sprint trains with multiple riders.

Fig. 11. Wind tunnel tests of a team time trial in the closed-circuit wind tunnel with closed test section at Eindhoven University of Technology in the Netherlands (photo by Bart van Overbeeke; reproduced with permission).

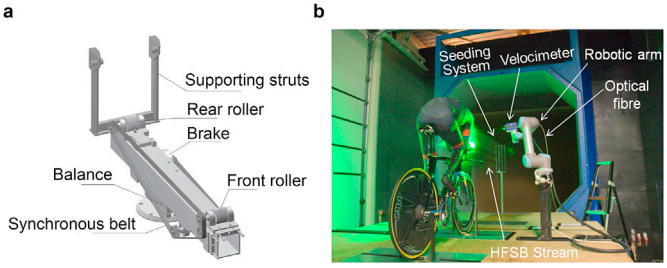

Fig. 12. (a) Force balance used for cycling aerodynamics testing that enables the rotation of the rear wheel and of the front wheel by a belt (source: Gibertini and Grassi, 2008; reproduced with permission from Springer Nature); (b) Particle image velocimetry (PIV) technique used by Jux et al. (2018) in the open jet wind tunnel at Delft University of Technology in the Netherlands (soure: Jux et al., 2018; CC BY 4.0).

buoyancy (Fischer, 2017; Mercker et al., 1997; Mercker and Wiedemann, 1996). However, these corrections are usually smaller than those required in closed test section WTs (Fischer, 2017; Mercker and Wiedemann, 1996).

WT experiments enable the measurement of different quantities related to cycling aerodynamics. Forces and moments are the most commonly measured variables, especially the aerodynamic drag, defined along the cyclist-bicycle direction (body axes). These variables are measured using a force balance, usually placed on or below the WT floor and connected to the bicycle wheel(s) by means of supporting struts (Fig. 12a). This balance can also be placed inside the turntable when this is elevated from the WT floor. This turntable not only facilitates the cyclist rotation and thus the potential reproduction of crosswind conditions, but it also acts as a splitter plate by "cutting" the boundary layer developed on the WT floor when the turntable is elevated from the floor. This flow boundary layer is not present in reality when a cyclist is riding through stagnant air and it may affect the forces acting on the cyclist, therefore its reduction or removal is aimed at during the tests. In vehicle aerodynamics this is sometimes achieved using suction or blowing systems as well as a moving ground plane. To the best of our knowledge, no moving ground plane has yet been used in cycling experiments: the argued reason is that the influence of a moving floor is minimal in cycling as opposed to vehicle aerodynamics, where a large portion of the car body is situated very close to the ground while in cycling only a small part of the bicycle with minimal width, i.e. the wheels, is situated close to the ground. Modern force balance systems also enable the wheels to rotate (Fig. 12a) improving the reproduction of real cyclist conditions where the wheels are rotating and the cyclist is pedaling at a given frequency. Despite being more realistic, the moving configuration reduces the test reproducibility due to the difficulty of a cyclist to keep the same exact position during pedaling and exactly the same pedaling frequency. This could be solved using a movable mannequin (Crouch et al., 2016) although the mannequins geometry especially at joints such as ankles, knees and hips will differ from that in reality. Another option is the use of camera systems to track the position of a real cyclist (Brownlie, 2019).

Other measurements are possible in WT testing, including velocity measurements using probes (Crouch et al., 2014) or optical methods (Chabroux et al., 2010; Barry et al., 2016; Jux et al., 2018; Terra et al., 2018), as shown in Fig. 12b for Particle Image Velocimetry (PIV), pressure measurements (Defraeye et al., 2010a, 2010b) and temperature measurements (Alam et al., 2010). Moreover flow visualization is possible using oil (Brownlie et al., 2009), smoke (Kyle, 1989) or tufts (Kyle, 1990).

Note that wind tunnel tests generally provide only the total drag of the combined cyclist-bicycle system. However, through surface pressure measurements and optical measurements, it is possible to obtain aerodynamic information pertaining to the drag of single components, such as helmets (e.g. Chabroux et al., 2010; Giappino et al., 2018) or body parts (e.g. Terra et al., 2018).

A comprehensive review of the WT testing methodology in cycling aerodynamics is provided in (Brownlie, 2019), where different protocols

for cycling tests in WTs are described and solutions to common testing issues are provided.

3.3.2. Computational fluid dynamics (CFD)

CFD in cycling aerodynamics is based on numerically solving approximate forms of the Navier-Stokes equations, where the two most commonly applied approximate forms are the Reynolds-Averaged Navier-Stokes (RANS) equations and the Large Eddy Simulation (LES) equations. Hybrid approaches, such as Detached Eddy Simulation (DES) and Scale-Adaptive Simulations (SAS), have also been used in cycling simulations (Fintelman et al., 2015; Godo et al., 2010, 2011; Griffith et al., 2014), however steady RANS remains by far the most commonly used approach. This is not only true for cycling aerodynamics but also holds in other fields such as building simulation (Blocken, 2018) and other aerodynamic applications (Casey and Wintergerste, 2000; Hanjalic, 2005). The RANS equations for the isothermal flow of an incompressible, homogeneous, Newtonian and isotropic fluid can be written as:

$$\frac{\partial U_i}{\partial x_i} = 0 \tag{17}$$

$$\frac{\partial U_i}{\partial t} + U_j \cdot \frac{\partial U_i}{\partial x_j} = -\frac{1}{\rho}\frac{\partial P}{\partial x_i} + \frac{1}{\rho}\frac{\partial}{\partial x_j}\left(2\mu S_{ji} - \rho\left(\overline{u_j' u_i'}\right)\right) \tag{18}$$

where U and u' are the time-averaged velocity and the velocity fluctuation, respectively, which together constitute the instantaneous velocity. ρ is the density, P the time-averaged pressure and S_{ji} the time-averaged strain-rate tensor. These equations are very similar to the original instantaneous Navier-Stokes equations, with the difference that averaged rather than instantaneous quantities are considered and that additional terms are present which are the elements of the Reynolds stress tensor, $\rho(\overline{u_j' u_i'})$. These terms represent the influence of the turbulence on the mean flow. However, it adds six unknowns to the problem which now has more unknowns than equations, rendering the system underdetermined: this is known as the closure problem of the RANS equations. Several so-called turbulence models have been proposed to close them and many of these models have been used and compared in cycling and para-cycling aerodynamics studies (Defraeye et al., 2010a; Fintelman et al., 2015; Malizia et al., 2019; Mannion et al., 2018c, 2019a).

Assessing the accuracy and reliability of a CFD simulation is an essential step in the CFD simulation process. It entails identifying, quantifying and reducing errors and uncertainties of CFD simulations by (solution) verification and by validation of the results by comparison with accurate experimental data. Two types of verification exist: code verification and solution verification (Franke et al., 2007; Oberkampf et al., 2004; Roy, 2005). Code verification is often performed by code developers and deals with the correctness and reliability of the code. Solution verification, or numerical error estimation (Oberkampf et al., 2004), is the process of quantification of the numerical errors, and includes round-off errors, iterative convergence errors and spatial and temporal discretization errors (Roy, 2005). Since the latter errors can be different for every type of simulation, solution verification needs to be performed for each simulation that is significantly different from others (AIAA, 1998; Roy, 2005). Validation is the process of quantifying the accuracy of the CFD simulation through comparisons with experimental data (Oberkampf et al., 2004; Roy, 2005) thus connected with the physics of the problem (Roy, 2005). The uncertainties in the computational simulation are indeed connected to the capability of the computational model to reproduce the reality (Casey and Wintergerste, 2000): some of these uncertainties derive from the turbulence modeling, the lack of knowledge of exact boundary conditions and/or geometry simplifications (Casey and Wintergerste, 2000). Procedures to quantify and reduce errors and uncertainties are provided by several CFD best practice guidelines for outdoor flows in the urban environment (Blocken, 2015; Blocken and Gualtieri, 2012; Franke et al., 2010, 2007; Tominaga et al., 2008), automotive external aerodynamics (Lanfrit, 2005), environmental modeling (Jakeman et al., 2006) and in general for industrial applications (Casey and Wintergerste, 2000).

As opposed to experimental methods, CFD simulations offer the advantage of providing so-called whole-flow field data (e.g. Blocken, 2014, 2015), i.e. the relevant parameters in the entire computational domain. As an example, Fig. 13a shows the phase-averaged streamwise vorticity contours in the vertical centerplane while Fig. 13b shows mean velocity streamlines around four cyclist bodies in a team pursuit. Moreover, forces and moments can be decomposed in each cyclist and bicycle zone, both in terms of viscous and pressure force components. For example, Defraeye et al. (2011) provided the drag values for the different cyclist body parts and Malizia and Blocken (2020) provided the drag of the different components that constitute a bicycle wheel. Finally, CFD simulations do not suffer by similarity constraints and blockage problems because they can be performed at full scale and in a computational domain that the user can easily select such that the blockage ratio is well below 5%.

3.3.3. Field tests

In field tests, relevant variables are measured in real time while a cyclist or a group of cyclists is riding. The measured quantities can be the oxygen consumption, $\dot{V}_{O_2}$, the power exerted by the cyclist, and/or the velocity. Subsequently, mathematical models can be used to infer the aerodynamic drag from the measured variables. Debraux et al. (2011) provided a complete review of these methods together with methodologies to assess the cyclist frontal area. Some of these methods are also briefly discussed here.

In coast down tests, a horizontal path is split in two zones: in the first zone the cyclist is accelerating from rest to a target speed; in the second zone the cyclist stops pedaling and the bicycle decelerates. In the latter, several infrared sensors are placed at known distances and used as timing switches (Tengattini and Bigazzi, 2018), see Fig. 14. To better reproduce

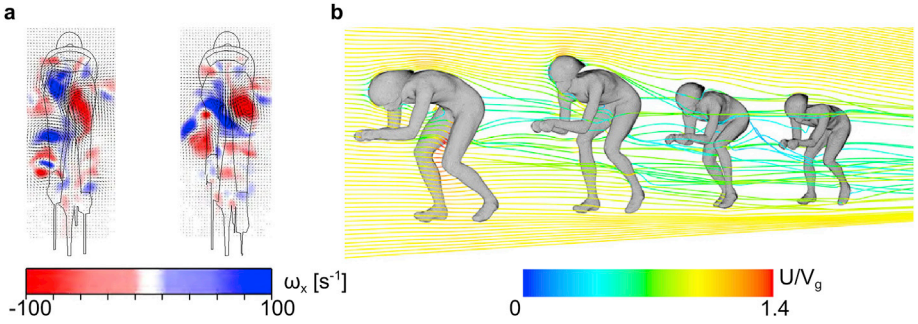

Fig. 13. (a) Phase-averaged streamwise vorticity contours in a vertical centerplane located 0.60 m downstream of the rear of the cyclist for two crank angles (source: Griffith et al., 2019; reproduced with permission); (b) Velocity colored mean streamlines for a four-cyclist team pursuit (adapted from Defraeye et al., 2014; reproduced with permission from the American Society of Mechanical Engineers - ASME).

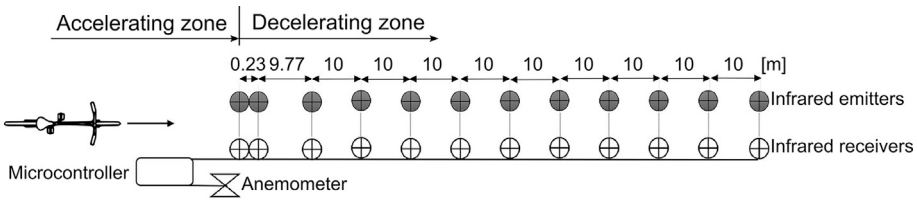

Fig. 14. Coast down test setup (adapted from Tengattini and Bigazzi, 2018; reproduced with permission from the American Society of Civil Engineers - ASCE). Units in [m].

real cycling conditions, the cyclist can keep pedaling in the second or measuring zone, however no thrust should be provided to the bicycle (Candau et al., 1999). From the relation between velocity and time, the drag area and the rolling resistance can be calculated as done for instance by Kyle (1979), Burns and Sullivan (1995), Candau et al. (1999) and Tengattini and Bigazzi (2018). Moreover, Burns and Sullivan (1995) and Kyle and Burke (1984) compared the results obtained by coast down tests with WT results and they generally found the drag force during the field tests to be larger, with Burns and Sullivan (1995) finding a better agreement for an upright position than for a more aerodynamic position using aero-bars. Kyle and Burke (1984) provided a few reasons for the larger values measured during the field tests: during the WT tests the wheels were kept static thus no contribution of the rotational drag due to the wheel rotation and rolling resistance could be measured, and the rider's position could have been slightly different in the two methods.

Note that a recent study proposed a different mathematical model to be used for the coast down tests, where drag and rolling resistance coefficients are also function of the speed (Baldissera, 2017). Previously, also Kyle (1988a, 2002) included an additional velocity dependent term for the rolling resistance, which was equal to $N \cdot C_{rr,2} \cdot V_g$, where N is the number of wheels and $C_{rr,2}$ the second rolling resistance coefficient. Kyle (1988a, 2002) reported a $C_{rr,2}$ measurement for a 17 inch (~0.43 m) wheel diameter by means of drum tests. It was found that $C_{rr,2}$ was equal to 0.0502 N s/m for the only wheel tested.

Linear regression is another method used during field tests, and it is based on the simultaneous measurement of power and velocity. Martin et al. (1998) applied the mathematical model described in Subsection 3.1, for 38 road cycling tests where the power was measured by a SRM power meter. They compared the measured power with the model predicted power and they obtained a $R^2 = 0.97$ between the two power values. Similar linear regression methods were used by Grappe et al. (1997) using a different power meter, the Max One. Moreover, Gibertini et al. (2010) and Belloli et al. (2014) compared the WT results with field tests both for a regular bicycle and for a Paralympic handcycle. Similar to Martin et al. (1998), Belloli et al. (2014) found large noise in instantaneous results of power and velocity, however after averaging the results for an entire lap of a track circuit, a good agreement was found with the WT tests. Gibertini et al. (2010) compared the aerodynamics and the comfort of three different positions for six cyclists. The field test results, provided as a ranking of the three positions for each cyclist, confirmed the WT results in terms of the best aerodynamic position for each cyclist. However, no quantitative results were provided, rendering any further conclusion about differences between the two different methods impossible. As opposed to WT tests and CFD simulations, field tests enable an evaluation of the cyclist's comfort and his/her biomechanical efficiency. Combined studies between cyclist aerodynamics and cyclist biomechanics were also done by Schade et al. (2016).

Aerodynamic drag can also be assessed towing a rider with a cable connected to a car (di Prampero et al., 1979; Dal Monte et al., 1983; Capelli et al., 1993), coasting down hills of known slope, where an equilibrium velocity is reached when forces due to aerodynamic and rolling resistance balance the acceleration given by the descent (described in Kyle and Burke, 1984); or by measuring the oxygen consumption of the cyclist while riding (Pugh, 1974; McCole et al., 1990; Hagberg and McCole, 1990).

Contrarily to WT tests and CFD simulations, the wind direction and magnitude cannot be controlled during field tests: the inherent variability and uncontrollable nature of the real meteorological boundary conditions represents one of the biggest limitations of this methodology. Even when testing inside indoor velodromes, the air speed, direction and turbulence intensity depend on the cyclist location along the track, i.e. if in the straight or corner sections (Fitzgerald et al., 2019). Furthermore, additional modifications to the airflow seen by the cyclist occur due to the presence of other cyclists, i.e. for multiple cyclists on a track, and by the cycle cadence (Fitzgerald et al., 2019).

More recently, large-scale stereoscopic PIV, generally used for WT measurements, has also been used to measure the aerodynamic drag and to obtain flow field visualizations for actual indoor and outdoor field tests (Spoelstra et al., 2019).

4. Bicycle aerodynamics

The bicycle is responsible for about 18–40% of the combined cyclist-bicycle system aerodynamic drag, depending on the cyclist position (Defraeye et al., 2010b; Kyle and Burke, 1984; Nonweiler, 1956). The bicycle consists of several components including frame, wheels and handlebar. The aerodynamic aspects of these main components are described in the following subsections, together with a last subsection focused on smaller but not unimportant components such as fork and cables.

4.1. Frame and tubes

4.1.1. Early developments (1890 – early 1970s)

Nowadays racing bicycles generally have a diamond-shaped frame. This type of frame was first introduced by Humber in 1890 (Sharp, 1896; Kyle and Weaver, 2004) (Fig. 15a) and used for the world hour record bicycles of Merckx in 1972 (Fig. 15b), of Moser in 1984 (Fig. 15c) and that of Campenaerts in 2019 (Fig. 15d). However, Moser's bicycle had a frame with curved tubes and a front wheel smaller than the rear wheel, whereas the bicycle of Campenaerts had a frame with different tube cross-sectional shapes compared to the previous two bicycles, i.e. circular for the bicycles of Merckx and Moser whereas streamlined for the bicycle of Campenaerts. Despite the fact that these bicycles kept a similar diamond-shaped frame for more than one century, successful and radical attempts to improve bicycle aerodynamics by changing the frame have been made, both at the end of 19th century and more recently. The first two aerodynamic improvements in bicycle frames were the recumbent bicycle and the streamlined enclosures for bicycles.

The recumbent or laid-back bicycle was first introduced by Charles Challand in 1895 (Hadland and Lessing, 2014; von Salvisberg, 1897; Wilson, 2004) (Fig. 16a). The crank was placed in front of the cyclist who as a result could ride in a more comfortable position. The potential of this bicycle was only recognized in 1932 when a second-category track cyclist, Francis Faure (Schmitz, 1990) started riding the recumbent bicycle designed by Charles Mochet and won several races. Fig. 16b shows Faure at the start of a race against other riders with regular racing bicycles. Faure on his recumbent bicycle had a much lower frontal area and therefore a substantial aerodynamic advantage (Wilson, 2004). Faure's greatest achievement was the world hour record in 1933 with a distance of 45,055 m, overcoming the previous 1914 record by Oscar Egg who

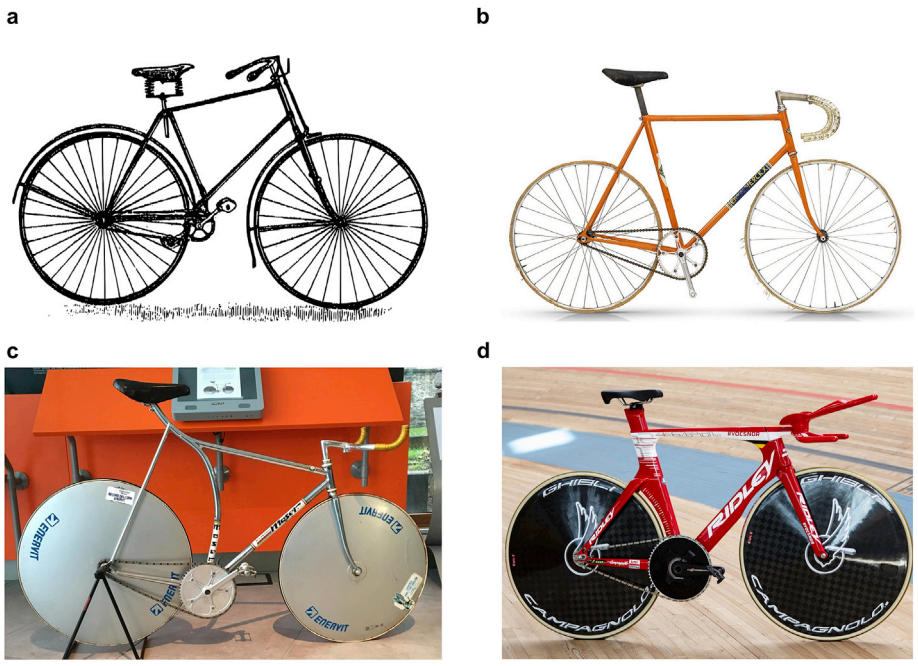

Fig. 15. (a) Humber's bicycle with diamond frame, built in 1890 (source: Sharp, 1896); (b) Bicycle of Merckx used for the world hour record in 1972 (reproduced with permission from Colnago); (c) Bicycle of Moser used for the world hour record in 1984 (reproduced with permission from Museo del Ciclismo Madonna del Ghisallo); (d) Bicycle of Campenaerts used for the world hour record in 2019 (reproduced with permission from Ridley).

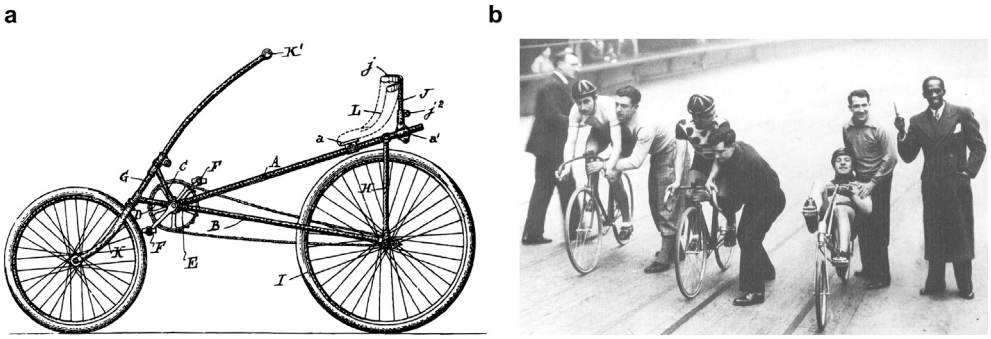

Fig. 16. (a) Challand recumbent bicycle, Swiss patent 11,429 (source: Hadland and Lessing, 2014). (b) Faure racing on Mochet's recumbent bicycle in 1934 (source: Schmitz, 2000).

attained 44,247 m in 1 h. However, in 1934 a new set of rules by the Union Cycliste Internationale (UCI), the world governing body of cycling, excluded both the recumbent bicycle and the associated record: the Mochet's recumbent was no longer recognized as a bicycle and Faure's record was moved to the category "special records set by machines without aerodynamic devices and propelled by human power" (Schmitz, 1990).

The first streamlined enclosures for bicycles were patented in 1913 by Bunau-Varilla (Schmitz, 1990) with British patent number 22,510 (Kyle, 2001). The combined bicycle and streamlined shell by Bunau-Varilla was known as Velo Torpille (Fig. 17a). The time trialist Marcel Berthet, who was competing against Oscar Egg for the world hour record, tested the Velo Torpille and successfully managed to break several records. In 1913 Berthet rode the 5 km on the Paris Vel D'Hiv indoor track in 5′39″3, thus achieving an average speed of 53.1 km/h, which is about 6 km/h faster than he could achieve on a standard racing bicycle of his time (Hadland and Lessing, 2014; Schmitz, 1990). However, in 1914 the UCI prohibited the use of any external aerodynamic devices (Schmitz, 1990).

The Velo Torpille was not the only streamlined device developed in those years. Other examples were the Coupe Vent in 1893, the Velo Fusée by Oscar Egg in 1932 (Fig. 17b); the Velodyne built by Marcel Riffard and driven by Marcel Berthet in 1933 (Fig. 17c) and the Velocar built by Georges Mochet, son of Charles, and driven by Francis Faure in 1939 (Fig. 17d). The latter two vehicles were a racing bicycle equipped with a streamlined enclosure and a recumbent bicycle equipped with a streamlined enclosure, respectively. Both were employed to break the world hour record, despite the fact that they were not officially recognized by the UCI (Schmitz, 2000). Berthet, 45 years old in 1933, drove the Velodyne up to a distance of 49,922 m in 1 h at sea level (altitude of about 160 m), about 500 m more than the distance traveled by Eddy Merckx in 1972 on a diamond-frame racing bicycle (Fig. 15b) at high altitude (about 2,300 m). Faure drove the Velocar up to 50,537 m in 1939 at sea level (about 30 m), being the first man to drive a two-wheel vehicle propelled by human power over 50 km in 1 h. Only in 1984 did Francesco Moser manage to break this record (51,151 m) at high altitude (about 2,300 m) using an aerodynamically optimized bicycle (Fig. 15c). A more detailed description of these recumbent and streamlined vehicles can be found in the literature (Abbott and Wilson, 1995; Hadland and Lessing, 2014; Kyle and Bassett, 2002; Kyle and Weaver, 2004; Schmitz, 2000, 1990; Wilson, 2004).

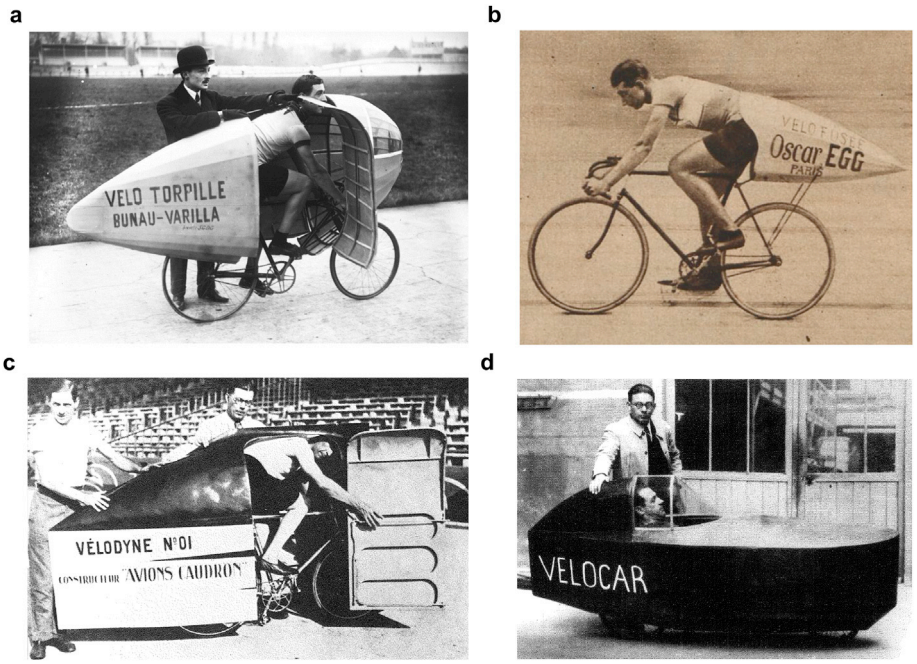

Fig. 17. (a) Velo Torpille by Bunau-Varilla and driven by Marcel Berthet in 1913 (reproduced with permission from "gallica.bnf.fr/BnF"); (b) Velo Fusée by Oscar Egg (1932) (source: "Le Miroir des sports", October 1920; reproduced with permission from "gallica.bnf.fr/BnF"); (c) Velodyne by Marcel Riffard and driven by Marcel Berthet in 1933 (source: Schmitz, 1990); (d) Velocar built by Georges Mochet and driven by Francis Faure in 1939 (source: Schmitz, 1990).

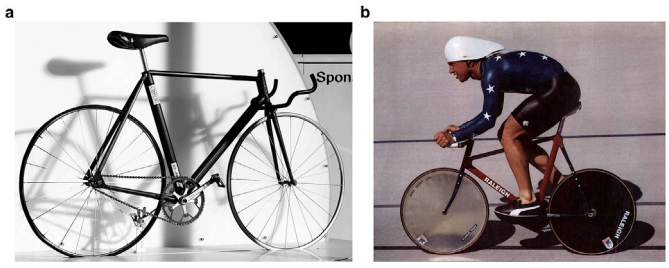

Fig. 18. (a) Maier Moussa carbon fiber bicycle with oval shape tubes, 1976 (reproduced with permission from Assos); (b) Elongated tubes on the 1984 time-trial pursuit "funny bicycle" (source: Kyle, 1986b). In this picture Steve Hegg was testing a pair of aerodynamic shoes on the bicycle (Kyle, 1986b).

4.1.2. Streamlined tubes and monocoque frames (late 1970s–1990s)

Apart from the above-mentioned exceptional examples, the bicycle frame in 1972 had remained almost unchanged compared to that at the beginning of the 20th century. Only in late 1970s, airfoil-shaped tubes started to be used for time-trial (TT) bicycle frames (Kyle, 1995a). As an example, Toni Maier Moussa used oval-shaped tubes (Kyle and Burke, 1984) for his carbon-fiber bicycle (Fig. 18a). In 1978, this bicycle was used during the track world championship by Daniel Gisiger, together with the first Lycra skinsuit. However, the 1984 world hour record by Moser was still achieved on a bicycle with a diamond frame and round tubes (Hinault and Genzling, 1988) (Fig. 15c). This frame was built with the purpose of allocating wheels of different sizes to obtain a lower frontal area, and for transferring more weight to the rear wheel: smaller wheels have a higher rolling resistance (Kyle, 2002) and therefore a frame able to transfer weight to the larger rear wheel was needed to achieve an optimal trade-off between drag reduction and low rolling resistance (Dal Monte et al., 1987). The practice of a smaller front wheel was already common in paced and motor-paced races where a smaller front wheel allowed the trailing cyclist to be closer to the pacer. Moreover, in the 1970s, bicycles of the former Eastern European countries already had a smaller front wheel and a sloping top tube to reduce the distance between the cyclists (Hinault and Genzling, 1988) thus achieving better drafting. Kyle (2002) reported WT and coast down test results confirming that drafting riders behind a leading rider reduced their drag by an additional 5% when they rode a bicycle with 24 inch (≈610 mm) wheels rather than with 27 inch (≈686 mm) wheels.

Two WT studies specifically focused on bicycle tubing (Kyle and Burke, 1984; Zdravkovich, 1992). Kyle and Burke (1984) tested three bicycles with tubes of different shapes: a "standard" track bicycle with rounded tubes and two "aero-bicycles" with teardrop shaped tubes of chord-to-width ratio 1.6 and 2.4 (Kyle, 1986a). The tests were performed as part of the design of the so-called "funny bicycles" used by the USA team in the 1984 Los Angeles Olympic Games (Fig. 18b). These bicycles were named "funny bicycles" because of their shape (Abbott and Wilson, 1995; Boardman, 2015): they had different combinations of disc wheel sizes with the smallest diameter down to 570 mm for the front wheel and 670 mm for the rear wheel, airfoil-shaped tubes, cowhorn airfoil-shaped handlebar and disc sprockets (Kyle, 2001). The WT tests were all performed at 48 km/h. Three different yaw angles (0°, 10°, 20°) were investigated for the standard track bicycle with rounded tube and for the aero-bicycle with 2.4 chord-to-width ratio tubes while only the 0° yaw angle was investigated for the aero-bicycle with the tubes with chord-to-width ratio 1.6. The bicycle equipped with the more elongated tubes (2.4) showed the best results in all conditions analyzed: the drag reduction was 41.4% for the isolated bicycle and 4.3% for the combined cyclist-bicycle system, compared to the standard track bicycle. When crosswind was considered, the drag reduction of the cyclist-bicycle system with the 2.4 ratio tubes further increased: −11.2% at 10° and −10.3% at 20° yaw angle (Kyle and Burke, 1984).

Zdravkovich (1992) applied splitter plates, i.e. plates with a small thickness, in the attempt to reduce drag on isolated wheels (see Subsection 4.2) and on a bicycle frame by suppressing the vortex shedding from these components. The test bicycle included the bicycle frame however without saddle, seat post and wheels due to limited WT test section size. The splitter plate length was defined based on the tube diameter, therefore splitter plates of different length were applied on tubes of different sizes while keeping the ratio between the splitter plate length and the tube diameter constant. The splitter plates were placed

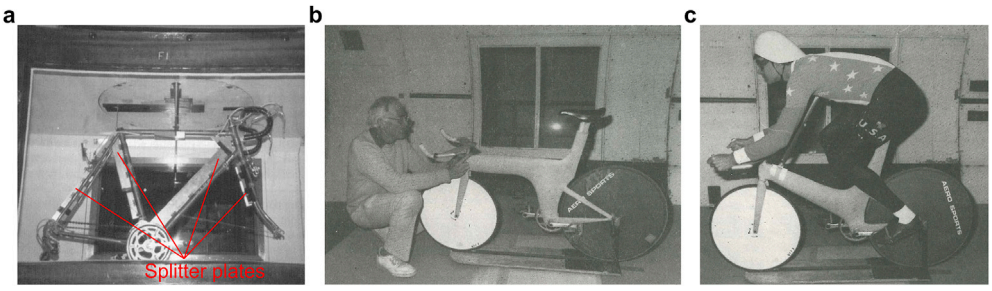

Fig. 19. (a) Bicycle equipped with splitter plates (source: Zdravkovich, 1992; reproduced with permission from Elsevier); (b) Monocoque bicycle with S-shape (source: Kyle, 1991b); (c) Monocoque bicycle with V-shape (source: Kyle, 1991b).

downstream to all tubes while no splitter plates were used on the handlebar and the top tube (Fig. 19a). The frame equipped with splitter plates had only a 4% drag reduction compared to the frame without splitter plates. Zdravkovich (1992) expected larger drag reduction, given that splitter plates were able to reduce the drag force of even 17% on isolated cylinders (Apelt et al., 1975, reported in Zdravkovich, 1992). This drag reduction was due to the vortex shedding suppression caused by the splitter plates placed in the leeward direction of a cylinder (Apelt et al., 1975; Zdravkovich, 1992). The frame was also tested without handlebar, concluding that this component contributed about 10% of the aerodynamic drag of the isolated frame. Moreover, Zdravkovich (1992) reported that the drag coefficient of the frame was Reynolds number independent between speeds of 20 km/h and 42 km/h.

Other studies compared bicycles with different frames, as done by Hagberg and McCole (1990) and McCole et al. (1990) who measured the oxygen consumption of 28 cyclists riding alone on a circuit at 40 km/h using a racing and an aerodynamic "funny bicycle", equipped with cowhorn handlebars, a 24 inch (≈610 mm) front wheel and a 28 inch (≈711 mm) rear disc wheel. Using the latter bicycle, the oxygen consumption decreased by 7 ± 4%. The uncertainty of 4% was not further detailed.

Kyle (1991b) reported WT tests performed between 1986 and 1990 on 20 bicycles either isolated or with a rider. These bicycles belonged to five different categories: road, TT, team pursuit, individual pursuit and triathlon bicycles. They reported a different repeatability of the experiments: "±0.13 N" and "±0.44 N" for the isolated bicycles and the cyclist-bicycle combinations, respectively. The lesser repeatability for tests with cyclists was explained by the difficulty to precisely reproduce the cyclist posture in every experiment. In all bicycle categories, the use of streamlined tubes produced lower drag. Moreover two individual bicycle pursuit prototypes with a monocoque or single-shell frame were tested in 1986 (Kyle, 1991b): one with an S shape (Fig. 19b) and one with a V shape (Fig. 19c). The tubing cross-section in both frames had an airfoil shape (NACA 0020) with a chord-to-width ratio of 5 to 1 in most of

Fig. 20. (a) Chris Boardman monocoque bicycle used in 1992 (reproduced with permission from "Paul Hudson/Flickr"); (b) Obree's world hour record bicycle in 1993 (reproduced with permission from Maximise Sport); (c) Chris Boardman's world hour record bicycle used in 1993 (reproduced with permission from "Paul O'Garra/Flickr"); (d) Miguel Indurain's world hour record bicycle in 1994 (source: Cicli Pinarello Spa, 2015); (e) Tony Rominger's world hour record bicycle in 1994 (reproduced with permission from Colnago); (f) Chris Boardman's world hour record bicycle in 1996 (reproduced with permission from "David Racklever/Flickr").

the frames and a minimum chord-to-width ratio of 3.5 to 1. Tests on the isolated monocoque bicycles gave a 16.7% drag reduction compared to the best aerodynamic bicycle with diamond frame. However, WT tests on combined cyclist and monocoque bicycles did not show any aerodynamic advantages of these bicycles compared to aerodynamic bicycles with diamond frame. Kyle (1991b) gave two explanations for this counter-intuitive finding: the difficulty to properly set the arms of the cyclist on these monocoque bicycles and the flow interaction in the area close to the legs and the frame. Developments of monocoque frame bicycles paused for few years after having been declared illegal by UCI in 1986 (Kyle, 2001), but they were resumed after monocoque bicycles had been readmitted in 1991 (Kyle, 2001). After their readmission in 1991, monocoque frames started to be studied and employed in races again. Hill (1993) and Burrows and Hadland (2008) described the monocoque frame bicycle (Fig. 20a) used by Chris Boardman to win the gold medal in the 4000 m individual pursuit of the Barcelona 1992 Olympic Games. This monocoque bicycle also had a single mono-blade supporting the front wheel (Fig. 20a), similar to the ones used in jet landing gears. WT tests on the isolated bicycle showed that this prototype with monocoque frame had 30% less drag than a conventional diamond-frame pursuit bicycle. However a 6.6% drag increase was measured compared to a conventional pursuit bicycle when the cyclist was included in the WT test, similar to the results described by Kyle (1991b). Hill (1993) however found that the drag increase was due to the handlebar configuration which influenced the cyclist posture: a cyclist should place himself or herself differently on a monocoque bicycle than on a conventional pursuit bicycle to minimize the aerodynamic drag. On a conventional bicycle the cyclist should use a very compact position to limit the airflow over the upper half of the bicycle, whereas on a monocoque bicycle the cyclist should position both arms so that the air can flow over the bicycle to exploit the low aerodynamic drag of the monocoque frame. With the monocoque optimized position, a 12% drag reduction was achieved compared to a conventional cyclist-bicycle combination. This bicycle was further developed by adding a nose in front of the headset and a foot in front of the bottom bracket (Fig. 20a), with the aim of smoothly directing the flow around the blunt shapes of the headset and the bottom bracket. These additions increased the drag reduction of the cyclist-bicycle system further up to 16% compared to a conventional cyclist-bicycle combination.

4.1.3. *Towards full integration of aerodynamics (1990s - 2020)*

By 1992, aerodynamics were fully integrated in bicycle designs. Not only monocoque bicycles were available, but also aerodynamic wheels (see Subsection 4.2), aero-bars (see Subsection 4.3) and other small components were developed taking aerodynamics into account (see Subsection 4.4). Graeme Obree introduced two new positions, nicknamed “tucked” and “superman”, which effectively reduced the aerodynamic drag. For details and pictures about these two positions see Subsection 4.3. Moreover, Obree’s bicycle, named “Old Faithful”, was self-built and did not follow the classical diamond-frame (Fig. 20b): a single oblique tube replaced the top and down tube, likely reducing the aerodynamic drag due to the reduction of the number of bicycle components. This aerodynamic development, together with advances in training techniques, physiology and nutrition (Kyle and Bassett, 2002), laid the foundation for the subsequent series of world hour records, which represented the most rapid increase since the introduction of the safety bicycle (Kyle and Bassett, 2002): more than 5 km in less than three years, see Fig. 21. The records are mentioned here in chronological order: (17/07/1993-51,596 m) Graeme Obree using his tucked position, aerodynamic wheels and self-built bicycle, Fig. 20b; (23/07/1993-52,270 m) Chris Boardman using a diamond-shaped monocoque bicycle with aero-bars and four-spoke wheels, Fig. 20c; (27/04/1994-52,713 m) Obree with the same bicycle and rider position as before; (02/09/1994-53,040 m) Miguel Indurain on a monocoque bicycle, aero-bars and disc wheels, Fig. 20d; (22/10/1994-53,832 m) Tony Rominger on a diamond-frame track bicycle, disc wheels and

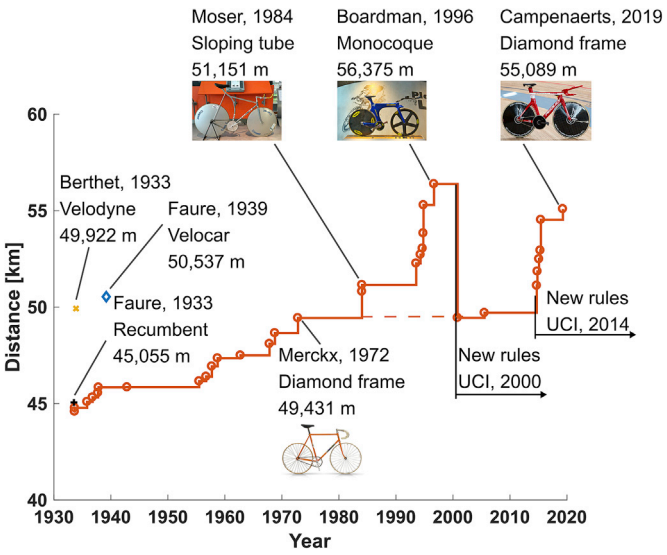

Fig. 21. World hour record from 1933. Several records where a special frame was used are highlighted (photos reproduced with permission from Museo del Ciclismo Madonna del Ghisallo; Colnago; “David Racklever/Flickr”; Ridley).

aero-bars, Fig. 20e; (05/11/1994-55,291 m) Tony Rominger with the same bicycle and rider position as before; (06/09/1996-56,375 m) Chris Boardman on a monocoque bicycle with five-spoke front wheel, disc rear wheel and extra-elongated tri-bars that enabled him to use the superman position used first by Obree, Fig. 20f. However, in 2000 the UCI created a new set of rules aimed at preventing the use of aerodynamic devices in cycling: only diamond-shaped frames, round frame-tubes, dropped handlebar, front and rear wheels with same diameter, wheels with 16–32 spokes and shallow-rim, and a bicycle minimum weight of 6.8 kg were allowed for world hour record attempts (Kyle and Bassett, 2002). Moreover, cyclists had to wear safety helmets without any aerodynamic features. As a result, the world hour record bicycle should look similar to the 1972 Merckx bicycle (Fig. 15b). On the other hand, more freedom was left for TT competitions, where disc wheels, aero-bars with limited length, aerodynamically shaped frame-tubes with a maximum chord-to-width ratio of 3 to 1 and aerodynamic helmets could still be used (Kyle and Bassett, 2002).

Between 1996 and 2000, other studies were performed on monocoque bicycles. Thompson (1998) described the design of the Australian “superbike”, a bicycle with a monocoque frame. The aerodynamic development was made by WT tests. The author reported the difficulty in obtaining accurate and repeatable tests using real riders. Therefore, first the athletes were replaced by a pair of lightweight polystyrene foam moving legs, and later also trunk, arms and head were included in the tests (Thompson, 2013). An electrical motor beneath the WT was responsible for the rotation of the rear wheel and through a belt the front wheel was also rotated. Comparing the power needed to ride at 55 km/h with the diamond frame bicycle used by the Australian national team in 1992 versus the 1996 “superbike” with a monocoque frame, a power reduction of about 15% was obtained for the latter.

Another aspect of the bicycle frame investigated in those years was the lateral spacing between the cyclist’s feet and the frame. Parker et al. (1996) performed WT tests of a track bicycle with a diamond frame, either without any enclosure covering the empty space between the tubes forming the diamond frame or with a cover between these tubes. Only a dummy cyclist lower half (feet, legs and pelvis) was included in the tests. Results show that for the open diamond frame bicycle, reducing the spacing between the feet from 8.25 in (21.0 cm) to the standard spacing of 4.25 in (10.8 cm) and beyond to 1.25 in (3.2 cm) always reduce the aerodynamic drag: a 1.1 N drag decrease was measured between the feet spacing of 4.25 in (10.8 cm) and 1.25 in (3.2 cm). Contrarily, the tests

using the covered diamond frame showed a drag decrease from the widest feet distance (8.25 in, 21.0 cm) to the standard distance (4.25 in, 10.8 cm) but a 0.4 N drag increase when the feet spacing was further reduced to 2.75 in (7.0 cm) followed by a drag decrease for the lowest spacing tested (1.25 in, 3.2 cm). The results show a clear interaction between the frame shape and the cyclist legs, which can also be used to design narrower bottom brackets. Note that the UCI rules now forbid the use of frame shapes other than diamond frames.

Despite the UCI restriction concerning frame shape and tube shape, with maximum chord to width ratio to 3 to 1, frame profiles kept being studied by bicycle companies but the results were generally not published and if they were, these studies had often not been subjected to rigorous peer review. An example is the 2010 report written by an American bicycle manufacturing company (Harder et al., 2010), where different isolated profiles, including truncated airfoils, were tested by means of both WT tests and CFD simulations to find the best profile to be applied on their bicycles.

More recently, in 2014, the UCI relaxed some of the aerodynamic limitations for the world hour record, raising new interest in this type of competition. The world hour record of Campenaerts in 2019 (55,089 m), was performed using an aerodynamic bicycle, aero-bars and aerodynamic wheels, see Fig. 15d.

4.2. Wheels

The first "aerodynamic" wheels appeared already in the 1890s, however, their use was scarce and since that time, no further evolution in the aerodynamic design of wheels had been recorded for a century. Only from 1984, new generations of aerodynamic wheels were designed. These wheels are described in Subsection 4.2.1. Next, the state-of-the-art of wheel aerodynamics is presented, where first WT test results are addressed (Subsection 4.2.2), next the issues in comparing different WT studies are highlighted (Subsection 4.2.3), and finally the results from CFD studies are outlined (Subsection 4.2.4).

4.2.1. Wheel types and general performance

The first "aerodynamic" wheel was a disc wheel, patented in 1892 by Arthur Comings Hide (Hide, 1892). This patent did not include claims about aerodynamic advantages, nevertheless the book by Sharp (1896) reports claims about a lower air resistance associated with these wheels. Hide also built a safety bicycle with a rear disc wheel and a four-spoke front wheel (Fig. 22a): these wheels were quite similar to the ones used in modern track bicycles (Fig. 20c in Subsection 4.1). Hide's design did not realize a breakthrough in cycling at the time and only little information about disc wheel use can be found in the literature. However, Schmitz (1990, 2000) and Abbott and Wilson (1995) reported and showed that these disc wheels were mounted in bicycles with streamlined enclosures in 1913 and 1914. One reason for the scarce use of these wheels could be their poor stability in crosswind conditions, especially when used as front wheels (Abbott and Wilson, 1995). This instability was recently confirmed by several authors (Edwards, 1986, as reported in Kyle, 1995a; Greenwell et al., 1995) who found that the pressure center of a disc wheel is located about 0.25 times the diameter in front of the wheel axle, hence the side force can cause substantial instability for these wheels when strong crosswinds are present. On the other hand, the center of pressure of spoked and tri-spoke wheels is about 0.13 times the diameter ahead of the wheel axle (Greenwell et al., 1995). As a result, given the same side force, the steering moment is only about half that of a disc wheel. In addition, the lower side force on spoked wheels than disc wheels also adds to a lower steering moment (Godo et al., 2010; Greenwell et al., 1995).

Disc wheels became popular only from 1984, after Moser established two world hour records using a bicycle developed by means of WT tests (Dal Monte et al., 1987) and equipped with lenticular wheels. These wheels were designed to have a streamlined shape using two convex shells, as in Figs. 15c and 22b (Dal Monte, 1988). In a recent interview, Dal Monte stated that this shape was inspired by the radar used in Awacs aircrafts (Crosetti, 2014). Dal Monte et al. (1987) reported tests of Moser himself in a WT on a bicycle equipped with both conventional spoked wheels and with lenticular wheels. During these tests the wind speed was fixed to 14 m/s and the wheels were kept static. Dal Monte et al. (1987) systematically tested different skinsuits, helmets and bicycle components, like lenticular wheels, aerodynamic crank, streamlined shoes and pedals, to optimize the aerodynamic drag of the combined cyclist-bicycle system. Moreover, the bicycle was equipped with a smaller front than rear wheel (660 mm and 711 mm diameter, respectively), since towing tests had previously indicated that this configuration was more aerodynamically advantageous (Dal Monte et al., 1983, reported in Dal Monte et al., 1987). However no quantitative results were provided about this drag reduction. Note that recent tests found a larger drag when the same cyclist-bicycle system was tested with rotating rather than static wheels and moving legs, from ≈6% higher (Crouch et al., 2017) to ≈30% higher (García-López et al., 2008). The moving legs and the rotating wheels are the causes for the larger measured drag. In particular, Kyle (1991c, 2002) measured 15%–30% higher drag for an isolated rotating wheel compared to an isolated static wheel.

The four-spoke wheels designed for the first time by Hide around in 1896 (Fig. 22a), were reinvented in the late 1980s. The reason to develop wheels with large and few spokes was to find a trade-off between aerodynamics and stability due to crosswind, the latter being a main issue for disc wheels. A tri-spoke wheel (Fig. 22c) patent was filed in 1988 (Hopkins and Principe, 1988) and WT tests reported in 1990 (Hopkins et al., 1990; Kyle, 1990). These tests showed a small drag difference, within the experimental error, between the new designed tri-spoke wheel

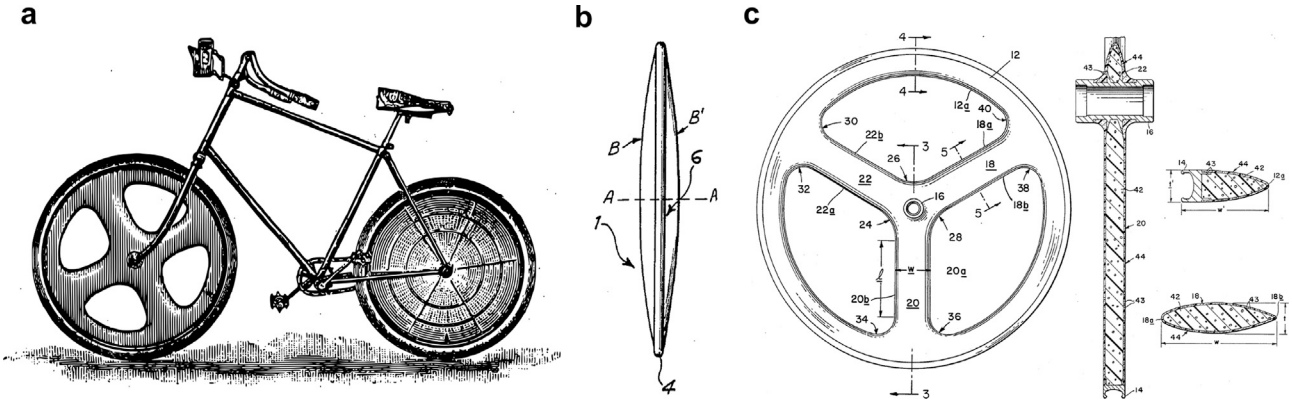

Fig. 22. (a) Safety bicycle with four-spoke front wheel and disc rear wheel, built by Hide (source: Sharp, 1896); (b) Lenticular wheel designed in 1984 (source: Dal Monte, 1988); (c) Tri-spoke wheel patent filed in 1988 (source: Hopkins and Principe, 1988).

and a lenticular wheel for both 0° and 10° yaw angle. At 10° yaw angle, both aerodynamic wheels had about 65%–75% lower drag than at 0° yaw angle. This behavior is called the "sail-effect", and it is caused by the generation of a lift force with a component parallel to the direction of motion. Compared to a full disc wheel, this tri-spoke wheel had only half of the disc wheel lateral surface area (Hopkins et al., 1990).

4.2.2. Wind tunnel studies

With the raised awareness of the importance of aerodynamics in cycling following Moser's world hour record (Hinault and Genzling, 1988) and contemporary WT tests of Kyle and Burke (1984) to optimize the aerodynamics of the cyclist-bicycle combination for the 1984 Olympic Games, the number of aerodynamic tests on bicycle wheels increased in those years. WT tests were the common method for investigating bicycle wheel aerodynamics. An overview of WT tests is provided in Table 3, where the table entries are the wheel type, the test-section cross-sectional dimensions, the speed tested, the yaw angles tested, the target parameters for which measurement results were provided and the fact whether or not rotational moment measurements were performed. The vast majority of previous WT tests cycling wheel aerodynamics were performed for isolated wheels. Here, the term isolated refers to the absence of the frame but with the inclusion of a slender support structure in WT tests, and with potential presence of a nearby flat surface, roller or rolling belt representing the ground. Indeed, the standard practice in testing cycling wheels is to focus on isolated wheels. While it is clear that the final goal is the drag reduction of the whole system of the bicycle – including all components – and rider, testing wheels together with the rest of the bicycle unavoidably renders the results on wheel performance dependent on the bicycle, which complicates a clear comparison. Nevertheless, also field tests of bicycles equipped with different wheels were also performed (Capelli et al., 1993; Hagberg and McCole, 1990; McCole et al., 1990). Concerning the field tests by Hagberg and McCole (1990) and McCole et al. (1990), where the $\dot{V}_{O_2}$ of the cyclists was measured when riding bicycles with different wheels, Lukes et al. (2005) argued that small performance differences could not be sensed by this type of tests.

These WT tests generally aimed at a comparison of commercially available wheels in terms of aerodynamic drag. The first systematic comparison of commercially available wheels was conducted by Kyle (1990, 1991c, 1995b, 2002), who tested more than 30 wheels, including disc wheels, aerodynamically-spoked (tri- and four-spoke) wheels and spoked wheels. Note that in the present paper, the term spoked wheels refers to wheels equipped with a high number of spokes, from 12 up to 36, which have small cross-sectional dimensions, in the order of few mm diameter or chord. The majority of these tests was performed with the wheel aligned with incoming flow, thus with a 0° yaw angle, and only few with yaw angles >0°. Overall, the aerodynamic drag was found to be lowest for lenticular and disc wheels, with a maximum drag difference of 16% between the best and worst performing disc wheel. The aerodynamically-spoked wheels had a larger deviation between different models, up to 38%, with the drag of the best performing models situated within the drag values of the disc wheels. The spoked wheels had the worst performance among the different wheels, with 50%–150% larger drag than the best disc wheel. The spoked wheels showed a large variability in results due to their different number of spokes, spoke shape, rim shape, rim depth and tire width. Nevertheless, a general trend that was discerned was that fewer spokes, deeper rims and narrower tires reduced the aerodynamic drag. Moreover, the best cross-sectional shapes for spokes were found to be bladed and oval, whereas the worst shape was a rounded one. Some examples of cross-sectional shapes are shown in Fig. 23 for commercially available spokes (Roues Artisanales, 2008). A few wheels were also tested at 10° yaw angle, equivalent to a mild crosswind. In this condition, lenticular, disc and tri-spoke wheels decreased their drag thanks to the sail effect. It should be noted that the drag force results provided by Kyle correspond to the sum of translational and rotational aerodynamic drag, the former measured by a force balance and the latter derived from the power needed to keep the wheel spinning. The rotational drag accounted for about 20–40% of the total drag, depending on the wheel (Kyle, 1995b). More recently, Jermy et al. (2008) confirmed the high impact of the rotational moment to the total power needed to translate and rotate a wheel. The rotational power had a higher contribution to the total drag than found in previous studies: 25–50% for disc wheels, 37–55% for aerodynamically-spoked wheels and 45–55% for spoked wheels (Jermy et al., 2008). Therefore a complete analysis of wheel aerodynamics has to consider both translational drag and the rotational drag. However, as shown in Table 3, other WT tests in the literature (Barry et al., 2012; Crane and Morton, 2018; Greenwell et al., 1995; Sayers and Stanley, 1994; Tew and Sayers, 1999; Zdravkovich, 1992) did not consider the rotational drag in their analyses. Besides the aerodynamic drag, Kyle (1995b) also discussed other parameters affecting the wheel performance: weight, moment of inertia, stiffness of the wheel and rolling resistance. An increase in wheel weight increases the rolling resistance and the potential energy component when slopes are present (see Eqs. (5)-(6)). Weight increase and its distribution also influence the wheel moment of inertia: a larger moment of inertia slows the acceleration of a wheel. Lastly, the rolling resistance also depends on the tire mounted on the wheel and the quality of the ground surface.

In addition to the previous commercially-available wheel comparisons, two studies (Zdravkovich, 1992; Sayers and Stanley, 1994) investigated if adding elements to spoked wheels could provide a drag

Table 3
Information on wind tunnel tests of wheel aerodynamics.

Reference	Test section [m^2] (W x H)[a]	Speed [km/h]	Yaw angle [°]	Wheel type[c]	Reported results[e]	Rotational moment measured
Kyle (1990, 1991c, 1995b, 2002)	0.61 × 0.91	24–73	0, 10	Sp; a-Sp; disc	D	Yes
Zdravkovich (1992)	1.20 × 0.91	20–42	0–25	p-Sp	C_D, C_S, C_Y[f]	No
Sayers and Stanley (1994)	0.87 × 0.58[b]	30–72	0	c-Sp	C_D[f]	No
Greenwell et al. (1995)	2.13 × 1.52	16–48	0–90	Sp; a-Sp; disc	C_D, C_S, C_Y[g]	No
Tew and Sayers (1999)	0.87 × 0.58[b]	30–55	0–30	Sp; a-Sp; disc	C_D, C_S[g]	No
Jermy et al. (2008)	1.20 × 0.90	30–50	0–50	Sp; a-Sp; disc	D, S, P	Yes
Barry et al. (2012)	4.00 × 2.60[b]	50	0–30	Sp; a-Sp; disc[d]	C_DA, C_SA, C_YA, C_RA	No
Crane and Morton (2018)	1.00 × 1.00[b]	32–59	0–12.6	Sp	C_DA, C_SA	No

[a] W = width; H = height.
[b] Open test section. The dimensions refer to the wind tunnel jet.
[c] Sp = spoked; a-Sp = aero-spoked wheels (tri-spoke, four-spoke and five-spoke wheels); p-Sp = spoked wheels with splitter plates; c-Sp = spoked wheels with cladding; disc = disc or lenticular wheels.
[d] Bicycle and mannequin included in the tests.
[e] D = drag; S = side force; C_D = drag coefficient; C_S = side force coefficient; C_Y = yawing moment coefficient; P = power; C_DA = drag area; C_SA = side force area; C_YA = yawing moment area; C_RA = rolling moment area.
[f] Coefficient computed using frontal area $2tr$, where t is the tire width and r the wheel radius including the tire.
[g] Coefficients computed using lateral area, πr^2, where r is the wheel radius including tire.

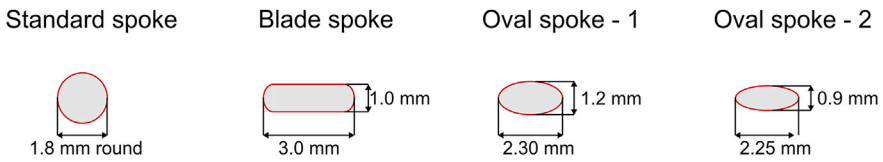

Fig. 23. Different cross-section shapes for spokes (adapted from Roues Artisanales, 2008).

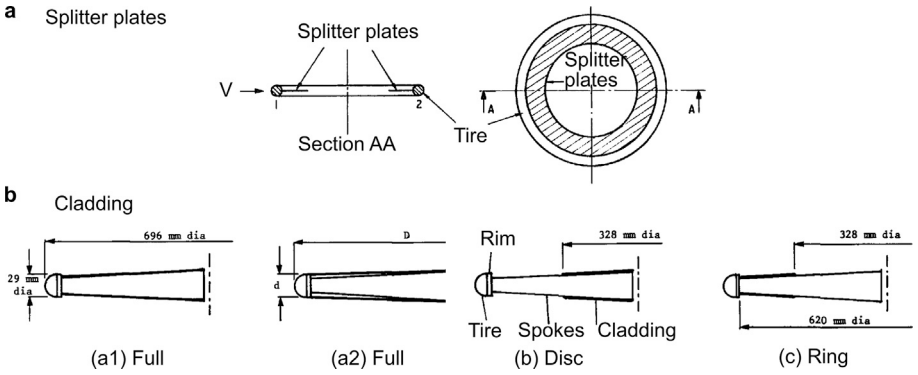

Fig. 24. (a) Splitter plates applied on a wheel (adapted from Zdravkovich, 1992; reproduced with permission from Elsevier); (b) Cladding applied around the spokes (adapted from Sayers and Stanley, 1994; reproduced with permission from Elsevier).

decrease. Zdravkovich (1992) tested a spoked wheel without and with splitter plates of different length (Fig. 24a). The splitter plates are thin plates placed circumferentially inside the wheel's rim. This idea originated from previous investigations on bluff bodies (Roshko, 1954; Apelt et al., 1973, 1975) where splitter plates were shown to reduce the vortex shedding from these bodies thus reducing their drag with up to 17% (Apelt et al., 1975, reported in Zdravkovich, 1992). For bicycle wheels, only a small drag reduction (<5%) was achieved using short splitter plates with a two tire-width length, whereas longer ones actually increased the drag with up to +5%. Zdravkovich (1992) argued that the reason for the small impact of splitter plates on wheel aerodynamics was the limited vortex shedding from the wheels. Zdravkovich (1992) also introduced a quantity named the shape factor, defined as the ratio of the wheel diameter to the tire width. Increasing the shape factor from 22 to 31, thus narrowing the tires, the drag coefficient increased with up to almost 40%. This was in contrast to the conclusions by Kyle (1990, 1991b), who stated that narrower tires were preferable from an aerodynamic point of view. This apparent contradiction is due to how the drag coefficient was defined, as explained by Greenwell et al. (1995): as will be outlined below in Subsection 4.2.3. Moreover, Zdravkovich (1992) found a high drag force sensitivity to yaw angle alignment: a 2° misalignment gave more than 10% difference in drag. A high yaw angle sensitivity in WT tests was later confirmed also by Greenwell et al. (1995). Sayers and Stanley (1994) added claddings of different shapes on wheels (Fig. 24b). These consisted of cardboard discs fitted over the spokes on each side of the wheel. The two partial cladding configurations namely disc, with cladding near the hub, and ring, with cladding near the rim, did not provide any drag coefficient reduction, whereas a full cladding improved the wheel drag, especially if no discontinuities or steps were present between the cladding and the rim, as shown in Fig. 24b for the a2-full case. The results by Sayers and Stanley (1994) were given in terms of drag coefficient similarly to Zdravkovich (1992). However, this choice did not influence their conclusions since the same tire type was employed in all the tests.

Greenwell et al. (1995) and Tew and Sayers (1999) investigated seven and six commercially-available wheels, respectively, by means of WT tests. Both studies tested the selected wheels, ranging from 36-spokes to tri-spoke and disc wheels, at different WT velocities and yaw angles. At zero yaw angle, "aerodynamic" wheels, namely deep-rim, tri-spoke and disc wheels, had smaller drag than "conventional" 36-spoke wheels in both studies. However, while all aerodynamic wheels had around a 25% drag reduction compared to the conventional 36-spokes wheel in Greenwell et al. (1995), this difference ranged between 50% and 70% in Tew and Sayers (1999), showing both a larger drag reduction and a larger difference in performance between the aerodynamic wheels. At yaw angles larger than 0° for a speed of 48 km/h, Greenwell et al. (1995) found that disc wheels significantly decreased their drag until it became negative at around 15° yaw angle, thus creating thrust. However, this behavior was not observed by Tew and Sayers (1999): the second worst drag coefficient was measured for a disc wheel at yaw angles larger than 15° at speeds equal or smaller 48 km/h. On the other hand the side force had a similar trend for similar wheel types between the two studies, with the side force value increasing almost linearly with yaw angle for all the wheels. One exception was noted by Tew and Sayers in the measured side force of disc wheel: it grew linearly from 0° to 5° and from 8° to 30°, whereas between 5° and 8° a sudden drop was measured. However, Gibertini and Grassi (2008) stated that this behavior was never observed in their WT measurements for similar typology of wheels. Greenwell et al. (1995) showed also that the maximum side force correlated well with the side area of each wheel, thus the larger the side area of the wheel, the higher the side force. High values of the side force could also cause high yawing instabilities. Moreover, Greenwell et al. (1995) did not consider any blockage correction in their study, stating that the blockage should be negligible. Both studies found a weak influence of the WT speed, especially for side force and turning moment. Greenwell et al. (1995) explained the low dependency on the Reynolds number by the argument that no laminar regions should be present on the wheels due to the flow transition caused by the tire tread and wheel rotation. Lastly, Greenwell et al. compared the results from different studies about spoked wheels at 0° yaw angle, finding that decreasing the number of spokes from 36 to 24 reduced significantly the aerodynamic drag coefficient, −35%, whereas a further reduction to 16 spokes reduced the drag an additional 10% compared to the 24 spokes configuration.

Recent WT tests on wheel aerodynamics also highlighted the role of the interaction between the tire and the rim. Crane and Morton (2018) tested six wheels combined with five different tires at yaw angles between 0° and 13°. The drag and side force area results were then averaged using weights accounting for the probability a certain yaw angle is encountered (Brownlie et al., 2010; Cooper, 2003, 2012) while travelling at 13.4 m/s. This type of average was called wind averaged drag area, or

wind averaged side force area, following the common name used in car and truck industry to describe this averaging technique (Cooper, 2003, 2012). The wind averaged drag area increased for larger ratios between the tire to rim width. This increase showed an almost linear dependence with the ratio between the tire to rim width, with the linear regression providing $R^2 = 0.87$. Crane and Morton (2018) did not provide the regression coefficients, however the present authors estimated that the slope of the line was around 0.034 m^2 and the intercept −0.012 m^2: a 10% wider tire may cause a drag difference of about 0.4 N at 13.4 m/s for a single wheel. Moreover, the wind averaged side force was mostly influenced by the rim depth rather than the tire and rim widths. Therefore, Crane and Morton (2018) suggested that wheel manufacturers should consider also different tires in their design process and that cyclists should mount tires that are at most as wide as the rim, as also suggested by Kyle (2002). Moreover, Hed and Haug (1991) in their patent also reported an improved aerodynamic when the ratio between the rim width to tire width is between 1.05 and 1.15, or vice versa when the tire width to rim width is between 0.87 and 0.95.

Even though it is standard practice to testing isolated cycling wheels, the final goal is to reduce the drag of the whole system of the bicycle – including all components – and the rider. Therefore it is necessary to study their interaction. Barry et al. (2012) tested five different wheels in a WT, including spoked, tri-spoke and disc. The tests were conducted using these wheels as the front wheel of a bicycle, with and without a mannequin. The rear wheel was a flat disc wheel for the tests without the mannequin and a lenticular disc wheel for the tests with the mannequin. Results showed different drag trends for the results with and without the mannequin. Generally, a front disc wheel provided the best, or among the best, drag area for yaw angles between 0° and 30° for the case without the mannequin and between 0° and 15° for the case with the mannequin. In the latter case, for yaw angles between 20° and 30°, the front disc wheel provided the worst results compared to other wheels with a sharp increase in the drag area. The deep-rim spoked and tri-spoke wheels gave overall lower drag area values compared to shallow-rim wheels and values close to those of the disc wheels for yaw angles between 0° and 15° for the case with the mannequin. Moreover, deep-rim spoked wheels and tri-spoke wheels had a lower side force area, yawing moment area and rolling moment area than disc wheels for all yaw angles, but higher than shallow-rim spoked wheels. Barry et al. (2012) highlighted that the latter two moments can cause an increase of the rolling resistance and reduce the handling of the bicycle and the performance of the cyclist, especially at high yaw angles.

4.2.3. Comparison of selected wind tunnel studies

In this subsection some specific WT studies are selected and their results are highlighted to show and explain apparent discrepancies and inconsistencies. First the contradiction between the results of Zdravkovich (1992) and Kyle (1990, 1991b) is discussed, next the results by Tew and Sayers (1999) and Greenwell et al. (1995) are compared. Finally, the discrepancies of the WT tests mentioned in (Godo et al., 2009, 2010, 2011) are addressed.

Zdravkovich (1992) concluded in the above-mentioned study that narrowing the tires caused a drag coefficient increase up to almost 40%. This was in contrast to the conclusions by Kyle (1990, 1991b) who stated that narrower tires were preferable from an aerodynamic point of view. This apparent contradiction was explained by Greenwell et al. (1995): Zdravkovich computed the wheel drag coefficient similarly to other bluff bodies, thus using as reference area the frontal area given by the multiplication of the tire width and the wheel diameter. However, the drag of different wheel components, like hub, rim and spokes, did not scale with the tire width, therefore Greenwell et al. (1995) suggested to use the drag area or a drag coefficient based on the full-wheel side area, equal to πr^2, with r the wheel radius, to compare the drag of different wheels. Based on this definition, the wheel tested by Zdravkovich (1992) with a narrow tire indeed had a lower drag area than the wheel with a wider tire (Greenwell et al., 1995). This revised conclusion confirmed the findings from Kyle (1990; 1991b).

Greenwell et al. (1995) and Tew and Sayers (1999) tested seven and six wheels, respectively. Among the tested wheels, two were used in both studies, namely the 16-spoke Campagnolo Shamal and the Specialized tri-spoke, therefore it is possible to quantitatively compare their drag results. At 0° yaw angle, a 37% and 16% lower drag was measured by Tew and Sayers (1999) than Greenwell et al. (1995) for the spoked and tri-spoke wheel, respectively. These tests were performed under different conditions. This can explain the different results found by Tew and Sayers (1999) versus Greenwell et al. (1995) on the same wheel: different WTs were employed; open test section in (Tew and Sayers, 1999) versus closed test section in (Greenwell et al., 1995), probably different tires were used, 20 mm width in (Tew and Sayers, 1999) versus not provided by (Greenwell et al., 1995), different wheel types were applied, a front wheel in (Tew and Sayers, 1999) and a rear wheel including gears in (Greenwell et al., 1995) and finally, different wheel supports were used; a single vertical strut in (Tew and Sayers, 1999) versus the rear part of a cut bicycle frame in (Greenwell et al., 1995).

Godo et al. (2009, 2010, 2011) did not perform any WT tests, however they compared their CFD results with WT results available in the literature or provided them by wheel manufacturers. Note that it is unclear whether the WT measurements provided by wheel manufacturers were subjected to scientific reporting and peer review, thus they should be considered with caution. The reported WT results presented a high drag discrepancy. For example, eight WT results were reported at 0° yaw angle for the for the Zipp808 spoked wheel, with a drag coefficient ranging between about 0.02 and 0.05, whereas only two different WT tests were reported for yaw angles up to 20°, with a drag coefficient discrepancy between these two sets of data ranging from 10% to 40%.

The above-mentioned different measurements results performed by different authors for the same wheel can be attributed to the lack of a uniform testing methodology. Indeed, even with the focus generally on isolated wheels, Crane and Morton (2018) pointed out that the testing protocols might significantly vary between different manufacturers and researchers. As indicated in Table 3, generally, all these studies were performed under different test conditions. In addition, Crane and Morton (2018) found a large sensitivity of the aerodynamic drag to the ratio between the tire width and the rim width, therefore the use of different tires in those studies could have also contributed to the drag discrepancies reported in this subsection.

4.2.4. CFD studies

After 2000, wheel aerodynamics started to be investigated also by means of CFD simulations. An overview is presented in Table 4, where the table entries are the wheel type, the dimensions of the computational domain, the size of the computational grid, the turbulence modeling approach, the rotation modeling approach and whether or not a comparison with WT tests was performed. Table 4 shows that the vast majority of previous CFD studies were performed for isolated wheels, in line with the standard practice in WT tests. Similar to Table 3, Table 4 shows that also CFD simulations are characterized by the lack of a uniform testing methodology, which can impede an inter-study comparison.

One of the first CFD studies on wheel aerodynamics was mentioned by Hanna (2002). Hanna reported that CFD simulations were performed to assess and quantify the presence of the sail effect of disc wheels when used at the rear of bicycles. For this purpose, two computational models were created with the same cyclist and bicycle but different rear wheel shape, i.e. spoked versus disc. Note that the spoked wheel considered was approximated by only the tire, rim and hub, thus without the spokes for computational economy. Both configurations were evaluated at a travelling speed of about 40 km/h, for a 90° crosswind ranging from 0 to about 48 km/h. In zero crosswind conditions, the combined cyclist-bicycle with rear disc wheel had a 2% lower drag compared to the case with the rear spoked wheel. This drag difference increased in crosswind conditions: for the case with 32 km/h crosswind (≈39° yaw angle), the drag aligned with the rider direction was 17% lower when

Table 4
Information on CFD simulations of wheel aerodynamics.

Reference	Wheel type[a]	Domain (W x H x L)[d]	Grid[f]	Turbulence modeling[g]	Rotational modeling[h]	Comparison with WT tests
Hanna (2002)	Sp; Disc[b]	n.a.	n.a.	n.a.	n.a.	No
Knupe and Farmer (2009)	Sp; a-Sp; disc	1.4 × 1.2 × 5.0 m^3 (2.0Ø × 1.7Ø × 7.1Ø)	1 M–6 M	Std k-ε	MRF	No
Godo et al. (2009, 2010)	Sp; a-Sp; disc	0.8 × 1.1 × 2.8 m^3 (1.2Ø × 1.5Ø × 4Ø)	3.8 M–16 M	SA-DES	MRF-RW	Yes
Godo et al. (2011)	Sp; a-Sp; disc[c]	Semi-ellipsoid[e]	6 M–10 M	SA-DDES	MRF-RW	Yes
Karabelas and Markatos (2012)	Sp	4.2 × 4.2 × 14.0 m^3 (6Ø × 6Ø × 20Ø)	250 k–522 k	URANS	SM	Yes[i]
Pogni and Petrone (2016)	Sp	1.5 × 1.2 × 2.0 m^3 (2.1Ø × 1.7Ø × 2.9Ø)	Up to 5 M	Std k-ε	MRF	No
Malizia et al. (2019)	Sp	7.7 × 7.7 × 11.2 m^3 (11.0Ø × 11.0Ø × 16.0Ø)	Up to 46 M	SA, Rk-ε, k-ω SST, γ k-ω	RW; MRF; MRF-RW	Yes
Malizia and Blocken (2020)	Sp	7.7 × 7.7 × 11.2 m^3 (11.0Ø × 11.0Ø × 16.0Ø)	Up to 41 M	k-ω SST	MRF-RW	Yes

[a] Sp = spoked; a-Sp = aero-spoked wheels (tri-spoke, four-spoke and five-spoke wheels); disc = disc or lenticular wheels.
[b] The spoked wheel included only the tire, rim and hub. The spokes were neglected.
[c] Front-half of a cut bicycle frame included in the simulations.
[d] Wheel diameter, Ø, assumed to be 0.7 m. Moreover, W = width, H = height and L = length of the computational domain.
[e] No size provided.
[f] "k" is used for thousands (10^3) and "M" for millions (10^6).
[g] Std k-ε = standard k-ε; SA = Spalart Allmaras; DES = detached eddy simulation; DDES = delayed detached eddy simulation; Rk-ε = realizable k-ε; k-ω SST = k-ω shear stress transport; γk-ω = k-ω SST with intermittency transition model; URANS = unsteady RANS with Re-Normalization Group k-ε turbulence model.
[h] RW = rotating wall; MRF = moving reference frame; MRF-RW = hybrid MRF and RW; SM = sliding mesh.
[i] Only comparison with WT test of static (i.e. non-rotating) wheel.

using the rear disc wheel rather than the rear spoked wheel. However, for the same 32 km/h crosswind, the side force on the cyclist-bicycle configuration with rear disc wheel doubled the one with spoked wheel. The text did not mention the detailed methodology description and result validation.

Subsequent CFD studies on wheel aerodynamics focused on isolated wheels, without any support or bicycle (Godo et al., 2010, 2009; Karabelas and Markatos, 2012; Knupe and Farmer, 2009; Malizia et al., 2019; Malizia and Blocken, 2020; Pogni and Petrone, 2016) with the exception of Godo et al. (2011) where the front fork and the front half of a cut bicycle frame were included (Table 4). The majority of these studies focused on comparing the aerodynamic performance of different wheel types, including spoked, tri-spoke and disc wheels, whereas Karabelas and Markatos (2012) and Pogni and Petrone (2016) only considered spoked wheels. In contrast, Malizia et al. (2019) focused on the CFD methodology used to investigate the aerodynamics of cycling spoked wheels and Malizia and Blocken (2020) focused on the impact of the ground and the type of ground-wheel contact modeling on the wheel aerodynamics, with highlights of the flow behavior around the wheel (Fig. 25).

The CFD studies by Godo et al. (2009, 2010, 2011) compared the performance of six wheels: one "conventional" shallow-rim wheel, three deep-rim spoked wheels with rims of different depth, one tri-spoke wheel and one disc wheel. Godo et al. (2009, 2010, 2011) found similar drag values for the spoked wheels at 0° yaw angle, while the tri-spoke and the disc wheel had about 6% and 18% lower drag than the spoked wheels, respectively. Increasing the yaw angle, the drag of the spoked wheels generally reduced up to around 10° yaw angle, after that it increased until the last yaw angle computed, 20°. However, the spoked wheels with deeper rims had a larger drag reduction than spoked wheels with shallow rims: for example, at 10° yaw angle the drag of the wheel with deepest rim was almost 60% lower than the drag of the same wheel at 0°. Contrarily, the drag of the tri-spoke wheel increased until around 8° yaw angle (+16%), after that it decreased; whereas the drag of the disc wheel drag decreased almost monotonically, with the exception of a drag increase at 10° and 12° yaw angle, reaching an almost zero drag condition for yaw angles between 16° and 20°. Similarly to previous WT studies (Greenwell et al., 1995; Tew and Sayers, 1999), the side force showed an almost linear increase with the yaw angle, with larger values when

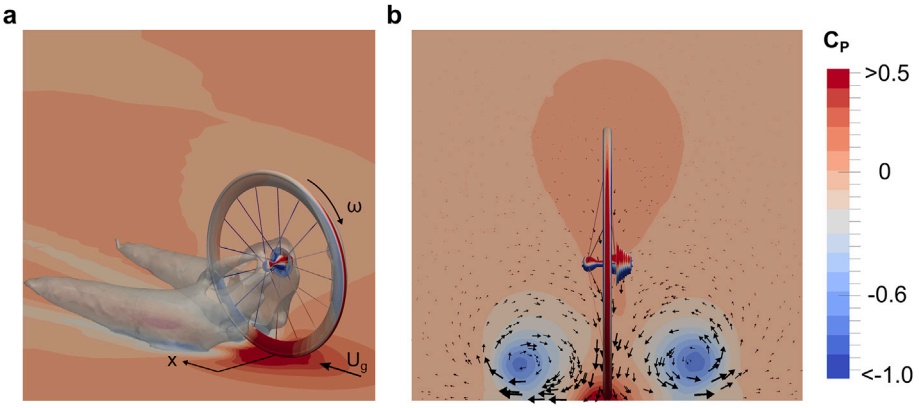

Fig. 25. (a) Isosurfaces of static pressure coefficient $C_P = -0.3$ (gray) together with C_P contours on the rotating wheel and on the ground; (b) vector plots and contours of C_P in a lateral vertical plane at a streamwise distance from the hub center x = +3/4Ø, where Ø is the wheel diameter equal to 700 mm (adapted from Malizia and Blocken, 2020).

deeper rims or disc wheels were used. Moreover, unstable turning moments, i.e. moments that tend to further increase the yaw angle, were found at all yaw angles for the disc wheel and the wheel with the deepest rim, 125 mm depth for the combined rim and tire, whereas stable turning moments, i.e. moments that tend to reduce the yaw angle, were found for all the other wheels, including the tri-spoke. Among all these studies, only the study by Godo et al. (2011) included the rotational power; its contribution to the total power was 9–10% for the tri-spoke wheel, 12–18% for the wheel with 75 mm depth of the combined rim and tire, and 17–24% for the deepest rim wheel considered, thus smaller than the results of Kyle (1995b) and Jermy et al. (2008). Lastly, Godo et al. (2011) found that the wheel type had a stronger effect on fork aerodynamics than the fork on wheel aerodynamics. Godo et al. (2009, 2010, 2011) did not perform any WT tests, however they compared their CFD results with WT results available in the literature or provided them by wheel manufacturers, as mentioned in Subsection 4.2.3. These WT results presented a high drag discrepancy. For example, two different WT tests were reported for the for the Zipp808 spoked wheel for yaw angles up to 20°, with a drag coefficient discrepancy between these two sets of data ranging from 10% to 40%. This situation with very large discrepancies in WT results is unfortunately detrimental for the confidence when comparing CFD and WT results: at different yaw angles, the computed drag coefficient was 20%–45% lower than the measured drag coefficient of one of the two sets, whereas the discrepancy with the other set of WT measurements ranged between −35% and +20%.

Karabelas and Markatos (2012) performed both CFD simulations and WT tests of a static spoked wheel, thus not rotating, together with CFD simulations of the same spoked wheel but rotating. For the static wheel case, the WT results showed a sensitivity of the aerodynamic forces to the inlet mean velocity for yaw angles between 0° and 45°: the drag coefficient for inlet velocities of 7 m/s and 9 m/s was about 5% and 15%, respectively, higher than the drag at 5 m/s. Contrarily, the CFD results showed negligible sensitivity of the drag coefficient to the inlet velocity tested: 5 m/s, 10 m/s and 20 m/s. The present authors hypothesize that this observation was caused by the turbulence model and near-wall modeling approach used by Karabelas and Markatos (2012), being the RNG k-ε model (Orszag et al., 1993) and the standard wall functions (Launder and Spalding, 1974). This combined approach is not able to compute the laminar-to-turbulent transition, therefore the flow will have been turbulent on the entire wheel for all the velocities tested, and as a result no drag variations due to laminar-to-turbulent transition could be captured. Moreover the CFD simulations systematically underestimated the WT results by 18%–40% for yaw angles in the range of 0°–45°. The only exception was the drag at 7.5° yaw angle, for which the measured drag had a significant drop, −18% and −31% compared to the measured drag at 0° and 15° yaw angle, respectively, consequently the CFD and WT results were in closer agreement for this particular yaw angle. The rotating-wheel CFD simulations showed a larger drag coefficient, about 20%, than static wheels. Moreover, the tire-rim combination was the main source of drag in all yaw angle configurations (≈65% at 0° yaw angle), then the 16 spokes (≈30% at 0°), and lastly the hub (≈5% at 0°). Two additional wheel models with different number of spokes, 8 and 32, were also created, and the results showed a drag decrease by lowering the number of spokes from 32 spokes to 16 spokes (≈−18%) and 8 spokes (≈−22%).

Two main problems in CFD simulations of wheel aerodynamics are the lack of uniform testing methodology and the large sensitivity of the results to the wide range of computational parameters to be set by the user. Some recent studies have attempted to address some of these issues by sensitivity analyses and the establishment of some guidelines for CFD simulations of isolated wheel aerodynamics. Malizia et al. (2019) focused on the impact of the computational grid resolution, the approach for wheel rotation modelling and the turbulence modelling on the computed translational and rotational drag. They showed that an adequate choice of these parameters is critical for accurate results to be obtained. From this analysis, a close agreement between the computed drag coefficient and that from WT results in the literature (Tew and Sayers, 1999) was achieved, with a drag coefficient discrepancy smaller than 3.4%. However, the analysis was limited to only one 16-spoke wheel, one yaw angle (0°) and one speed (13.41 m/s). However in the CFD simulations of Malizia et al. (2019) the ground was neglected to resemble the experimental conditions in (Tew and Sayers, 1999). The impact of the presence of the ground and the type of ground-wheel contact modeling on wheel aerodynamics was later studied by Malizia and Blocken (2020). In addition, a description of the flow behavior around the wheel was also provided; Fig. 25 shows a high pressure in the front section of the tire, hub and gears, and on the wheel and ground near their area of contact. Two low pressure regions were generated in the wake of the hub and gears, which reached first the wheel rear bottom section then the ground. These low pressure regions are characterized by a counter rotating flow, which caused a downwash in the wheel's wake and a high pressure region on the ground downstream the wheel.

4.3. Handlebar

The handlebar is one of the three points of contact between cyclist and bicycle, together with the saddle and the pedals. It has evolved from the wooden bar used in the Draisienne (Fig. 26a) over the dropped handlebar in late 19th Century (Fig. 26b) to advanced bars such as the 3D printed titanium handlebar (Cicli Pinarello Spa, 2015) used in 2015 by Wiggins for his 2015 world hour record (Fig. 26c) or by Primož Roglič in his 2019 Vuelta TT (Fig. 26d). The aerodynamic design of a handlebar follows two strategies: optimizing the handlebar shape in terms of its aerodynamics, e.g. a more streamlined shape; and optimizing its shape to enable the cyclist to take a more aerodynamic posture, both in terms of reduced drag coefficient and reduced frontal area, without substantially limiting his or her power output.

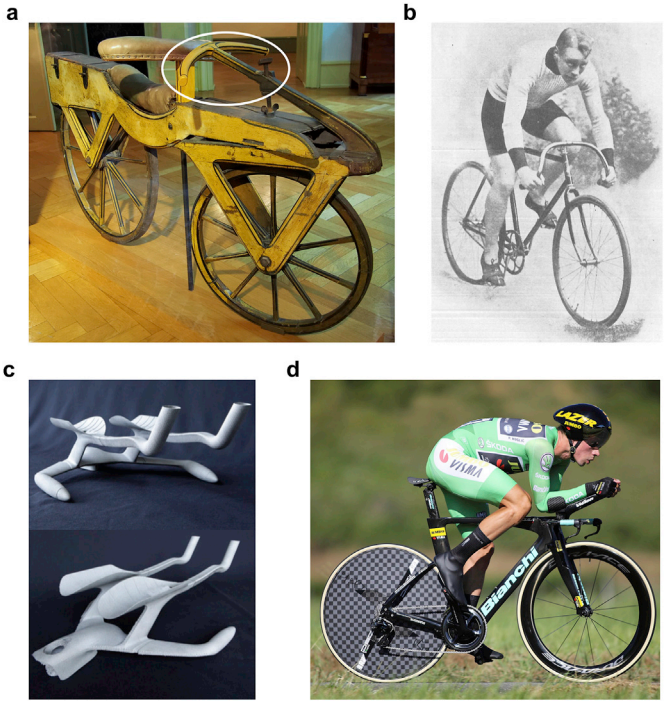

Fig. 26. (a) Wooden bar, highlighted with white circle, used in the Draisienne bicycle (reproduced with permission from "edk7/Flickr"); (b) Dropped handlebar used in cycling races in 1894 (source: Gronen and Lemke, 1987); (c) 3D printed titanium handlebar of Wiggins', world hour record bicycle (source: Cicli Pinarello Spa, 2015); (d) Team Jumbo-Visma rider Primož Roglič using a 3D printed handlebar during the individual time-trial of the Vuelta 2019 (source: Cor Vos Agency; reproduced witih permission).

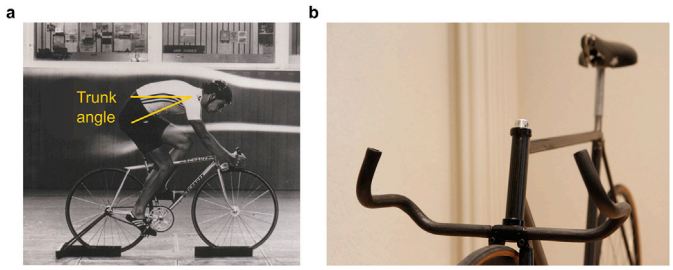

Fig. 27. (a) Aerodynamic tests of the aerodynamic Schauff bicycle equipped with cow-horns, the cyclist trunk angle is indicated in red (reproduced with permission from Schauff); (b) Cow-horn handlebar connected to front fork on bicycle by Maier Moussa in 1976 (reproduced with permission from Assos).

4.3.1. *Dropped bars, cow-horn bars and tri-bars*

Already in the early 20th century, different handlebar shapes were commercially available (Hadland and Lessing, 2014). The most common in competitions was the dropped handlebar, which is still widely used. There is no official date about its first use but already in 1894 bicycles were equipped with this type of handlebar (Gronen and Lemke, 1987; Kyle and Weaver, 2004), as shown in Fig. 26b. This handlebar enables the cyclist to reduce the frontal area by crouching forward and reducing the trunk angle, i.e. the angle between the horizontal and the trunk (Fig. 27a). The influence of the frontal area on aerodynamic performance was already known at the end of the 19th century, not only empirically but also through mathematical models of cyclist performances (Bourlet, 1894). However it is not clear how widespread this knowledge was at that time. Note also that general conclusions on drag reduction can only be drawn after considering both the frontal area and drag coefficient and more specifically their product, the drag area C_DA: although a lower frontal area generally provides lower drag values in cycling, there are cases where cyclists with larger frontal area have lower drag values than other cyclists with smaller frontal area (e.g. in Barry et al., 2015; Blocken et al., 2018a; Edwards and Byrnes, 2007).

The idea of reducing the frontal area to increase cyclist performance came back around the 1970s, when new handlebar locations and handlebar shapes were introduced. The former refers to connecting the handlebar at a lower position along the head tube instead of on top of it, whereas the latter refers to a reverse curvature of the hand grips compared to the dropped handlebar; this handlebar was known as "cow-horn" or "bull-horn". One example of a cow-horn handlebar not connected on the head tube is shown in Fig. 27b. It dates back to 1976 and was designed by Maier Moussa for his carbon fiber bicycle (Boardman, 2015). This handlebar was connected directly to the forks of the front wheel. A similar handlebar was used by Lothar Thoms who won the 1,000 m track TT at the 1980 Olympic Games in Moscow with the time of 1′02″955, establishing the new world record. The previous 1,000 m track TT world record was set only one month earlier by Urs Freuler with the time of 1′05″582, more than 2 s slower than Thoms. Cow-horn shaped handlebars were also connected on top of the head tube, for instance in the world hour record bicycle of Moser (Fig. 15c) or in the "funny bicycles" of the 1984 USA Olympic cycling team (Fig. 18b). A further evolution of the cow-horn handlebar was the design by Ménard in 1980 (Hinault and Genzling, 1988) for the 1983 Gitane Delta bicycle (Fig. 28a and b). Ménard replaced the common circular horizontal bar of this handlebar with an airplane-wing shaped horizontal bar (Fig. 28a) and a bicycle equipped with this handlebar was also driven by Laurent Fignon in the 1984 prologue of the Tour de France (Fig. 28b). Similarly, Schauff attached a streamlined-shaped handlebar (Kyle, 2001) at the bottom of the head tube (Figs. 27a and 28c) for their aerodynamic bicycles (Kyle, 2001) designed between 1979 and 1980 (Schauff, 2018). This bicycle was used in the 1983 track cycling world championship.

At the 1984 RAAM race (Race Across AMerica), Jim Elliot equipped his bicycle with a forearm support mounted centrally on his handlebar (Boardman, 2015). This support both reduced his arm-muscle stress and lowered his frontal area, and presumably his total drag. This design was further developed and used by Pete Penseyres (Boardman, 2015), 1986 RAAM race winner. The new handlebar enabled him not only to support his forearms but also to keep his hands in front of him (Fig. 29a) (Boardman, 2015). The first commercially available version of this handlebar, called clip-on handlebar, aero-bars or tri-bars, was patented by Lennon in 1987 (US patent 4,750,754; filed in January 1987), see Fig. 29b, and successfully used in many TT races, for instance LeMond won the individual TT of the 1989 Tour de France using this type of handlebar.

4.3.2. *The special handlebars by Obree*

Following the idea of frontal area reduction, Graeme Obree developed a new bicycle, the "Old Faithful". Obree reduced his frontal area riding on this bicycle by placing his hands near the chest and shoulder, thus shielding his arms from the wind ("tucked in") in a very crouched position (Fig. 29c). This position was kept using an ad-hoc handlebar, which was flat and narrow, with an oval cross section (Boardman, 2015). Using this bicycle and position, Obree broke the world hour record twice, in 1993 (51,596 m) and in 1994 (52,713 m). In between, Boardman broke the world hour record (52,270 m) on a monocoque track bicycle equipped with aero-bars (see Subsection 4.1 and Fig. 20c). However, in 1994 the UCI introduced new regulations about the saddle position, which had to be situated at least 50 mm behind a vertical line passing through the bottom bracket axle, and about the distance between chest and handlebar, such that "daylight" should be visible (Boardman, 2015). After the introduction of these rules, Obree was disqualified during the 1994 Men's individual pursuit world championship and his tucked position was banned. Despite the new rules, the world hour record was broken another three times by the end of 1994: once by Miguel Indurain (53,040 m) and twice by Tomy Rominger (53,832 m and 55,291 m), see Section 4.1, Figs. 20 and 21. All the bicycles used for these hour records were equipped with aero-bars. After the tucked position being banned, Obree in 1995 equipped his bicycle with aero-bars and started adapting

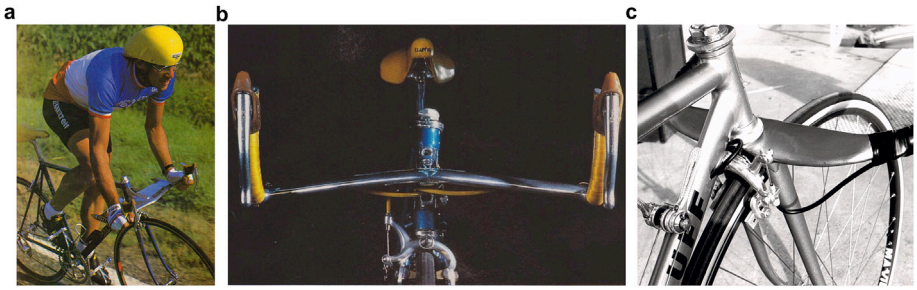

Fig. 28. (a) Gitane Delta bicycle with airplane-wing handlebar used by Fignon in the 1984 Tour de France (source: "Miroir du Cyclisme", July 1984); (b) Front view of the Gitane Delta airplane handlebar (source: "Miroir du Cyclisme", January 1985); (c) Streamlined handlebar attached at the bottom of the head tube and mounted on the aerodynamic Schauff bicycle (reproduced with permission from Schauff).

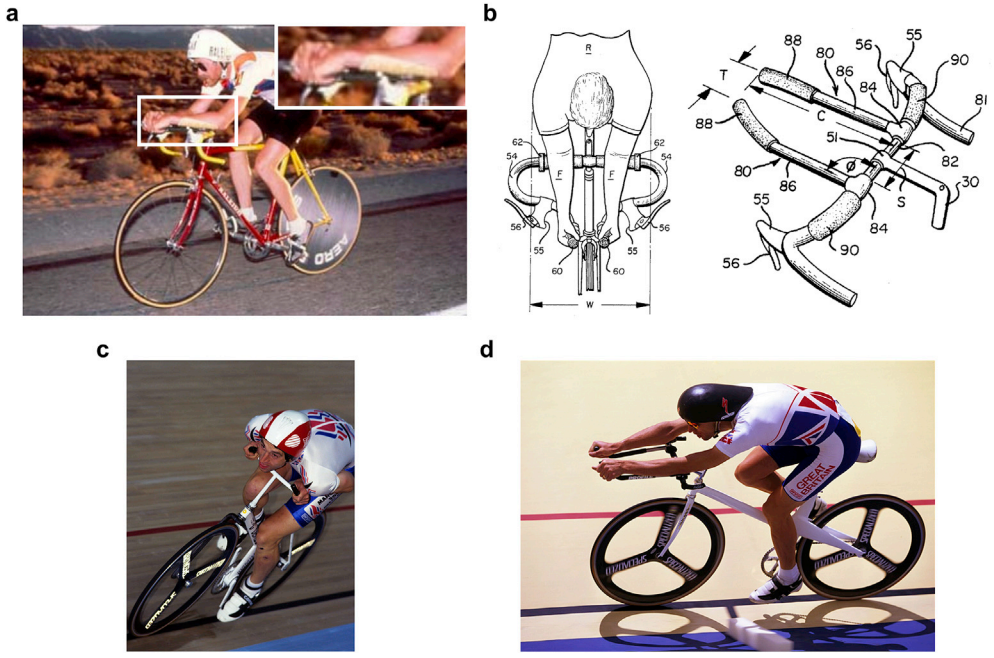

Fig. 29. (a) Clip-on supports for forearms used by Pete Penseyres during the 1986 RAAM race (reproduced with permission from "www.ultracycling.com"); (b) Two types of clip-on handlebar patented by Dan C. Lennon (US patent 4,754,750); (c) Special handlebar used by Obree in his tucked position (reproduced with permission from Graham Watson); (d) Special extended tri-bars used by Obree during the 1985 world championships for his superman position (reproduced with permission from Graham Watson).

his position to the new type of handlebar (Obree, 2005). After several rides, Obree found that the best position for himself was with his arms as high up and stretched out as much as possible (Obree, 2005), see Fig. 29d. In this completely stretched position, Obree was able to reduce his frontal area and to have a more streamlined position than possible with shorter aero-bars. Obree used this position for the individual pursuit of the world cup series, and after winning the Australian race in 1995, an Australian newspaper printed a picture of Obree while using his new position, with the title "superman": from that moment on, this position was commonly nicknamed the "superman" position (Obree, 2005). Adopting this position, Obree also won the world pursuit title in 1995. Other riders also adopted this position, such as Chris Boardman who broke the world hour record in 1996. However, new UCI rules forbade also this position at the end of 1996.

4.3.3. *Wind tunnel tests and CFD simulations*

Several studies about the aerodynamic impact of the handlebar are summarized in Table 5. The first studies where different handlebar positions and shapes were tested to reduce the cyclist drag were performed by Dal Monte et al. (1987) and Kyle (1989) by means of WT tests. Dal Monte et al. (1987) tested two handlebar heights on Moser's world hour record bicycle, finding that a lower height reduced the total drag. This bicycle was equipped with a cow-horn handlebar. Kyle (1989) investigated the impact of cow-horn and tri-bar handlebars on the combined cyclist-bicycle aerodynamics (Fig. 30a and b). The latter handlebar was similar to the one employed by LeMond in the last stage, an individual TT, of the 1989 Tour de France. This clip-on handlebar provided a drag

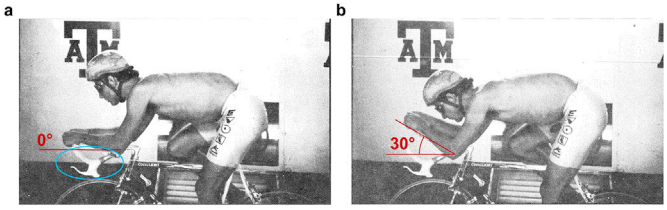

Fig. 30. (a) Tri-bar aligned with the horizontal (0°), the cow-horn handlebar is indicated by the ellipse; (b) Tri-bar at 30° from the horizontal. Pictures adapted from Kyle (1989).

reduction for the cyclist-bicycle combination between 13.7% and 15.5% compared to the tests with a cow-horn handlebar. Two reasons were given by Kyle (1989) to explain this result: (i) the clip-on handlebar enabled the cyclist to keep a more streamlined posture, with a flatter back and a lower frontal area; and (ii) a substantial portion of the cyclist's body could be shielded by the arms. An optimization study of the clip-on handlebar was also performed, both in terms of bar inclination and elbow pad position. The elbow pads are the supports on the handlebar where the elbows lay. The best aerodynamic performance was obtained by positioning the pads inward rather than outward. The upward tilting of the bars (Fig. 30b) gave higher drag for two different elbow positions (+1.2% and +4.2%) and lower drag for one elbow position (−1.1%) compared to flat bars (Fig. 30a). However tilted bars still performed better than cow-horn handlebars.

Studies aimed at finding the best clip-on handlebar aerodynamic

Table 5
Information on wind tunnel tests of handlebar aerodynamics.

	Handlebar	Test section [m^2] (W × H)[a]	Speed [km/h]	Measurements[d]
Dal Monte et al. (1987)	Cow-horn	11[b,c]	54	C_DA
Kyle (1989)	Cow-horn & Clip-on	3.0 × 2.1	48	D
Oggiano et al. (2008)	Clip-on	2.7 × 1.8	52	ΔD
Underwood and Jermy (2010)	Clip-on	1.5 × 1.5[c]	41	ΔD; ΔP
Underwood and Jermy (2013)	Clip-on	1.5 × 1.5[c]	42	C_DA

[a] W = width; H = height.
[b] The jet used in this open test-section wind tunnel had a semi-circular shape, therefore only the jet diameter is provided.
[c] Open test section. The dimensions refer to the wind-tunnel jet.
[d] D = drag [N]; C_DA = drag area [m^2]; ΔD = drag differences [N]; ΔP = power differences [W].

setup were also performed by Oggiano et al. (2008) and Underwood and Jermy (2013), both using WTs, see Table 5. The former tested 11 different cyclists on a TT bicycle using three handlebar positions. The results from the WT tests showed that a combined movement of the handlebar of 20 mm down and of 20 mm forward reduced the aerodynamic drag between 3.1% and 5.8% compared to the reference position of each cyclist. The latter tested 14 pedaling cyclists in a WT, focusing both on handlebar height and pad separation. Underwood and Jermy (2013) found a larger influence of the handlebar height than the pad separation in the drag optimization process for male cyclists, while both handlebar height and pad separation seemed equally important for female cyclists. Moreover, 10 of 14 cyclists obtained a drag reduction using lower handlebar heights thanks to the lower frontal area. For the remaining cyclists, it was argued that low handlebar positions forced them to raise the head to keep the line of vision, thus increasing their drag. The optimum pad separation was highly athlete dependent and a unique trend could not be found. Moreover, Underwood and Jermy (2013) suggested to choose a pad separation that facilitates the cyclist to keep the head low while maintaining the line of vision, since the pad separation had a smaller impact on the aerodynamic drag than the handlebar height. Lastly, they concluded that there was not a single handlebar position that provided the minimum drag for all the cyclists, so the optimal handlebar configuration was cyclist dependent.

Underwood and Jermy (2010) investigated the influence of the position of the hands on a clip-on handlebar. Eight cyclists were placed in a WT using their own TT position and equipment, only changing their hand position during the tests. Moreover, the cyclists were pedaling during the tests and the WT speed was set to 11.4 m/s, the maximum achievable by their WT. The drag results were then extrapolated for a speed of 15.6 m/s and 14.7 m/s respectively for male and female cyclists, and they were reported in terms of drag difference [N]. The four hand positions were defined as normal hand position (Fig. 31a), thumbs inside (Fig. 31b), fist grip (Fig. 31c) and arrow grip (Fig. 31d). The normal hand position was used as reference. Placing the thumbs inside, a higher drag was measured for four of the eight cyclists while a significantly lower drag was measured only for one cyclist (−1.09 N). Using the fist grip and arrow hand positions, no cyclists experienced a higher drag than with the normal hand position, several did not experience any significant drag differences whereas a drag reduction was achieved for three and four athletes, respectively: between 0.03 N and 0.19 N for the fist grip hand position and between 0.30 N and 1.17 N for the arrow hand position that came out as the best position among the four tested.

The last aspect investigated about handlebar aerodynamics is the cross-sectional shape, as done by Wurnitsch et al. (2010). Their aim was the design of a custom TT handlebar, developed starting from measurements of the upper limb muscular activity with the cross-sectional profile chosen according to the results of numerical simulations. These simulations were performed using a 2D potential flow method coupled with boundary layer equations on four possible handlebar cross-sectional shapes: Van de Vooren, NACA 16-033, Newman and wedge profiles (Fig. 32a). The lowest aerodynamic drag was achieved by the NACA 16-033 profile, respectively 2%, 6% and 20% lower than Van de Vooren, Newman and wedge profiles. The NACA profile was therefore used for the final design of a custom TT handlebar (Fig. 32b).

4.4. Other equipment

From the early 1980s, some TT bicycles have been designed taking into account also the aerodynamic behavior of small components, like cables, pedals and water bottles. Two examples were the Gitane Profil TT bicycle in 1980 (Cycles Gitane, 1980) and the aerodynamic Schauff developed between 1979 and 1980, and used for races in 1981 (US patent Des. 269,962 filed in 1980 by Hans Schauff).

The Gitane Profil was one of the first TT bicycles tested by means of WT tests. These tests allowed to discriminate between bicycle components in terms of aerodynamic drag reduction. The tubes, including the seat post, were elongated and not circular for aerodynamic purposes. Furthermore cables were concealed inside the frame and the handlebar (Fig. 33a), the front breaks were placed behind the fork (Fig. 33a) and the bicycle was equipped with an aerodynamic water bottle (Fig. 33b). Moreover fillets were carefully brazed to obtain a smooth transition between the tubes.

The aerodynamic Schauff was also tested in a WT, see Fig. 27a in Subsection 4.3. This bicycle had a streamlined-shaped handlebar, see Fig. 28c in Section 4.3, internal cables and both front and rear brakes placed behind the fork and the seat-stays, respectively (Figs. 28c and 34a). Moreover the bicycle had an aerodynamic appendix behind the seat tube near the saddle (Fig. 34a).

In 1980, Shimano produced a new group-set where each bicycle component was aerodynamically optimized by frontal area reduction and/or streamlining (Shimano, 1980). For example, Fig. 34b and c show their 1980 aerodynamic free-hub, aero-bottle, derailleurs and pedals. However, this group-set did not become popular and it was discontinued few years after its first production (Kyle, 2001), despite its claimed superior aerodynamic performance. The aerodynamic studies in late 1970s and early 1980s were indeed often not taken in serious consideration and only after 1984, aerodynamics succeeded in achieving a breakthrough in cycling (Hinault and Genzling, 1988). That year, Moser realized the new world hour record (51,151 m) and the USA cycling team raced in the Olympic Games with aerodynamic bicycles, winning 9 out of 24 medals in the cycling competitions, although it should be mentioned that the Soviet Union and former Eastern bloc countries such as the DDR (East Germany) boycotted those Olympic Games.

The aerodynamic influence of small components was also studied by Kyle during the development of the so called “funny bicycle”, used by the USA team in the Olympic Games of 1984. Kyle and Burke (1984) and Kyle (1998b, 1995a) provided tables with the drag reduction/increase obtained by changing large bicycle elements like wheels, helmets and frames but also by changing small elements like pedals and water bottles. In each table, only the speed of 48 km/h was specified, while no information was given about the reference drag of the combined cyclist-bicycle system, the bicycle used and the cyclist position. With the scope of giving a reference value to the readers, the present authors report that in Kyle and Burke (1984) and Kyle (1998b, 1995a), drag values of about 31 N–36 N were measured at 48 km/h for a cyclist on a “standard” track bicycle, thus not a prototype bicycle. Using an aerodynamic crank together with a single front full-disc sprocket 52T reduced the drag by 0.14 N and by 0.21 N compared to a standard crank with a single sprocket 52T or a set of two standard sprockets 42T/52T, respectively. Replacing the standard water bottle with an aero water bottle further reduced the drag (0.13 N) and also replacing standard shifters with aero shifters gave an aerodynamic advantage (0.08 N). Note that shifters were still located on the downtube and not on the handlebar and that finger-tip shifters should provide further advantages in terms of drag reduction. Removal of all cables also provided advantages in terms of aerodynamic drag: the drag of isolated cables in crossflow was found to be 0.16 N/m while the drag of sheathed cables (5 mm diameter), i.e. the cables together with the cable housing, was 0.50 N/m in crossflow. In addition to the aforementioned aerodynamic improvements, several other suggestions were provided by Kyle (1995a) to reduce the drag of small details: wheel-mounting nuts should be recessed into the tubes or rounded, bolts or quick-release systems should be eliminated and joints between different frame components should include fillets to smoothen the airflow around them.

A smooth bicycle shape without joints is achievable when creating a bicycle as a single monocoque, thus a single shell frame. An example is the 1992 monocoque frame bicycle used by Boardman (Fig. 35a and Fig. 20a in Subsection 4.1). This bicycle had a mono-blade fork: it used a single blade to connect the frame and the wheel, instead of the common forks with two legs (Hill, 1993). In addition the mono-blade fork had an airfoil-shape. A quantification of the drag reduction due to this single element was not provided, however it can reasonably be argued that using one single blade

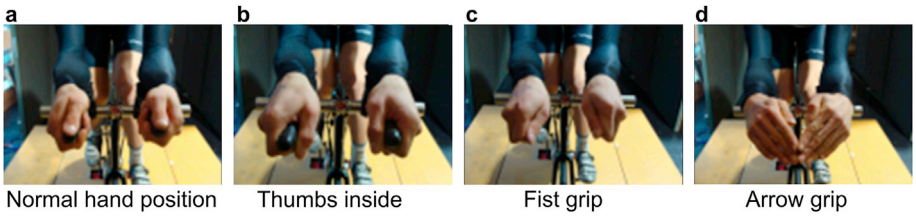

Fig. 31. (a) Normal hand position; (b) Thumbs inside; (c) Fist grip; (d) Arrow grip (adapted from Underwood and Jermy, 2010; reproduced with permission from Elsevier).

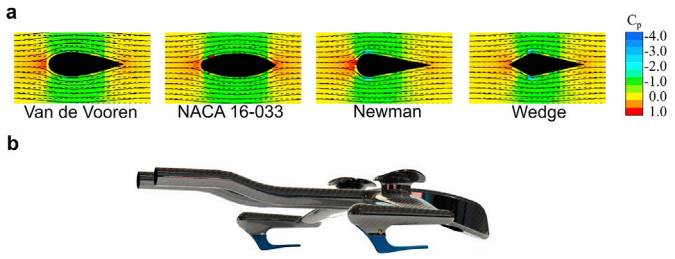

Fig. 32. (a) Different handlebar horizontal tube profiles analyzed (adapted from Wurnitsch et al., 2010); (b) Optimized handlebar design (source: Wurnitsch et al., 2010; reproduced with permission from Elsevier).

instead of a fork with two legs should provide a considerable reduction in the aerodynamic drag since the flow is less disturbed due to the absence of one fork's leg. However, single-leg fork bicycles were not new, actually one of the first examples of such as bicycle was the "Invincible" Safety of Surrey Machinists Co. in 1888 (Sharp, 1896) (Fig. 35b), although aerodynamic performance was likely not a target here.

The fork shape is also important for the overall aerodynamic characteristics of the bicycle. Martin and Cobb (2002) found that streamlined tubes are aerodynamically efficient not only for the frame, but also for the forks. Forks with airfoil-shaped legs reduced the drag of the cyclist-bicycle combination by 2.5% compared to that of a cyclist riding a bicycle equipped with a fork consisting of oval-shaped legs. On the other hand, oversized circular-shaped fork legs had a drag that was about 2.3% higher than oval-shaped fork legs.

Another important aerodynamic detail is the space between the fork and the front wheel, since the fork can be placed farther away from the wheel or closer to the wheel. Placing it farther away from the wheels was used for example by the UK team in the Olympic Games in 2012 (Boardman, 2015), whereas placing it closer was chosen for the bicycle used in the 2015 world hour record achievement by Wiggins (Cicli Pinarello Spa, 2015). The latter is described in a white paper of the manufacturing company, which states that a fork closer to the wheel generated less drag force for their bicycle (Cicli Pinarello Spa, 2015). It should be noted that this publication and the results reported in it were not peer reviewed and it refers to only one bicycle and one set of disc wheels. The present authors argue that a different behavior might likely be observed with different wheel types, e.g. disc or spoked wheels. Further CFD simulations and/or WTs tests with different bicycles and wheels are therefore needed to understand the flow topology resulting from the interaction between wheel and fork and its effects on the aerodynamic performance.

In the last few years, there has also been a transition from rim brakes to disc brakes. The presence of a new element attached to the bicycle frame opens room to designers to aerodynamically optimize the interaction between these brakes, the wheels and the frame. An example from an internal

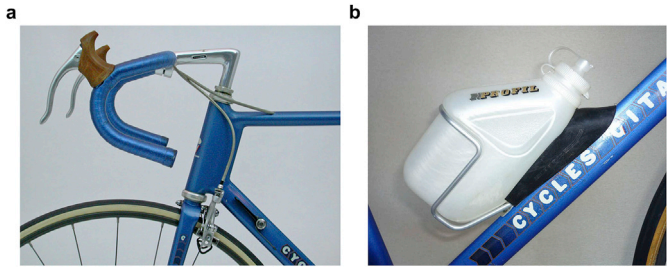

Fig. 33. (a) Gitane Profil with front breaks placed behind the fork and cables concealed inside the frame (reproduced with permission from "www.speedbicycles.ch"); (b) Gitane Profil with aerodynamic water bottle (reproduced with permission from "http://www.velocompetition.com").

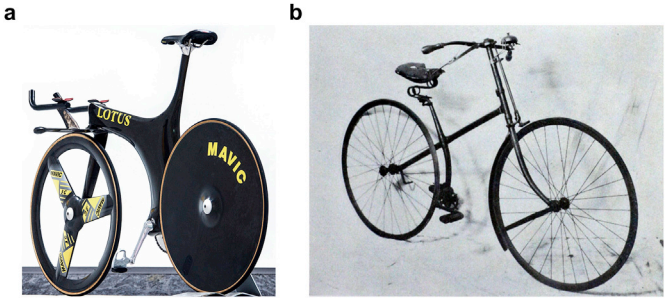

Fig. 35. (a) Bicycle with monocoque frame and mono-blade fork in the bicycle used by Boardman in the Olympic Games in 1992 (reproduced with permission from "father_TU/Flickr"); (b) Single-leg fork used in the "Invincible" safety bicycle of Surrey Machinists Co., dated 1888 (reproduced with permission from Grace's Guide to British Industrial History, 2016).

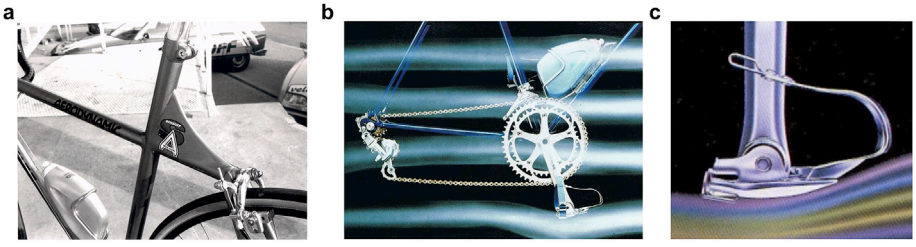

Fig. 34. (a) Aerodynamic appendices behind the seat tube in the aerodynamic Schauff bicycle (reproduced with permission from Schauff); (b) Shimano first aerodynamically optimized group-set (source: Shimano catalogue 1980); (c) Detail of the aerodynamically optimized pedal by Shimano (source: Shimano catalogue 1981).

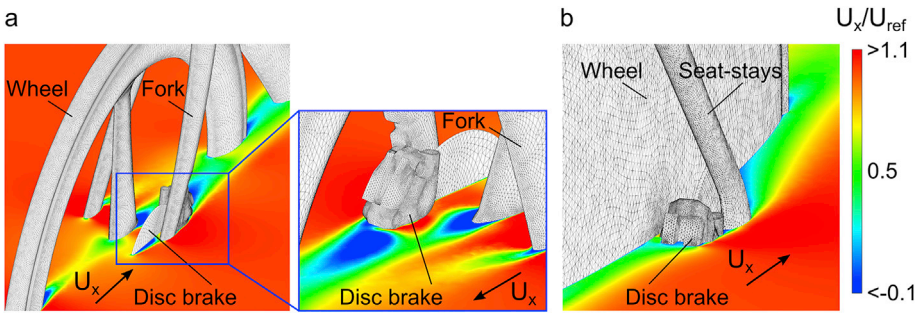

Fig. 36. Contours of streamwise velocity U_x in a horizontal plane showing the interaction between disk brakes, frame and wheels.

CFD study for a contemporary leading bicycle manufacturer is shown in Fig. 36.

5. Summary, conclusions and future perspectives

The present review paper addresses cycling aerodynamics with primary focus on the racing bicycle and its main components, both from an historical perspective and from a quantitative point of view. It consists of three parts. In the first part, a brief history of the bicycle is provided, from the first bicycle, the so-called "Draisienne" in 1817, to the commonly accepted first modern bicycle, "the Rover Safety" in 1885. The second part presents both the mathematical models that describe the cycling physics, and the methods to assess the aerodynamic forces and moments, i.e. field tests, wind tunnel (WT) measurements and computational fluid dynamics (CFD) simulations. The last part focuses on the aerodynamics of the bicycle and its components, with subsections dealing with each main bicycle element, frame, wheels and handlebar, and a subsection describing the aerodynamics of small bicycle elements, such as cable, forks and water bottles. In each subsection the historical evolution of each component is first presented, with references to relevant records and important achievements. Next, the actual state-of-the-art is discussed. The aerodynamics of a cyclist and its wearable equipment, like skinsuits and helmets, and the impact of drafting on cycling performance will be treated in a follow-up paper of the present review paper.

In summary, the aerodynamic drag is of major importance in cycling since it is the major resistive force, up to 90%, for cyclists riding on flat terrain at high speeds. The present paper shows that already in the late 1890s and early 1900s a certain degree of knowledge – mainly empirical – was present about the impact of aerodynamics on cycling: the first cycling mathematical models were available (Bourlet, 1894), and a first aerodynamic improvement phase included the first recumbent bicycles and streamlined enclosures for bicycles that were designed in 1895 and in 1913, respectively, and disc wheels, fours spoke wheels and dropped handlebar were available around the 1890s. In addition, there were races where cyclists drafted in the wake of multi-tandem bicycles, motorcycles or trains already in late 1800s, in which the cyclists reached speeds beyond 100 km/h. However, to the best of authors knowledge, noteworthy aerodynamic innovations did not occur in cycling after the UCI non-recognized world hour record of Faure in 1939 (50,537 m in 1 h), achieved driving a recumbent bicycle with a streamlined enclosure, and up to the 1970s, albeit that the first WT tests on cyclist reduced-scale models and real cyclists were already performed in the 1950s. The latter tests quantitatively showed the impact of aerodynamics in cycling.

A second bicycle aerodynamic improvement phase started in the late 1970s and early 1980s, with the first streamlined tubes used for bicycle frames, streamlined handlebars mounted at different positions along the head tube, aerodynamic water bottles and concealed cables. This rediscovery of the influence of cycling aerodynamics culminated with the world hour record of Moser in 1984, achieved on a bicycle tested in a WT and equipped with a pair of modern disc wheels. As stated by Hinault and Genzling (1988): "*It wasn't until Francesco Moser broke the world hour record in 1984 on a bicycle with sloping frame and disk wheels that aerodynamic studies on cyclists were taken seriously*". Since then, the aerodynamic research in cycling has increased rapidly, year after year, despite the introduction of UCI rules aimed at preserving the bicycle appearance and limiting the role of innovation and technology in cycling performance (Kyle, 2001; Schmitz, 1990).

One of the bicycle components that has been most regulated is the frame. The frame is the core constituent of a bicycle. In the 1990s, monocoque bicycle frames were introduced, which not only significantly improved the aerodynamic performance of the bicycle but also drastically changed the bicycle shape. The latter pushed the UCI to ban them in 2000 by enforcing the use of diamond-frames, although a moderate use of aerodynamic shapes for the tubes was and is still allowed. While the UCI rules provide constraints regarding the frame of the bicycle, they still leave ample room for aerodynamic optimization of the bicycle. The drag of the frame can still be further reduced varying the tubes shape, length and angles, albeit the aerodynamic optimization should not be done at the expenses of the cyclist biomechanical efficiency, which is linked with the capability of a cyclist to produce power.

A second main component of the bicycle whose aerodynamics has been largely studied is the wheel. Studies are often not limited to a single yaw condition, zero degrees, but also to other yaw conditions, so the impact of crosswinds on wheel aerodynamics can be assessed. The crosswind might generate the so called "sail effect", i.e. the generation of a lift force with a component on the wheel streamwise direction: this lift component helps reducing the drag force acting on the wheel streamwise direction. This effect is more pronounced for disc wheels, tri-spoke wheels and spoked wheels with deep-rim. On the other hand, the side force is generally higher for these type of wheels and may cause turning instabilities and difficulties for the cyclist to ride straight. Moreover, lowering the number of spokes and decreasing the tire width have a beneficial impact on the aerodynamic drag, thus the performance of the cyclist. Therefore the aerodynamic optimization of the wheel needs to consider not only the aerodynamic drag, but also the side force, the rotational and yawing moments at different yaw angles. However, large discrepancies are present in the results from different studies, both experimental and computational, causing a reduction in confidence in the current testing and simulations methods. It is therefore necessary to define, for the wheel and the bicycle, protocols and guidelines to perform accurate and uniform WT tests and CFD simulations, so results from different researchers and manufacturers can be better compared. Future research would also benefit from comparisons between results of CFD simulations and detailed flow field measurements obtained in WT tests. Additional field measurements would also help the transfer of knowledge, gained in a controlled environment such as in WT tests and CFD simulations, to the real world, where environmental conditions like the wind play an important role.

The standard practice in WT tests and CFD simulations of wheel aerodynamics is to focus on an isolated wheel. The term isolated refers to the absence of the frame but with the inclusion of a slender support structure in WT tests, and with potential presence of a nearby flat surface, roller or rolling belt representing the ground. On the one hand, this focus on isolated wheels is justified because testing the wheels together with

the rest of the bicycle and the rider will unavoidably render the results on wheel performance dependent on the bicycle and on the rider, which complicates a clear inter-comparison of different wheels. A uniform WT testing and CFD simulation methodology should also be clear and not unnecessary complicated, which advocates tests that do not include the bicycle, let alone the rider. On the other hand, the final goal is the drag reduction of the whole system of the bicycle – including all components. Therefore, both types of WT tests and CFD simulations are necessary. Future research and development should focus on uniform and unambiguous testing methodologies but also on more integrated assessments using with WT testing, CFD and field testing.

Also for other components like the handlebar, the impact of the aerodynamics should not only be assessed on the bare bicycle, given that besides the direct aerodynamic impact of the handlebar on the total cyclist-bicycle drag, there is a – large – indirect contribution on the total drag due to its interaction with the cyclist position: a different handlebar might enable the cyclist to keep a more aerodynamic position on the bicycle. Therefore studies on handlebar aerodynamics are intrinsically connected with the aerodynamics of the cyclist position, nevertheless handlebar shape optimization might still bring aerodynamic gains useful to improve the performance of elite cyclists. In writing this review paper, the authors have also observed difficulties to present generalized results that could apply to all the cyclists about the optimal aerodynamic configuration for aero-bars: elite cyclists need personalized handlebars, thus they need to be either personally tested in a WT or 3D scanned so that a 3D printed model can be realized and tested in a WT or the 3D scan used in a CFD simulation. Future studies should also analyze a large sample of cyclists and try to find correlations between the handlebar position and cyclist anthropometric quantities such as height and arm length.

Small bicycle components can also provide aerodynamic gains which can help elite cyclists to further improve their performance. However, the aerodynamic impact of these small elements might be difficult to measure in a WT as the drag differences between different versions of the same small bicycle component can reside within the measuring accuracy of the force balances. On the other hand, CFD simulations enable the computation of the drag caused by each bicycle element, therefore CFD simulations have the potential to provide further insights in the aerodynamic optimization of small bicycle equipment.

This review has shown that by far most previous quantitative and published studies were performed by WT tests, and that field testing and CFD appeared less often used. However, it should be noted that this review and therefore also this view is mainly based on published information provided in books, journal articles and proceedings of international conferences. It is well-known that field testing is intensively applied in practice, as well as wind tunnel testing, while CFD is much less often used. CFD holds considerable advantages but also considerable disadvantages, and both must be carefully weighed against each other for every specific project. CFD does provide whole-flow field data and therefore provides the largest degree of physical insight in the aerodynamic behavior of the bicycle and its components, as mentioned above. On the other hand, CFD for bicycle aerodynamics is very time-consuming and prone to error. The correct reproduction of separation and reattachment lines, vortex shedding and associated phenomena require very high near-wall grid resolutions and advanced turbulence modelling. The grids should generally contain wall-adjacent cells with sizes down to 0.020 mm (Blocken et al., 2018a, 2018b). This implies that a computational grid for a single bicycle easily contains several tens of millions of computational cells. These stringent grid requirements in combination with the large sensitivity of the CFD results to the wide range of computational parameters that have to be chosen by the user call for the establishment of specific CFD best practice guidelines for bicycle aerodynamics, similar to those that have been developed for other aerodynamics applications in the past two decades, such as building aerodynamics (Blocken, 2015; Blocken and Gualtieri, 2012; Franke et al., 2007, 2010; Tominaga et al., 2008) and automotive external aerodynamics (Lanfrit, 2005).

The complexity of bicycle aerodynamics does not only entail difficulties in terms of WT tests, CFD simulations, field testing and practical design considerations. It also provides continuing challenges and opportunities, as this complexity and the many degrees of design freedom that remain leave ample room for further aerodynamic innovations and improvements.

Declaration of competing interest

The authors declare that they have no known competing financial interests or personal relationships that could have appeared to influence the work reported in this paper.

CRediT authorship contribution statement

Fabio Malizia: Conceptualization, Investigation, Writing - original draft, Writing - review & editing, Visualization, Funding acquisition. **Bert Blocken:** Conceptualization, Writing - review & editing, Supervision, Funding acquisition.

Acknowledgements

During the work on this paper the first author has been employed sequentially by KU Leuven in Belgium and by Eindhoven University of Technology (TU/e) in the Netherlands. He expresses his gratitude to VLAIO (Flemish Agency for Innovation and Entrepreneurship) for the PhD scholarship (dossier nr. IWT.141701) for his work at KU Leuven. The authors thank Team Jumbo-Visma and ANSYS CFD for the partnership in cycling aerodynamics that has inspired parts of this paper. The authors also thank the Groupama-FDJ cycling team and Lapierre Bikes for the collaboration in bicycle aerodynamics that has equally inspired parts of this paper. The authors are grateful to all the photographers, manufacturers and online libraries for providing copyright permission to reproduce their photos. The authors are also very grateful to the anonymous reviewers for their very valuable and constructive comments on this paper.

References

Abbott, A.V., Wilson, D.G., 1995. Human-Powered Vehicles. Human Kinetics Publishers, Champaign, IL, USA.

AIAA, 1998. Guide for the verification and validation of computational fluid dynamics simulations. In: AIAA G-077-1998, AIAA Standards, vol. 77. American Institute of Aeronautics and Astronautics, Inc., Reston (VA).

Alam, F., Chowdhury, H., Elmir, Z., Sayogo, A., Love, J., Subic, A., 2010. An experimental study of thermal comfort and aerodynamic efficiency of recreational and racing bicycle helmets. Procedia Eng. 2, 2413–2418.

Anderson, J.D.J., 1997. A History of Aerodynamics. Cambridge University Press, Cambridge.

Anderson, J.D.J., 1984. Fundamentals of Aerodynamics. McGraw-Hill Higher Education.

Apelt, C.J., West, G.S., Szewczyk, A.A., 1975. The effects of wake splitter plates on, and the flow past, a circular cylinder in the range $10^4<Re<5x10^4$, part II. J. Fluid Mech. 71, 145–160.

Apelt, C.J., West, G.S., Szewczyk, A.A., 1973. The effects of wake splitter plates on, and the flow past, a circular cylinder in the range $10^4<Re<5x10^4$, part I. J. Fluid Mech. 61, 187–198.

Baldissera, P., 2017. Proposal of a coast-down model including speed dependent coefficients for the retarding forces. Proc. Inst. Mech. Eng. P J. Sports Eng. Technol. 231, 154–163.

Barlow, J.B., Rae, W.H., Pope, A., 1999. Low-Speed Wind Tunnel Testing. John Wiley & Sons, Inc.

Barry, N., Burton, D., Crouch, T., Sheridan, J., Luescher, R., 2012. Effect of crosswinds and wheel selection on the aerodynamic behavior of a cyclist. Procedia Eng. 34, 20–25.

Barry, N., Burton, D., Sheridan, J., Thompson, M., Brown, N.A.T., 2016. Flow field interactions between two tandem cyclists. Exp. Fluid 57, 1–14.

Barry, N., Burton, D., Sheridan, J., Thompson, M., Brown, N.A.T., 2015. Aerodynamic performance and riding posture in road cycling and triathlon. Proc. Inst. Mech. Eng. P J. Sports Eng. Technol. 229, 28–38.

Belloli, M., Cheli, F., Bayati, I., Giappino, S., Robustelli, F., 2014. Handbike aerodynamics : wind tunnel versus track tests. Procedia Eng. 72, 750–755.

Blocken, B., 2018. LES over RANS in building simulation for outdoor and indoor applications: a foregone conclusion? Build. Simul. 11, 821–870.

Blocken, B., 2015. Computational Fluid Dynamics for urban physics: importance, scales, possibilities, limitations and ten tips and tricks towards accurate and reliable simulations. Build. Environ. 91, 219–245.
Blocken, B., 2014. 50 years of computational wind engineering: past, present and future. J. Wind Eng. Ind. Aerod.
Blocken, B., Gualtieri, C., 2012. Ten iterative steps for model development and evaluation applied to computational fluid dynamics for environmental fluid mechanics. Environ. Model. Software.
Blocken, B., van Druenen, T., Toparlar, Y., Andrianne, T., 2018a. Aerodynamic analysis of different cyclist hill descent positions. J. Wind Eng. Ind. Aerod. 181, 27–45.
Blocken, B., van Druenen, T., Toparlar, Y., Malizia, F., Mannion, P., Andrianne, T., Marchal, T., Maas, G.-J., Diepens, J., 2018b. Aerodynamic drag in cycling pelotons: new insights by CFD simulation and wind tunnel testing. J. Wind Eng. Ind. Aerod. 179, 319–337.
Boardman, C., 2015. The biography of the modern bike. Cassell.
Bouny, É., 1899. Étude expérimentale du coup de pédale. Paris.
Bourlet, C., 1894. Traité des bicycles et bicyclettes. Gauthier-Villars et fils, Paris.
Brownlie, L., Aihara, Y., Carbo, J., Harber, E., Henry, R., Ilcheva, I., Ostafichuk, P., 2016. The use of vortex generators to reduce the aerodynamic drag of athletic apparel. In: 11th Conf. Int. Sport. Eng. Assoc. ISEA 2016, vol. 147, pp. 20–25.
Brownlie, L., Kyle, C., Carbo, J., Demarest, N., Harber, E., MacDonald, R., Nordstrom, M., 2009. Streamlining the time trial apparel of cyclists: the Nike swift spin project. Sports Technol. 2, 53–60.
Brownlie, L., Ostafichuk, P., Tews, E., Muller, H., Briggs, E., Franks, K., 2010. The wind-averaged aerodynamic drag of competitive time trial cycling helmets. Procedia Eng. 2, 2419–2424.
Brownlie, L.W., 2019. Wind tunnels: design considerations in wind tunnel testing of cyclists. In: Pallis, J.M., McNitt-Gray, J.L., Hung, G.K. (Eds.), Biomechanical Principles and Applications in Sports. Springer, Cham, pp. 57–86.
Burns, S.P., Sullivan, J.P., 1995. Aerodynamic of the rider bicycle combination. Cycl. Sci. 8–10, 22–23.
Burrows, M., Hadland, T., 2008. Bicycle Design. Snowbooks.
Candau, R.B., Grappe, F., Ménard, M., Barbier, B., Millet, G.Y., Hoffman, M.D., Belli, A.R., Rouillon, J.D., 1999. Simplified decelearation method for assessment of resistive forces in cycling. Med. Sci. Sports Exerc. 1441–1447.
Capelli, C., Rosa, G., Butti, F., Ferretti, G., Veicsteinas, A., Di Prampero, P., 1993. Energy cost and efficiency of riding aerodynamics bicycles. Eur. J. Appl. Physiol. 67, 144–149.
Capelli, C., Schena, F., Zamparo, P., Dal Monte, A., Faina, M., Di Prampero, P.E., 1998. Energetics of best performances in track cycling. Med. Sci. Sports Exerc. 30, 614–624.
Casa, D.J., 1999. Exercise in the heat. I. Fundamentals of thermal physiology, performance implications, and dehydration. J. Athl. Train. 34, 246–252.
Casey, M., Wintergerste, T., 2000. ERCOFTAC - Special Interest Group on "Quality and Trust in Industrial CFD" - Best Practice Guidelines. European Research Community on Flow, Turbulence and Combustion.
Chabroux, V., Mba, M.N., Sainton, P., Favier, D., 2010. Wake characteristics of time trial helmets using PIV-3C technique. Techniques, 05–08.
Chowdhury, H., Alam, F., Subic, A., 2010. Aerodynamic performance evaluation of sports textile. Procedia Eng. 2, 2517–2522.
Cicli Pinarello Spa, 2015. Pinarello Bolide Hr White Paper 1.0 ©, pp. 1–11.
Cooper, K., 1998. Bluff-Body Blockage Corrections In Closed- And Open-Test-Section Wind Tunnels. Agard Ag-336 6.
Cooper, K.R., 2012. SAE Wind Tunnel Test Procedure for Trucks and Buses.
Cooper, K.R., 2003. Truck Aerodynamics Reborn - Lessons from the Past.
Crane, R., Morton, C., 2018. Drag and side force analysis on bicycle wheel-tire combinations. J. Fluids Eng. Trans. ASME 140, 1–8.
Crosetti, M., 2014. Una bici oltre i confini e Moser fece il marziano, il suo record ha 30 anni. La Repubb.
Crouch, T.N., Burton, D., Brown, N.A.T., Thompson, M.C., Sheridan, J., 2014. Flow topology in the wake of a cyclist and its effect on aerodynamic drag. J. Fluid Mech. 748, 5–35.
Crouch, T.N., Burton, D., LaBry, Z.A., Blair, K.B., 2017. Riding against the wind: a review of competition cycling aerodynamics. Sports Eng. 20, 81–110.
Crouch, T.N., Burton, D., Thompson, M.C., Brown, N.A.T., Sheridan, J., 2016. Dynamic leg-motion and its effect on the aerodynamic performance of cyclists. J. Fluid Struct. 65, 121–137.
Cummings, A., 1997. Cycling in the wind. Eur. J. Phys. 18, 176–179.
Cycles Gitane, 1980. Bernard Hinault présente la gamme des cycles Gitane.
Dahn, K., Mai, L., Poland, J., Jenkins, C., 1991. Frictional resistance in bicycle wheel bearings. Cycl. Sci. 3, 28–32.
Dal Monte, A., 1988. Streamlined wheel for bicycle, 4, 732,428.
Dal Monte, A., Leonardi, L.M., Menchinelli, C., Marini, C., 1987. A new bicycle design based on biomechanics and advanced technology. Int. J. Sport Biomech. 287–292.
Dal Monte, A., Martini, A., Antonini, G., Garbelli, D., Cinelli, C., 1983. Ciclismo ed aerodinamica. In: Scuola Dello Sport CONI.
Debraux, P., Grappe, F., Manolova, A.V., Bertucci, W., 2011. Aerodynamic drag in cycling: methods of assessment. Sports BioMech. 10, 197–218.
Defraeye, T., Blocken, B., Koninckx, E., Hespel, P., Carmeliet, J., 2010a. Computational fluid dynamics analysis of cyclist aerodynamics: performance of different turbulence-modelling and boundary-layer modelling approaches. J. Biomech. 43, 2281–2287.
Defraeye, T., Blocken, B., Koninckx, E., Hespel, P., Carmeliet, J., 2010b. Aerodynamic study of different cyclist positions: CFD analysis and full-scale wind-tunnel tests. J. Biomech. 43, 1262–1268.
Defraeye, T., Blocken, B., Koninckx, E., Hespel, P., Carmeliet, J., 2011. Computational fluid dynamics analysis of drag and convective heat transfer of individual body segments for different cyclist positions. J. Biomech. 44, 1695–1701.
Defraeye, T., Blocken, B., Koninckx, E., Hespel, P., Verboven, P., Nicolai, B., Carmeliet, J., 2014. Cyclist drag in team pursuit: influence of cyclist sequence, stature, and arm spacing. J. Biomech. Eng. 136, 1–9.
di Prampero, P.E., Cortili, G., Mognoni, P., Saibene, F., 1979. Equation of motion of a cyclist. J. Appl. Physiol. 47, 201–206.
Drais, K., 1817. LODA, eine neu erfundene Fahrmaschine. Badwochenblatt für die Großherzogliche Stadt Bad.
Drais, K., 1816. Ein Wagen, der ohne Pferde läuft, erfunden von dem Freiherrn von Drais in Mannheim. Neues Mag.
Earl of Albemarle, Hillier, G.L., 1896. Cycling, fifth ed. Longmans, Green, and Co., London and Bombay.
Edwards, A.G., Byrnes, W.C., 2007. Aerodynamic characteristics as determinants of the drafting effect in cycling. Med. Sci. Sports Exerc. 39, 170–176.
Edwards, E., 1986. Aerodinamic Stability of Front Disc Wheels.
ESDU, 1980. Blockage Corrections for Bluff Bodies in Confined Flows, March 1998. Engineering Sciences Data Unit.
Faria, E.W., Parker, D.L., Faria, I.E., 2005a. The science of cycling: physiology and training - Part 1. Sports Med. 35, 285–312.
Faria, E.W., Parker, D.L., Faria, I.E., 2005b. The science of cycling: factors affecting performance - Part 2. Sports Med. 35, 313–337.
Ferretti, G., 2015. Energetics of Muscular Exercise, Energetics of Muscular Exercise.
Fintelman, D.M., Hemida, H., Sterling, M., Li, F.X., 2015. CFD simulations of the flow around a cyclist subjected to crosswinds. J. Wind Eng. Ind. Aerod. 144, 31–41.
Fischer, O., 2017. Investigation of Correction Methods for Interference Effects in Open-Jet Wind Tunnels. Springer Vieweg.
Fitzgerald, S., Kelso, R., Grimshaw, P., Warr, A., 2019. Measurement of the air velocity and turbulence in a simulated track cycling team pursuit race. J. Wind Eng. Ind. Aerod. 190, 322–330.
Flanagan, M.J., 1996. Considerations for data quality and uncertainty in testing of bicycle aerodynamics. Cycl. Sci. 7–10, 22.
Fonda, B., Šarabon, N., 2012. Biomechanics and energetics of uphill cycling: a review. Kinesiology 44, 5–17.
Franke, J., Hellsten, A., Schlünzen, H., Carissimo, B., 2010. The best practise guideline for the CFD simulation of flows in the urban environment : an outcome of COST 732. In: The Fifth International Symposium on Computational Wind Engineering (CWE2010), pp. 1–10.
Franke, J., Hellsten, A., Schlünzen, H., Carissimo, B., 2007. Best Practice Guideline for the CFD Simulation of Flows in the Urban Environment. COST action 732.
García-López, J., Rodríguez-Marroyo, J.A., Juneau, C.-E., Peleteiro, J., Martínez, A.C., Villa, J.G., 2008. Reference values and improvement of aerodynamic drag in professional cyclists. J. Sports Sci. 26, 277–286.
Genta, G., Morello, L., 2009. The Automotive Chassis - Volume 2: System Design. Springer.
Giacomelli, R., 1930. The aerodynamics of Leonardo da Vinci. J. R. Aeronaut. Soc. 34, 1016–1038.
Giappino, S., Omarini, S., Schito, P., Somaschini, S., Belloli, M., Tenni, M., 2018. Cyclist aerodynamics: a comparison between wind tunnel tests and CFD simulations for helmet design. In: In-Vento 2018: XV Conference of the Italian Association for Wind Engineering, Naples (Italy).
Gibertini, G., Campanardi, G., Guercilena, L., Macchi, C., 2010. Cycling aerodynamics: wind tunnel testing versus track testing. IFMBE Proc. 31, 10–13. IFMBE.
Gibertini, G., Grassi, D., 2008. Cycling aerodynamics. In: Nørstrud, Helge (Ed.), Sport Aerodynamics. Springer, Vienna, pp. 23–48.
Godo, M., Corson, D., Legensky, S., 2010. A comparative aerodynamic study of commercial bicycle wheels using CFD. In: 48th AIAA Aerosp. Sci. Meet. Incl. New Horizons Forum Aerosp. Expo, vol. 35, pp. 1–31.
Godo, M.N., Corson, D., Legensky, S.M., 2009. An aerodynamic study of bicycle wheel performance using CFD. In: 47th AIAA Aerosp. Sci. Meet. Incl. New Horizons Forum Aerosp. Expo, pp. 1–21, 12065.
Godo, M.N., Corson, D., Legensky, S.M., Manager, F.P., Analyst, S., Park, C., Manager, G., 2011. A Practical Analysis of Unsteady Flow Around a Bicycle Wheel, Fork and Partial Frame Using CFD, pp. 1–25.
Grace's Guide to British Industrial History, 2016. Surrey machinist Co [WWW Document]. https://gracesguide.co.uk/Surrey_Machinist_Co, 6.17.19.
Grappe, F., Candau, R., Belli, A., Rouillon, J.D., 1997. Aerodynamic drag in field cycling. Ergonomics 40, 1299–1311.
Greenwell, D.I., Wood, N.J., Bridge, E.K.L., Addy, R.J., 1995. Aerodynamic characteristics of low-drag bicycle wheels. Aeronaut. J. 99, 109–120.
Griffith, M.D., Crouch, T.N., Thompson, M.C., Burton, D., Sheridan, J., Brown, N.A.T., 2014. Computational fluid dynamics study of the effect of leg position on cyclist aerodynamic drag. J. Fluids Eng. Trans. ASME 136, 1–9.
Griffith, M.D., Crouch, T.N., Burton, D., Sheridan, J., Brown, N.A.T., Thompson, M.C., 2019. A numerical model for the time-dependent wake of a pedalling cyclist. Proc. Inst. Mech. Eng. P J. Sports Eng. Technol.
Gronen, W., Lemke, W., 1987. Geschichte des Radsports. Fuchs-Druck und Verlag.
Guye, C.E., 1893. Moyen de déterminer expérimentalement le travail effectué par un vélocipédiste. La Nat 1039, 346–347.
Hadland, T., Lessing, H.-E., 2014. Bicycle Design. The MIT Press, Cambridge, Massachusetts.
Hagberg, J.M., McCole, S.D., 1990. The effect of drafting and aerodynamic equipment on the energy expenditure during cycling. Cycl. Sci.
Hanjalic, K., 2005. Will RANS survive LES? A view of perspectives. J. Fluid Eng. 127, 831.
Hanna, R.K., 2002. Can CFD make a performance difference in Sport ?. In: 4th Int. Conf. Eng. Sport, pp. 17–30.
Harder, P., Cusack, D., Matson, C., Lavery, M., 2010. Airfoil Development for the Trek Speed Concept Triathlon Bicycle.

Hed, S.A., Haug, R.B., 1991. Bicycle Rim and Wheel, vol. 5, 061,013.
Heijmans, J., Mallon, B., 2011. Historical Dictionary of Cycling. The Scarecrow Press Inc., Plymouth (UK).
Herlihy, D.V., 2004. Bicycle: the History. Yale Univ. Press, New Haven.
Hide, A.C., 1892. Wheel for velocipedes, 478,191.
Hill, R.D., 1993. The design and the development of the Lotus Sport pursuit bicycle. Proc. Inst. Mech. Eng. Part D J. Automob. Eng. 207, 285–294.
Hinault, B., Genzling, C., 1988. Road Racing: Technique & Training, English ed. Velo-news Corporation.
Hoerner, S.F., 1965. Fluid Dynamic Drag. Published by the author, New York (USA).
Hopkins, M.W., Principe, F.S., 1988. Vehicle wheel, 4,919,490.
Hopkins, M.W., Principe, F.S., Kelleher, K.J., 1990. Beyond materials: du Pont's aerodynamic bicycle wheel. In: 35th International SAMPE Symposium.
Íniguez-De-La-Torre, I., Íniguez, J., 2006. Cycling and wind: does sidewind brake? Eur. J. Phys. 27, 71–74.
Isvan, O., 1984. The effect of winds on a bicyclist's speed. Bike Technol. 1–6.
Jakeman, A.J., Letcher, R.A., Norton, J.P., 2006. Ten iterative steps in development and evaluation of environmental models. Environ. Model. Software 21, 602–614.
Jermy, M., Moore, J., Bloomfield, M., 2008. Translational and rotational aerodynamic drag of composite construction bicycle wheels. Proc. Inst. Mech. Eng. P J. Sports Eng. Technol. 222, 91–102.
Jeukendrup, A.E., Martin, J., 2001. Improving cycling performance: how should we spend our time and money. Sports Med. 31, 559–569.
Joyner, M.J., Coyle, E.F., 2008. Endurance exercise performance: the physiology of champions. J. Physiol. 586, 35–44.
Jux, C., Sciacchitano, A., Schneiders, J.F.G., Scarano, F., 2018. Robotic volumetric PIV of a full-scale cyclist. Exp. Fluid 59, 0.
Karabelas, S.J., Markatos, N.C., 2012. Aerodynamics of fixed and rotating spoked cycling wheels. J. Fluid Eng. 134, 011102.
Kawamura, T.M., 1953. Wind Drag of Bicycles. Tokyo.
Knupe, J., Farmer, D., 2009. Aerodynamics of High Performance Race Bicycle Wheels, pp. 1–15.
Kobayashi, K., 1993. Histoire du vélocipède de Drais à Michaux, 1817 - 1870: mythes et réalités. Tokyo.
Kyle, C.R., 2002. Selecting cycling equipment. In: Burke, E.R. (Ed.), High Tech Cycling. Human Kinetics Books, Champaign, IL, USA, pp. 1–48.
Kyle, C.R., 2001. Bicycle aerodynamics and the Union Cycliste Internationale: the conflict between technology and regulations. In: Transactions, 11th Cycling History Conference, Osaka, Japan, August 23-25, 2000. Vanderplas Publications, San Francisco, pp. 118–131.
Kyle, C.R., 1995a. Bicycle aerodynamics. In: Human-Powered Vehicles. Human Kinetics Publishers, Champaign, IL, USA, pp. 141–155.
Kyle, C.R., 1995b. Aero wheel performance. Cycl. Sci. 6–9, 20–21.
Kyle, C.R., 1991a. The effect of crosswinds upon time trials. Cycl. Sci. 51–56.
Kyle, C.R., 1991b. Wind tunnel tests of aero bicycles. Cycl. Sci. 3, 57–61.
Kyle, C.R., 1991c. New aero wheel tests. Cycl. Sci. 27–30.
Kyle, C.R., 1990. Wind tunnel tests of bicycle wheels and helmets. Cycl. Sci. 27–30.
Kyle, C.R., 1989. The aerodynamics of handlebars and helmets. Cycl. Sci. 22–25.
Kyle, C.R., 1988a. Sunraycer, wheels, tires and brakes. In: Lecture 3-3, G.M. Sunraycer Case History. Society of Automotive Engineers, Warrendale, Pennsylvania.
Kyle, C.R., 1988b. The mechanics and aerodynamics of cycling. In: Burke, E.R., Newsom, M.M. (Eds.), Medical and Scientific Aspects of Cycling. Human Kinetics Publishers, pp. 235–251.
Kyle, C.R., 1986a. Equipment design criteria for the competitive cyclist. In: Burke, E.R. (Ed.), Science of Cycling. Human Kinetics Books, Champaign, IL, USA, pp. 137–144.
Kyle, C.R., 1986b. Athletic Clothing. Sci. Am. 254, 104–110.
Kyle, C.R., 1979. Reduction of wind resistance and power output of racing cyclists and runners travelling in groups. Ergonomics 22, 387–397.
Kyle, C.R., Bassett, D.R.J., 2002. The cycling world hour record. In: Burke, E.R. (Ed.), High Tech Cycling. Human Kinetics Books, Champaign, IL, USA, pp. 175–196.
Kyle, C.R., Burke, E.R., 1984. Improving the racing bicycle. Mech. Eng. 34–45.
Kyle, C.R., Weaver, M.D., 2004. Aerodynamics of human-powered vehicles. Proc. Inst. Mech. Eng. Part A J. Power Energy 218, 141–154.
Lallement, P., 1866. Improvement in velocipedes, 59,915.
Lanfrit, M., 2005. Best Practice Guidelines for Handling Automotive External Aerodynamics with FLUENT. Version 1.2. Fluent Deutschl. GmbH Birkenweg 14a 64295 Darmstadt/Germany.
Launder, B.E., Spalding, D.B., 1974. The numerical computation of turbulent flows. Comput. Methods Appl. Mech. Eng. 3, 269–289.
Lennon, D.C., 1987. Bicycle and handlebar system, 4,750,754.
Lessing, H.-H., 2003a. Automobilität - Karl Drais und die unglaublichen Anfänge. Maxime Verlag, Leipzig.
Lessing, H.-H., 2003b. The velocipede of 1819 in America. Cycle Hist. 13.
Lessing, H.-H., 2001. What led to the invention of the early bicycle? Cycle Hist. 11.
Lessing, H.-H., 1996. Cycling or roller skating: the resistibler rise of personal mobility. Cycle Hist. 5.
Lukes, R.A., Chin, S.B., Haake, S.J., 2005. The understanding and development of cycling aerodynamics. Sports Eng. 8, 59–74.
Malizia, F., Blocken, B., 2020. CFD Simulations of an Isolated Cycling Spoked Wheel: Impact of the Ground and Wheel/ground Contact Modeling. Eur. J. Mech. / B Fluids 82. July–August, 21-38.
Malizia, F., Montazeri, H., Blocken, B., 2019. CFD simulations of spoked wheel aerodynamics in cycling: impact of computational parameters. J. Wind Eng. Ind. Aerod. 194.
Mannion, P., Toparlar, Y., Blocken, B., Clifford, E., Andrianne, T., Hajdukiewicz, M., 2018a. Aerodynamic drag in competitive tandem para-cycling: road race versus time-trial positions. J. Wind Eng. Ind. Aerod. 179, 92–101.
Mannion, P., Toparlar, Y., Blocken, B., Clifford, E., Andrianne, T., Hajdukiewicz, M., 2018b. Analysis of crosswind aerodynamics for competitive hand-cycling. J. Wind Eng. Ind. Aerod.
Mannion, P., Toparlar, Y., Blocken, B., Hajdukiewicz, M., Andrianne, T., Clifford, E., 2018c. Improving CFD prediction of drag on Paralympic tandem athletes: influence of grid resolution and turbulence model. Sports Eng. 21, 123–135.
Mannion, P., Toparlar, Y., Blocken, B., Hajdukiewicz, M., Andrianne, T., Clifford, E., 2019a. Computational fluid dynamics analysis of hand-cycle aerodynamics with static wheels: sensitivity analyses and impact of wheel selection. Proc. Inst. Mech. Eng. P J. Sports Eng. Technol.
Mannion, P., Toparlar, Y., Clifford, E., Hajdukiewicz, M., Andrianne, T., Blocken, B., 2019b. On the effects of crosswinds in tandem aerodynamics: an experimental and computational study. Eur. J. Mech. B Fluid 74, 68–80.
Mannion, P., Toparlar, Y., Clifford, E., Hajdukiewicz, M., Andrianne, T., Blocken, B., 2019c. The impact of arm-crank position on the drag of a paralympic hand-cyclist. Comput. Methods Biomech. Biomed. Eng.
Martin, J., Cobb, J., 2002. Bicycle frame, wheels and tires. In: Jeukendrup, A. (Ed.), High Performance Cycling. Human Kinetics, pp. 113–127.
Martin, J.C., Davidson, C.J., Pardyjak, E.R., 2007. Understanding sprint-cycling performance: the integration of muscle power, resistance, and modeling. Int. J. Sports Physiol. Perform. 2, 5–21.
Martin, J.C., Milliken, D.L., Cobb, J.E., McFadden, K.L., Coggan, A.R., 1998. Validation of a mathematical model for road cycling.pdf. J. Appl. Biomech. 14, 276–291.
Maskell, E.C., 1963. A Theory of Blockage Effects on Bluff Bodies and Stalled Wings in a Closed Wind Tunnel. Aeronautical Research Council, Reports and Memoranda. N: 3400.
McCole, S.D., Claney, K., Conte, J.-C., Anderson, R., Hagberg, J.M., 1990. Energy expenditure during bicycling. J. Appl. Physiol. 68, 748–753.
Mercker, E., 1986. A blockage correction for automotive testing in a wind tunnel with closed test section. J. Wind Eng. Ind. Aerod. 22, 149–167.
Mercker, E., Wickern, G., Weidemann, J., 1997. Contemplation of nozzle blockage in open jet wind-tunnels in view of different 'Q' determination techniques. In: SAE Technical Papers.
Mercker, E., Wiedemann, J., 1996. On the correction of interference effects in open jet wind tunnels. Soc. Automot. Eng.
Morton, R.H., Hodgson, D.J., 1996. The relationship between power output and endurance: a brief review. Eur. J. Appl. Physiol. Occup. Physiol. 73, 491–502.
Nonweiler, T., 1956. The Air Resistance of Racing Cyclists.
Oberkampf, W.L., Trucano, T.G., Hirsch, C., 2004. Verification, validation, and predictive capability in computational engineering and physics. Appl. Mech. Rev. 57, 345.
Obree, G., 2005. Flying Scotsman: Cycling to Triumph through My Darkest Hours. Velo Press, Boulder, Colorado (USA).
Oggiano, L., Brownlie, L., Troynikov, O., Bardal, L.M., Sæter, C., Sætran, L.R., 2013. A review on skin suits and sport garment aerodynamics: guidelines and state of the art. In: Procedia Engineering, pp. 91–98.
Oggiano, L., Leirdal, S., Sætran, L., Ettema, G., 2008. Aerodynamic optimization and energy saving of cycling postures for international elite level cyclists. In: Proceedings of 7th ISEA Conference 2008. Biarritz, June 2-6, 2008.
Oggiano, L., Sætran, L., Løset, S., Winther, R., 2007. Reducing the athlete's aerodynamical resistance. J. Comput. Appl. Mech. 8.
Orszag, S.A., Yakhot, V., Flannery, W.S., Boysan, F., Choudhury, D., Maruzewski, J., Patel, B., 1993. Renormalization group modeling and turbulence simulations. In: International Conference on Near-Wall Turbulent Flows. Tempe, Arizona.
Parker, B.A., Franke, M.E., Elledge, A.W., 1996. Bicycle aerodynamics and recent testing. In: 34th AIAA Aerospace Sciences Meeting, Reno, NV, 15–18 Jan 1996.
Pogni, M., Petrone, N., 2016. Comparison of the aerodynamic performance of five racing bicycle wheels by means of CFD calculations. Procedia Eng. 147, 74–80.
Pugh, L.G.C.E., 1974. The relation of oxygen intake and speed in competition cycling and comparative observations on the bicycle ergometer. J. Physiol. 241, 795–808.
Ritchie, A., 2011. Quest for Speed. Cycle Publishing/Van der Plas Publications.
Roshko, A., 1954. On the Drag and Shedding Frequency of Two-Dimensional Bluff Bodies.
Roues Artisanales, 2008. Aerodynamics Tests [WWW Document]. http://www.rouesartisanales.com/article-15505311.html, 10.13.18.
Rover Cycle Company Limited, 1898. Rover Cycles for 1898: Catalogue and Price List.
Roy, C.J., 2005. Review of code and solution verification procedures for computational simulation. J. Comput. Phys. 205, 131–156.
Sayers, A.T., Stanley, P., 1994. Drag force on rotating racing cycle wheels. J. Wind Eng. Ind. Aerod. 53, 431–440.
Schade, D., Froncioni, A., Natrup, J., 2016. A new approach to measure position stability on the bike in time trial performance – a pilot study. J. Sci. Cycl. 5, 57–58.
Schauff, J., 2018. Private communication. (Accessed 24 October 2018).
Schmitz, A., 2000. Human Power: the Forgotten Energy. Hadland, Coventry.
Schmitz, A., 1990. Why your bicycle has not changed for 106 years. Cycl. Sci. 2, 3–8.
Scott, R.P., 1889. Cycling Art, Energy and Locomotion. J. B. Lippincott Company, Philadelphia.
Shanebrook, J.R., Jaszczak, R.D., 1976. Aerodynamic drag analysis of runners. Med. Sci. Sports 8, 43–45.
Sharp, A., 1896. Bicycles & Tricycles. Longmans, Green, and Co., London; New York and Bombay.
Shimano, 1980. Shimano Aerodynamics Catalogue.
Spoelstra, A., de Martino Norante, L., Terra, W., Sciacchitano, A., Scarano, F., 2019. On-site cycling drag analysis with the Ring of Fire. Exp. Fluid 60, 1–16.

Spurkland, L., Bardal, L.M., Sætran, L., Oggiano, L., 2015. Low aerodynamic drag suit for cycling: design and testing. In: Proceedings of the 3rd International Congress on Sport Sciences Research and Technology Support (IcSPORTS 2015), pp. 89–96.
Starley, J., Hillman, W., 1870. Wheels and Driving Gear for Velocipedes. British patent n. 2236.
Tengattini, S., Bigazzi, A., 2018. Validation of an outdoor coast-down test to measure bicycle resistance parameters. J. Transport. Eng. Part A Syst. 144, 04018031.
Terra, W., Sciacchitano, A., Scarano, F., 2018. A novel approach for skin suit aerodynamic optimization using local momentum deficit. In: ISEA 2018: 12th Conference of the International Sports Engineering Association "Engineering of Sport.".
Tew, G.S., Sayers, A.T., 1999. Aerodynamics of yawed racing cycle wheels. J. Wind Eng. Ind. Aerod. 82, 209–222.
Thompson, L., 2013. The racing bicycle. In: Routledge Handbook of Sports Technology and Engineering, pp. 111–129.
Thompson, L., 1998. Engineering the world's fastest bicycle. In: 2nd International Conference on the Engineering of Sport.
Tominaga, Y., Mochida, A., Yoshie, R., Kataoka, H., Nozu, T., Yoshikawa, M., Shirasawa, T., 2008. AIJ guidelines for practical applications of CFD to pedestrian wind environment around buildings. J. Wind Eng. Ind. Aerod. 96, 1749–1761.
Underwood, L., Jermy, M., 2013. Optimal handlebar position for track cyclists. Sports Eng. 16, 81–90.
Underwood, L., Jermy, M., 2010. Optimal hand position for individual pursuit athletes. Procedia Eng. 2, 2425–2429.
von Salvisberg, P., 1897. Der Radfahrsport in Bild und Wort. Olms Presse, Munich.
Wilson, D.G., 2004. Bicycling Science, third ed. The MIT Press.
Woodforde, J., 1980. The Story of the Bicycle. Routledge & Kegan Paul, London, Boston and Henley.
Wurnitsch, W., Siebert, M., Litzenberger, S., Sabo, A., 2010. Development of an individually customizable integral carbon aerobar based on sEMG measurements of the upper limbs. In: Procedia Engineering, pp. 2631–2635.
Zdravkovich, M.M., 1992. Aerodynamics of bicycle wheel and frame. J. Wind Eng. Ind. Aerod. 40, 55–70.